Transition metal oxides for combustion and depollution processes

Nicolas Bion, Fabien Can, Xavier Courtois, Daniel Duprez

In "Metal Oxides in Heterogeneous Catalysis"
Ed. JC Vedrine (Elsevier Publ.), Chapter 6, p. 287-353 (2018)
DOI: 10.1016/B978-0-12-811631-9.00006-5
ISBN: 978-0-12-811631-9

Chapter 6

Transition metal oxides for combustion and depollution processes

N. Bion, F. Can, X. Courtois, D. Duprez*

IC2MP, Université de Poitiers, CNRS UMR 7285, 4 Rue Michel Brunet, TSA 51106, 86073 Poitiers Cedex, France

Keywords

Total oxidation on oxides, carbon monoxide oxidation, methane combustion, COV oxidation, NO decomposition, NO oxidation, NH_3 oxidation, wet air oxidation.

Abstract

Transition metal oxides (M = Mn, Co, Fe, Ni,...) are potential catalysts for application in combustion and depollution processes. Owing to huge improvements in their preparation, perovskites, spinels, hexaaaluminates and some other oxide structures can replace noble metals in a number of processes. In this chapter, the most recent advances in the use of oxides for total oxidation (CO, methane, COV, wet air oxidation) and for the treatment of nitrogen compounds (NOx, NH_3, urea) will be reviewed. In every case, the most probable mechanism (Langmuir-Hinshelwood, Eley-Rideal, Mars-van Krevelen,...) and the nature of active sites (M^{n+}/M^{n+1} ion pairs, acid-base sites,...) as well as the role of reactive oxygen species will be examined in the light of recent results and up-to-date concepts. Finally the outstanding progresses in the oxide synthesis allow to apply these concepts to the development of extremely active and more stable catalysts.

6.1. Introduction

In 1815, H. Davy invented the safety lamp for miners consisting in a mesh screen enrolled around the flame, thus protected from methane and dusts of the gallery. Some years later, Davy improved his invention by adding a Pt filament close to the flame [1]. This filament continued to burn the oil even though the flame was blown out allowing the gallery to remain brightly lit for a while. It was the first clear demonstration of the action of Pt for hydrocarbon combustion, the beginnings of the Catalysis Science [2]. Given the high prize of platinum and other noble metals, many efforts have been made in the 19th century to replace these metals by oxide catalysts for catalyzing hydrocarbon combustion. But it was rapidly established that oxides showed a high tendency to form oxygenated intermediates during combustion. And in fact, during the second part of the 19th century, the objective of many researchers has been to make these oxides highly selective. All these studies led to an extraordinary development of new processes for Chemical Industry [3,4,5]. A turning point in history of Catalysis by oxides was the First World War. Chemical war with poison gases (chlorine, phosgene, yperite,...) led to equip soldiers with protecting masks containing absorbent filters. These filters were improved by adding a catalyst favoring adsorption and elimination of decomposition products at ambient temperature (CO and other VOC), especially for use in confined spaces. One of the best catalysts was hopcalite, a mixture of Mn and Cu oxides (improved by addition of Co or Ag oxides). Hopcalite was discovered by scientists of the John Hopkins University (hop) associated with the University of California (cal) in the last years of the war and described in 1920 [6] and in more detail in 1941 [7]. Nearly a century later, hopcalite and more generally copper-manganese mixed oxides continue to attract intensive researches for improving their synthesis [8,9], their stability [10] and for various applications in VOC oxidation [11,12,13].

Activity of single oxides for total oxidation is generally linked to the presence of $M^{n+}/M^{(n+1)+}$ ion pairs associated to oxygen vacancies, essential for the adsorption or the heterolytic splitting of the molecule (CO, hydrocarbons,...) and for O_2 activation. It is the reason why oxides such as Co_3O_4, Fe_3O_4,... which intrinsically possess two valences of the metal in their structure, are taken as good candidates for oxidation reactions [14,15,16], even in absence of noble metal [17]. The density of active sites depending on the crystal face (mainly 111, 110), the oxide shape (nanorods, nanosheets, nanocubes, ...) plays a major role in oxidation reactions [18].

However, mixed oxides M_1M_2Ox have generally superior performances owing to the presence of very active $M_1^{n+}/M_2^{(n+1)+}$ ion pairs. Hopcalites $CuMnO_2$ (see above) or CoFeOx [19,20,21] are good examples of such catalytic materials. In these materials, M_1 and M_2 may initially have the same charge but they adapt the right valence under the reaction conditions: the reductant-to-oxygen ratio is then a critical parameter for a good activity. In certain mixed oxides, the metal M_1, not reducible and inactive *per se*, is able to induce a partial reduction of M_2: the active site is a $M_2^{n+}/M_2^{(n+1)+}$ ion pair stabilized by the presence of M1. $LaMnO_3$ and $LaCoO_3$ perovskites are remarkable examples of this category of materials [22,23,24]. There is coexistence of Mn^{4+} and Mn^{3+} ions in $LaMnO_3$ while Co^{3+} and Co^{2+} ions are present together in $LaCoO_3$. It is the reason why the conventional nomenclature of these perovskites is $LaMnO_{3+\delta}$ and $LaCoO_{3-\delta}$ respectively, with δ = 0.15 for the manganite and δ = 0.1-0.3 for the cobaltite. Substitution of one or two cations of the binary oxides by other elements is a classical way to improve activity of the oxide catalysts widely used in oxidation reactions (perovskites,

hexaaluminates, spinels, ...). Some indication will be given about this strategy but it is not possible to be exhaustive because of the huge number of studies dealing with ternary and quaternary oxides, particularly in the vast world of perovskite-based materials. In parallel with oxides and mixed oxides prepared by sophisticated methods, waste derived materials were developed as active oxidation catalysts. A number of industrial wastes (for instance, red muds from aluminum industry) contain several oxides (iron, manganese, ...) which are currently used in oxidation. Bennett et al. have recently reviewed these applications [25].

Carbon-Hydrogen bond activation is a crucial step of the reactivity of noble metals for alkane oxidation [26,27]. On these metals, adsorbed O species can diffuse rapidly at the catalyst surface to reach the site where the reactant (CO, hydrocarbons, VOC,...) is adsorbed [28]. Oxygen mobility over oxides is generally much slower and may become a determining step in the catalytic reaction. As this will be seen in section 6.2, the so-called Mars and Van Krevelen mechanism, adapted for total oxidation, requires a significant mobility at the surface or inside the solid [29]. It is the reason why O mobility was investigated, mainly by $^{16}O/^{18}O$ exchange, on single oxides [30], perovskites [31], hexaaluminates [32,33] or Yttrium-Stabilized Zirconia (YSZ) [34,35].

After a short overview of the mechanisms of reaction with CH_4 and CO as model reactant (section 6.2), the complete oxidation reactions will be reviewed by class of compound: carbon monoxide (section 6.3), methane (section 6.4), other hydrocarbons and oxygenates (section 6.5), other VOC (Cl- and S-containing compounds, section 6.6), automotive soots (section 6.7), nitrogen compounds within their implication in DeNOx catalysis (section 6.8). All these oxidation reactions are carried out in gas phase. An interesting application of oxide catalysts concerns their use in aqueous phase for the so-called wet-air oxidation, which will be reviewed in section 6.9. For evident reason of space in this chapter and because several reviews were already published on the same topics, priority will be given to the most recent investigations, in the 2012-2016 period.

6.2. Overview on the mechanisms of total oxidation reactions over metal oxides

6.6.1 Different types of mechanisms for total oxidation

Recently, Liang and Fang have reviewed the different types of mechanisms that can predict the oxidation kinetics of various organic compounds, mainly hydrocarbons [36]. In the *Langmuir-Hinshelwood* (LH) mechanism, both hydrocarbon and oxygen are chemisorbed on the catalysts surface and react according to a bimolecular reaction. If the hydrocarbon and oxygen compete for the same sites, the kinetic derivation of the LH mechanism leads to the classical rate equation:

$$r_{LH} = k_C \frac{K_C P_C . K_O P_O}{(1 + K_C P_C + K_O P_O)^2} \qquad (6.1)$$

where r is the rate of HC consumption, k_C, the kinetic constant, P_C and P_O, the partial pressure of HC and oxygen, K_C and K_O their respective adsorption constants. Depending on the relative adsorption strength of HC or O_2, kinetic orders may vary from -1 for the most strongly adsorbed reactant to +1 for the reactant that is weakly adsorbed. If the hydrocarbon and oxygen are adsorbed on distinct sites, the equation becomes:

$$r_{LH} = k_C \frac{K_C P_C . K_O P_O}{(1 + K_C P_C)\,(1 + K_O P_O)} \qquad (6.2)$$

Positive orders are then observed for all the reactants.

In the *Eley-Rideal* (ER) mechanism, O_2 is too weakly adsorbed so that it reacts directly from the gas phase with the adsorbed hydrocarbon molecule. The kinetic derivation of this mechanism leads to the following rate equation:

$$r_{ER} = k_C \frac{K_C P_C . P_O}{(1 + K_C P_C)} \quad (6.3a)$$

The kinetic order is +1 with respect to oxygen and comprised between zero (HC strongly adsorbed) and +1 (HC weakly adsorbed) for the hydrocarbon.

But, in fact, the reverse (gas phase HC or CO reacts with adsorbed O) can occur. Eq. 6.3a becomes:

$$r_{ER} = k_O \frac{K_O P_O . P_C}{(1 + K_O P_O)} \quad (6.3b)$$

The *Mars and van Krevelen* (MvK) mechanism was initially proposed to explain the kinetic of selective oxidation reactions over vanadium oxide catalysts [29]. In this mechanism, the hydrocarbon is oxidized by the metal cation with concomitant insertion of the oxygen of the surface leading to CO_2, H_2O and an oxygen vacancy (rate of this step: r_C; kinetic constant: k_C) while the oxygen vacancy is refilled by gaseous O_2 (rate r_O; kinetic constant: k_O). The steady state is reached for $r_C = r_O$, which leads to rate equation:

$$r_{MkV} = \frac{k_C P_C . k_O P_O}{\nu k_C P_C + k_O P_O} \quad (6.4)$$

where ν is the overall stoichiometry of the reaction (one molecule of HC requires ν moles of O_2). As discussed by Vannice [37], this mechanism implies that (i) both oxidation step and reoxidation of the surface are of first order with respect to HC and O_2, respectively, (ii) O surface sites are free of carbon intermediates.

In the literature specific of perovskite-based catalysts, oxidation mechanisms are often presented as "*suprafacial*" or "*intrafacial*" mechanisms [23,38,39,40]. Suprafacial mechanisms mean that only surface oxygens are involved in the catalytic reaction: they correspond to LH or ER classical mechanisms, but also to the MvK mechanism in which the steps of O abstraction and O vacancy refilling are restricted to surface atoms. In intrafacial mechanisms, bulk oxygens are involved in the oxidation reaction. This is typically the case of MvK mechanisms with participation of all the oxygens of the oxide network.

6.6.2 Mechanisms of carbon monoxide oxidation

Kinetics and mechanisms of CO oxidation over transition metal oxides was reviewed by Royer and Duprez in 2011 [16]. Reaction kinetics depend very much on the nature of oxide, its exposed facet, its pretreatment (reducing or oxidizing, in wet or dry atmospheres, etc…). Figure 6.1 illustrates the effect of oxide pretreatment on the activity of several oxides for CO oxidation. This figure shows that the most active oxides (with the lowest T1/2) are also the most sensitive catalysts to moisture in the gases (representative points above the diagonal).

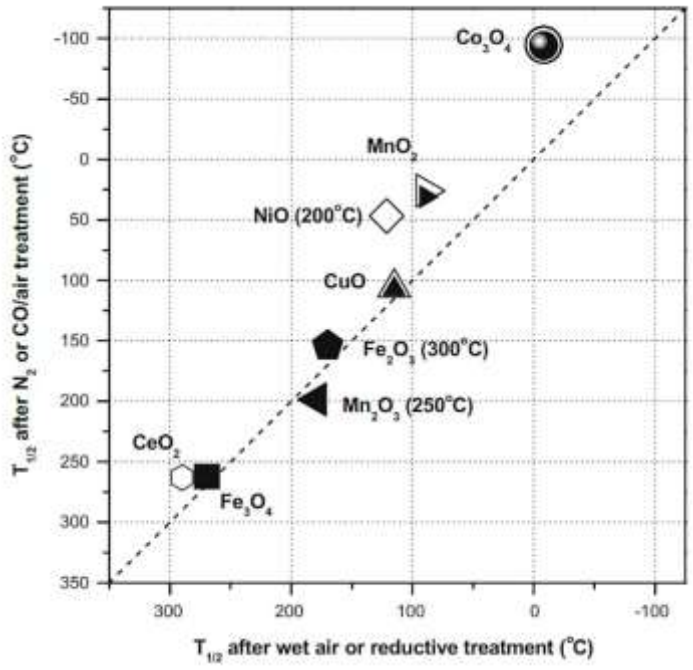

Figure 6.1. Activity of various oxides in CO oxidation. Temperature T1/2 for a 50% conversion after pretreatment in dry N2 or in a 1%CO/air mixture as a function of T1/2 after pretreatment in wet air or in reducing atmosphere. The pretreatments were carried out at 150°C or at the temperature noted in parentheses. Reaction conditions: 0.15 g catalyst sample, 1.0 vol% CO in air, 50 mL/min. From ref. 41

All the mechanisms depicted in 6.2.1 were proposed for CO oxidation. However, LH and ER mechanisms seem to represent, at the best, kinetics, spectroscopic and ^{18}O labeled experiments carried out at low temperature. For instance, Yu et al. have proposed the following reaction scheme for CO oxidation over Co_3O_4 at -80°C [41]:

$$CO + Co^{3+} \rightarrow CO{-}Co^{3+} \quad (6.5a)$$

$$O_2 + Co^{3+}{-}V_O{-}Co^{3+} \rightarrow Co^{3+}{-}O_2^{-}{-}Co^{2+} \quad (6.5b)$$

$$CO{-}Co^{3+} + Co^{3+}{-}O_2^{-}{-}Co^{2+} \rightarrow CO_2(g) + Co^{3+} + Co^{3+}{-}O^{-}{-}Co^{2+} \quad (6.5c)$$

$$CO{-}Co^{3+} + Co^{3+}{-}O^{-}{-}Co^{2+} \rightarrow CO_2 + Co^{3+}{-}V_O{-}Co^{3+} \quad (6.5d)$$

This sequence of elementary steps corresponds to a L-H mechanism with adsorption of CO and O_2 on different sites (Co^{3+} for CO and an oxygen vacancy between two adjacent Co ions), which explains why relatively close positive orders with respect to O_2 and CO were obtained (between 0.2 and 0.5). This mechanism is coherent with the model of surface structure of Co_3O_4 developed by Broqvist et al. for their DFT study [42]. However, in the Broqvist's model, there are two types of surface oxygens (denoted O_W and O_S) whose abstraction requires different energies. A MvK mechanism cannot thus be discarded in which each of these oxygens plays an inequivalent role in adsorption and surface reaction. Yu et al. have also noticed that the high activity of Co_3O_4 can be linked to a metal-oxygen bond energy much lower in this oxide than in inactive (TiO_2) or less active oxides (MnO_2 for instance).

Mechanisms of CO oxidation over oxide catalysts may depend on the exposed face. Therefore, mechanistic studies with polycrystalline solids can lead to erroneous interpretations. For instance, CO oxidation over the (100) face of α-Fe_2O_3 seems to follow an E-R mechanism with gaseous CO reacting on O_{ads} while a LH mechanism would be favored on the oxygen terminated (0001) surface [43,44]. The postulated E-R mechanism on the (100) face of Fe_2O_3 was proven on the basis of FTIR and ^{18}O labeling studies. Iron oxide surface is essentially covered by adsorbed oxygen and CO_2. Intermediates such as monodentate carbonates are detected by DRIFT but there is no evidence of adsorbed CO in the course of the reaction [44]. However, the mechanism on Fe_2O_3 (100) would be more complex than a classical E-R mechanism. DFT studies reveal that a first molecule of CO is strongly bound to some Fe ions of the surface, which destabilizes the other O-Fe bonds [43]. A second molecule of CO could then approach the surface and react with the O atoms weakly bound to Fe. The E-R mechanism corresponds to this last step of the overall process as depicted in eq. 6.6.

$$Fe_2O_3 + CO_g \rightarrow Fe_2O_3(CO) \quad (6.6a)$$

$$Fe_2O_3(CO) \rightarrow Fe_2O_2(CO) + CO_{2g} \quad (6.6b)$$

$$Fe_2O_2(CO) + O_2 \rightarrow [Fe_2O_2(CO)]O_2 \quad (6.6c)$$

$$[Fe_2O_2(CO)]O_2 + CO_g \rightarrow Fe_2O_3(CO) + CO_{2g} \quad (6.6d)$$

6.6.3 Mechanisms of methane oxidation

Methane is an hydrocarbon extremely refractory to oxidation. Palladium-based materials are the most active catalysts for methane combustion [45,46]. Oxidation generally starts at 300-350°C. Even though they operate at higher temperatures, oxide catalysts and especially perovskites can be good alternatives to the use of noble metals [23], particularly for heat production [47]. As for CO oxidation, the reaction can obey different mechanisms depending on the oxide used as catalyst. The simplest model is the *L-H mechanism* with co-adsorption of CH_4 and O_2 on the same sites formed by a Metal-Oxygen pair of the oxide surface. In the study of Pengpanich et al. [48], this mechanism leads to the best fitting for the kinetics of CH_4 oxidation over CeO_2-ZrO_2 mixed oxides. The resulting rate expression is analogous to that of Eq. 6.1 with terms of O2 adsorption in $P_O^{1/2}$ instead of P_O. Penganich et al. found that oxygen was more strongly adsorbed than CH_4, adsorption energy of O_2 on $Ce_{0.75}Zr_{0.25}O_2$ being 2.4 times higher than that of methane in the 400-600°C temperature range of reaction. A close examination of the data of Penganich et al. shows that the L-H model was ascertained on the basis of the coefficient of correlation (R^2=0.994) better than that of an E-R model with CH_4 reacting on adsorbed oxygen (R2=0.929 for Eq. 6.3b with a term in $P_O^{1/2}$ instead of P_O).

Contrasting with the previous study, Belessi et al. showed that the CH_4 oxidation reaction on ferrite-like perovskite catalysts obeyed an E-R mechanism, rather than a L-H model [49]. They also demonstrated that the E-R rate equation could be assimilated to power-law kinetics with apparent orders close to the experimental values (Eq. 6.7).

$$r_{ER} = k_O \frac{(K_O P_O)^{1/2}.P_{CH_4}}{1+(K_O P_O)^{1/2}} \approx k'_O (K_O P_O)^{0.5-a} P_{CH_4}{}^{b} \qquad (6.7)$$

Experimental orders, measured in the 420- 620°C temperature range, are comprised between 0 and 0.5 for O_2 and close to 1 for methane, which is in full agreement with Eq. 6.7.

Methane oxidation requires high temperature of reaction, above 400°C for most oxides. Oxygen mobility can thus be very high, which allows MvK mechanisms to occur. For instance, Zavada et al. showed that CH_4 oxidation over Co_3O_4 shifted gradually from a suprafacial mechanism of the E-R type at 400°C to a MvK mechanism implying cobalt-oxo species above 600°C [50]. Changes of mechanisms may also occur depending on the catalyst composition. By studying CH_4 oxidation over a series of $Ce_xSn_{(1-x)}O_2$ catalysts, Liu et al. concluded that the MvK model was preferred over the Sn-rich catalysts [51]. Figure 6.2 illustrates the reaction scheme proposed by Liu et al.

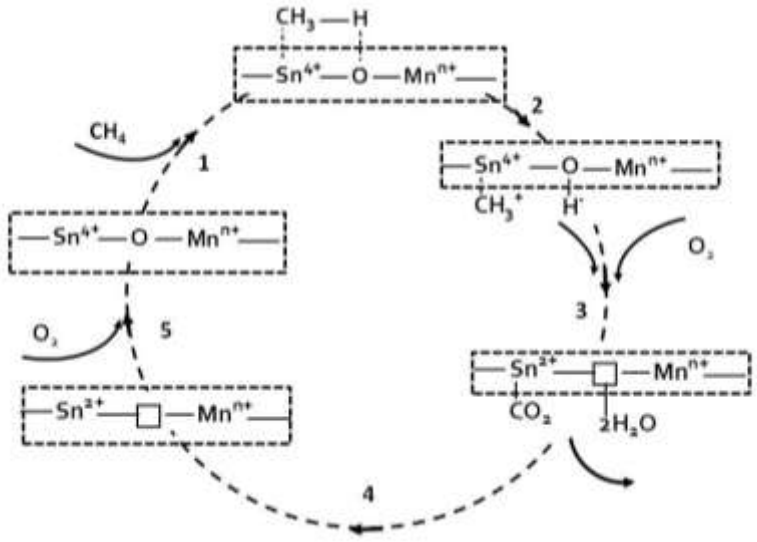

Figure 6.2. Mars and van Krevelen (MvK) mechanism of methane oxidation over $Ce_xSn_{(1-x)}O_2$ catalysts. From ref. [51].

Similarly, by coupling *in situ* electrical conductivity and CH_4 oxidation measurements over a series of $LaCo_xFe_{(1-x)}O_3$ perovskites, Popescu et al. established that the reaction obeyed a MvK mechanism on $LaFeO_3$ while a suprafacial mechanism was preferred on $LaCoO_3$ [52]. Both mechanisms can occur on $LaCo_xFe_{(1-x)}O_3$ perovskites. To clearly demonstrate the role of oxygen mobility in MvK mechanisms, it is necessary to add a component to the oxide catalyst allowing a fast CH_4 activation. A dual bed catalyst constituted of $LaMnO_3$ and YSZ (yttrium-stabilized zirconia) showed exceptional performance for O_2 activation, much better than with any of the individual components [34,35]. To take advantage of this property in CH_4 oxidation, a small amount of palladium was added to YSZ allowing good activation of the CH_4 molecule.

6.3 Oxidation of carbon monoxide

CO, which is highly toxic, is an important constituent of the automotive exhaust gases and its abatement is crucial not only to limit the environment pollution but also to prevent health damage or death. The CO molecule is also inevitably produced in the reforming process which aims to generate hydrogen. When hydrogen is produced to feed a proton-exchanged membrane fuel cell, few ppm of CO can cause dramatic poisoning of the electrode. Low-temperature CO oxidation is then essential to prevent the deactivation of the cell. It certainly makes the catalytic CO oxidation one of the most investigated catalytic reactions. Precious metals such as Au, Pt, Pd, and Rh supported catalysts are highly active for catalytic CO oxidation. However the increasing price as well as decreasing reserves of noble metals makes essential the development of cheaper catalysts constituted of more abundant metals but with comparable catalytic activity. Transition metal oxide catalysts appear as very interesting alternative of the noble metal-based catalysts and reviews regularly update the works which report a better comprehension of the catalytic mechanism as well as the optimization of the transition metal oxide-based formulation with improved catalytic performances [16]. Cobalt, Cerium, Manganese, Iron and Copper oxides are among the most studied samples for catalytic CO oxidation.

6.3.1 Cobalt oxide

For half a century, unsupported Co_3O_4 is known as very active base oxide catalyst for CO oxidation [53]. A significant result was obtained by Haruta et al.[54] who reported that in very dried conditions of reactant flow, CO oxidation was observed over the Co3O4 metal oxide at temperatures as low as -54°C. With this study, they also demonstrated that the cobalt oxide was dramatically sensitive to the presence of water traces (Figure 6.3). Indeed they clearly observed the inhibiting effect of water by comparing the light-off temperature T_{50} which increased from -54 °C for 850 ppb H_2O up to 50 °C for 3 ppm H_2O and 90°C for 0.6% H_2O.

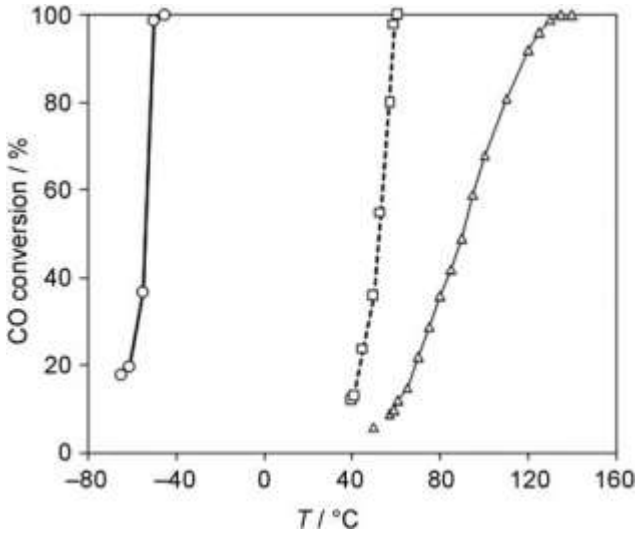

Figure 6.3 : Effect of water on CO conversion over Co_3O_4. Dry conditions: 850 ppb H_2O (trapping of moisture on zeolite at 80 °C); normal conditions: 3 ppm H_2O; wet conditions 6000 ppm H_2O: dry (o); normal (□); wet (Δ).Taken from Ref. [54].

Contrary to H_2O, CO_2 is not an inhibitor but the formation of carbonate species might lead to a deactivation of the catalyst when the reaction is performed at low temperatures. However, Jansson et al.[55] showed that carbonyls, carbonates and other surface C species were not directly responsible of cobalt oxide deactivation. They concluded suggesting that the slow deactivation during the reaction was likely due to a surface restructuration hindering the Co^{2+}/Co^{3+} redox at the origin of the good activity. They also demonstrated that the active sites of the Co_3O_4 were regenerated with oxidative step at 250 °C.

Recent research focused on nanostructured cobalt oxide catalysts [56,57,58]. Co_3O_4 has a spinel structure with a cubic close-packed array of O^{2-} in which one eighth of the tetrahedral sites and half of the octahedral sites are occupied by Co^{2+} and Co^{3+} respectively. Xie et al. reported in 2009 a remarkable illustration of the structure-reactivity relationship [59]. The activity as well as the stability of Co_3O_4 for CO oxidation reaction was considerably improved by changing the morphology of the oxide from spherical nanoparticles to nanorods. The difference of activity was associated to the surface enrichment in nanorods of Co^{3+} sites which are known as active site for the CO adsorption [60]. Indeed the (110) planes which contain mainly Co^{3+} sites are preferentially exposed in the nanorods while the spherical nanoparticles of Co_3O_4 are only enclosed of Co^{2+}-containing (111) and (001) planes. Morphology-dependent activity of Co_3O_4 was confirmed by Hu et al [61]. These authors showed that Co_3O_4 nanobelts which have a predominance of (011) facets were much more active than nanocubes terminated by the (001) planes. Contrary to Xie et al., they calculated a difference of TOF depending on the exposed crystal plane with TOF of Co^{3+} sites on (011) planes 2.7 times higher than those on (001) planes. Note that the crystal sizes of nanorods, nanobelts or nanocubes described previously are larger than 10 nm. Recently Iablokov et al. reported a study which aims to investigate the size effect in the CO oxidation activity over cobalt oxide catalysts by varying the size of the Co_3O_4 nanoparticles 3.5 and 12.2 nm [62]. They concluded that the CO oxidation was clearly structure sensitive over Co_3O_4 with higher activity for 5 to 8 nm particles and they again confirmed the crucial role of Co^{3+} by establishing a correlation between the Co^{3+} trivalent oxidation state and the CO oxidation rate using X-ray photoelectron spectroscopy. For smaller and larger particles the intrinsic activity decreased drastically (Figure 6.4). It completes the precursor work reported by Yu Yao in which the intrinsic activity varied little with BET surface area in the case of large particles [53].

Finally, the influence on CO oxidation activity of the pretreatment effect for low-temperature calcined Co_3O_4 oxides was reported [63]. Typically, when calcined below 400 °C, a pre-treatment of Co_3O_4 in dry air, in inert or reducing oxidizing dry atmospheres (N_2 or CO/air) in the temperature range of 150–250 °C induces the formation of surface oxygen vacancies resulting in an enhancement of the catalytic activity at a temperature as low as -80 °C.

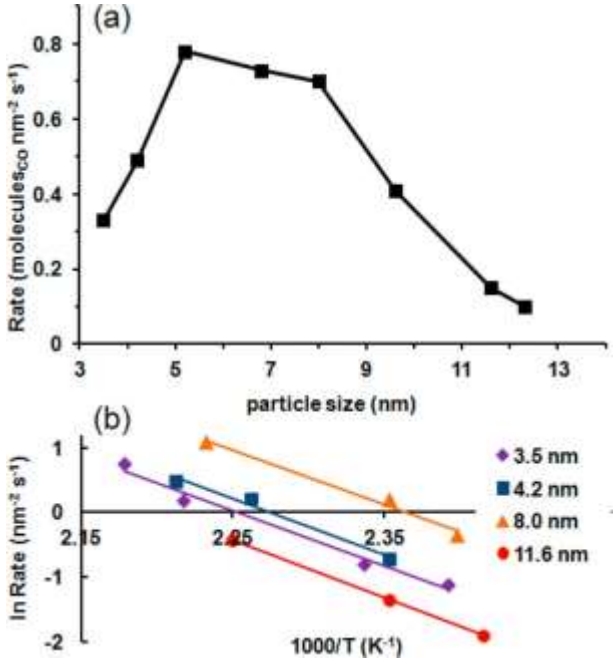

Figure 6.4: (a) CO oxidation activity (CO + O_2, 2% each, 150 °C) vs particle size, (b) Arrhenius plots for Co_3O_4/MCF-17 samples. Taken from [62]

6.3.2 Cerium oxides

The considerable attention that has received cerium oxide in numerous catalytic reactions is generally associated to the redox properties of this oxide [64]. For example, the application in automobile industry of ceria and ceria-based oxides as component of the Three-Way Catalysts (TWC) is related to their capacity to store and release oxygen, classically known as Oxygen Storage Capacity (OSC). The pioneering work to measure OSC in cerium-based oxides was established by Yao et al. who used the transient oxidation of CO in absence of O2 in the gas-phase using a pulse injection method [65]. The measurement is based on the fact that the CO oxidation proceeds over ceria via a Mars–van Krevelen mechanism involving the participation of O atoms from the lattice by oxygen vacancy generation and their subsequent replenishment with gas-phase oxygen [66]. The association of $^{16}O/^{18}O$ isotopic exchange and OSC measurements were shown very powerful to investigate the oxygen activation process [67] as well as oxygen diffusivities on the surface and bulk of the ceria and ceria-based-materials [68,69]. By combining the FTIR spectroscopy to these techniques, correlation was obtained between adsorption and exchange of superoxide O_2^- species and OSC values measured at 400°C [70]. Fornasiero et al. very recently published an exhaustive review in which the main results obtained by OSC measurement and correlation with CO oxidation have been largely described [71]. Recent literature on CO oxidation over pure ceria focused on the structure-activity relationship [56,72,73]. Contrary to cobalt oxide, a consensus was rapidly found on the basis of studies over polycrystalline materials that the CO oxidation was a structure sensitive reaction on ceria [74]. Recent advances in nanostructured ceria synthesis [75] and in transmission electron microscopy enabled a better determination of the most active facets and theoretical studies confirmed the influence of the crystallographic plane on the CO adsorption and the oxygen vacancy formation [76]. The higher catalytic activity in CO oxidation is obtained in nanorods that preferentially exposed (110) planes. This morphology also

exhibits the higher lattice oxygen mobility as determined by oxygen isotopic exchange. There is a very good correlation between oxygen mobility and CO oxidation which follow the same trends: rods with (110) and (100) facets > cubes with (100) facets > octahedra with (111) facets [72]. Another important correlation exists between the concentration of large-sized oxygen vacancy clusters and the reactivity of ceria nanoparticles [77]. An elegant illustration of the crucial role of oxygen vacancies was given by Gao et al. who prepared pits confined in three-atomic-layer thin ceria sheet as model material to study the CO oxidation at different sites [78,79]. The creation of this coordinately unsaturated pit-surrounded cerium sites (average coordination numbers of 4.6) induces the generation of more oxygen vacancies. It results in very active sites not only for O_2 activation but also for CO adsorption and diffusion. As a consequence the specific nanostructure lowered the apparent activation energy of CO oxidation from 122.9 to 61.7 kJ mol^{-1} and drastically decreased the CO conversion temperatures (Figure 6.5).

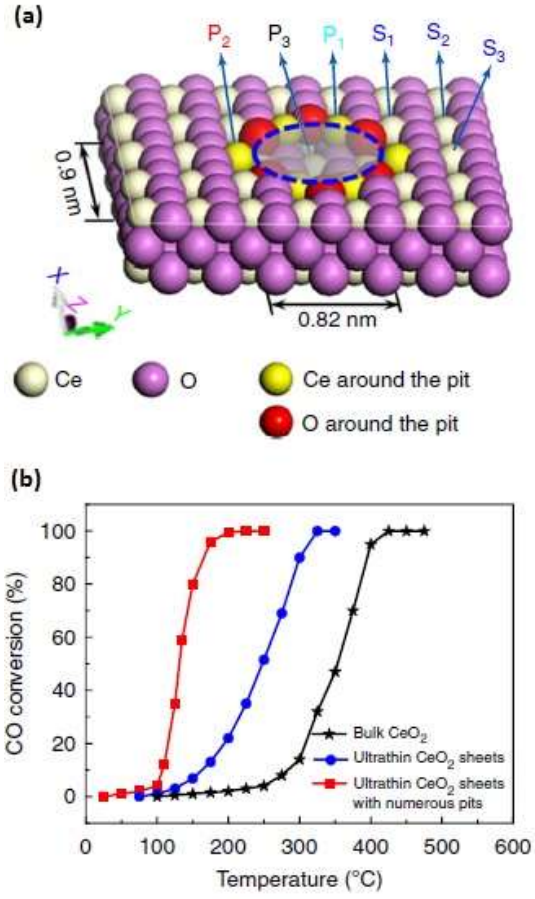

Figure 6.5 : (a) Overhead and top views of schematic structures for the three-atom-thick CeO_2 sheets with a pit size of 0.90 nm x 0.82 nm; the CO molecules prefer to adsorb at P2 site, while the O_2 molecules tend to adsorb and dissociate at the adjacent P1 sites. (b) Catalytic activity for CO oxidation versus reaction temperatures (experimental error: ±3%). Taken from [78]

6.3.3 Manganese oxides

Gao et al. studied the doping of α-MnO_2 by transition metal like Fe, Ni, Co and Cu for the CO oxidation reaction. On the basis of experimental data and DFT calculations, the authors concluded that the better activity of Cu doping (Figure 6.6) is associated with the easier formation of oxygen vacancies in the MnO_2 lattice which is considered as the rate-determining step for CO oxidation [80].

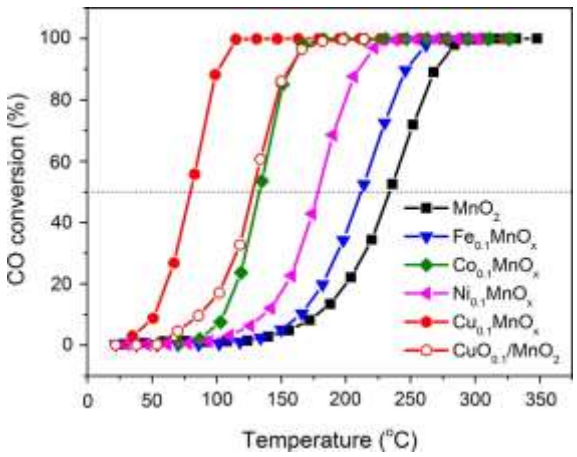

Figure 6.6: CO oxidation activity tests of the MnO_2, $CuO_{0.1}/MnO_2$, and Fe-, Co-, Ni-, and Cu-doped MnO_2 catalysts. Taken from [80]

α-MnO_2 was chosen because other authors previously synthesized α-, β-, γ-, and δ-MnO_2 nanorods by the hydrothermal method and compared their catalytic performances [81]. An effect of the phase structure was clearly evidenced since the activities of the catalysts decreased in the order α- ≈ δ - > γ- > β-MnO_2. The low activity of β-MnO_2 phase was associated with a collapse of its structure during the Mars-Van Krevelen type redox cycle. Indeed during the cycle, CO is oxidized with lattice oxygen leading to the transformation of MnO_2 in the intermediate Mn_2O_3 and Mn_3O_4 oxides which are reoxidized by gas-phase O_2. The reoxidation of Mn_2O_3 and Mn_3O_4 into MnO_2 is controversial if we consider the work of Stobbe et *al.* who reported that Mn_2O_3 corresponds to the highest obtainable manganese valency because further oxidation to MnO_2 can only occur under extremely high oxygen pressures [82]. The existence of intermediate structure of a non-stoichiometric manganese oxide could explain the good activity of α-≈ δ- MnO_2 as reported by Iablokov et al. who directly synthesized by oxalate precipitation and temperature-programmed reduction the non-stoichiometric MnO_x phases with x=1.61…1.67. Such intermediate phases were found much more active than Mn_2O_3 and Mn_3O_4 [62] . Xu et al. reported an elegant study by real time in situ and operando RAMAN spectroscopy in which the Langmuir-Hinshelwood mechanism would be predominant on α -Mn_2O_3 at low temperature (below 200°C) despite the suggestion of an intermediate Mn_jO_k ($1 < j < 2$, $1 < k < 3$, and $1 < k/j < 1.5$) phase formed on the near-surface region during CO adsorption. By performing temperature-programmed surface reaction, CO oxidation was found to proceed through Mars van Krevelen only when temperature reached 350°C [83].

Nanostructured $Ce_{0.7}Mn_{0.3}O_{2-\delta}$ solid solutions, prepared by Venkataswamy et al. simple coprecipitation method, are able to oxidize CO at lower temperature than pure ceria when calcined at 500 °C. Deep characterization showed that the presence of dual valences for both Ce (4+ or 3+) and Mn (3+ and 2+) cations and the very good activity is associated to the incorporation of highly dispersed Mn^{2+}/Mn^{3+} in the ceria matrix which increases the concentration of oxygen vacancies, still at the origin of oxidation activity [84].

6.3.4 Perovskite catalysts

Perovskite, $LnBO_3$ in which Ln is a lanthanide (usually La) and B cation possesses two valence states like Mn, Co or Fe is active for CO oxidation [22,23]. In 2013, our group reviewed the catalytic performances of perovskite in

CO oxidation reaction which is governed by a suprafacial mechanism involving only surface oxygen species[16]. For several decades, $LaMnO_3$ (manganites) and $LaCoO_3$ (cobaltites) are considered as the most active ABO_3 compositions for the reaction. Because of the participation of surface oxygen atoms in the mechanism, numerous studies focused on the development of new synthesis routes in order to enhance the specific surface area. Barnard et al. prepared $LaCoO_3$ by calcination of mixed hydroxide precursors and reported that the rate for CO oxidation exhibited a linear dependence with the surface area [85]. Shu et al. developed a complexation technique with additional introduction of zinc nitrate to synthesize cobaltite. After calcination ZnO is removed resulting in a 30 $m^2\ g^{-1}$ $LaCoO_3$ higher than the 9 $m^2\ g^{-1}$ obtained with conventional complexation method. The sample with high surface area also showed the best catalytic performances for oxidation of CO [86]. Another way to increase the surface area of perovskite was the utilization of the reactive grinding method which permits to Levasseur *et al.* to obtain $LaCoO_3$ with 35 $m^2\ g^{-1}$ surface area and good activity in CO oxidation [87].

The partial substitution of the A and B cations was also intensively investigated to improve the catalytic performances of the perovskite catalysts. La substituted by Sr has usually given the best activity: preferential substitution rate in $La_{1-x}Sr_xCoO_3$ has been found for x=0.3 and 0.8 [88]. The same improvement of the activity for the Sr incorporation was observed for manganite perovskites even if the optimal composition was depending on the reaction temperature [89]: $La_{0.4}Sr_{0.6}MnO_3$ was the most active for low temperature (below 200°C) while $La_{0.8}Sr_{0.2}MnO_3$ gives the highest activity for CO oxidation performed above 250°C. In this last work, the substitution of B cation was also studied like in numerous other papers in order to modify the redox properties of the perovskite. The manganese substitution by the copper induced a higher activity which originated from the increase of oxygen mobility and the reductive non-stoichiometry in the substituted solids. Cu also allows to increase the activity of pure $LaFeO_3$ and $^{18}O/^{16}O$ isotopic exchange experiments revealed that bulk oxygen atoms of Cu-substituted materials can participate in the CO oxidation reaction [90]. Finally the possibility of a simultaneous substitution of A and B cations makes almost infinite the number of compositions and their impact on the CO oxidation activity.

6.4 Methane oxidation

The total oxidation of methane or catalytic combustion of methane has been also widely studied for many years. Indeed this process is an alternative to conventional thermal combustion for power generation but also enables the limitations of pollutant emissions from natural gas or methane combustion devices. It is important to keep in mind that methane has a Global Warming Potential (GWP) twenty-three times higher than carbon dioxide. With the recent increase of shale-gas development, Howarth et al. estimated that 3.6% to 7.9% of the methane from shale-gas production escapes to the atmosphere over the life-time of a well [91]. The growing of lean-burn natural gas vehicules which require the abatement of emissions of methane at low-temperature is also expected in most of the industrial countries. The noble-metal catalysts are considered as very active for methane combustion [92] and among them supported-Pd catalyst is certainly the most studied [45,93] but transition metal catalysts are also regarded as alternative catalysts and a recent review illustrates this interest [94]. Here we will focus some single oxides and will explore the research performed on perovskite and hexaaluminate catalysts.

6.4.1 Single oxides

Like for carbon monoxide oxidation, cobalt oxide attracts considerable attention for methane catalytic combustion [57,94]. A clear morphology effect has been shown for the combustion of methane over nanostructures Co_3O_4. Hu et al. [95] prepared nanosheets, nanobelts and nanocubes by a hydrothermal process using cobalt hydroxide precursor and subsequent thermal decomposition. The catalytic performances followed the trend : nanosheets with (112) planes predominantly exposed > nanocubes with (011) exposed planes > nanobelts with (001) exposed facets. A similar trend was also observed for the redox properties. A more open structure was revealed for the (112) planes resulting in a lower electric energy barrier for C-H bond breaking compared with other exposed close packing planes. Highly porous Co_3O_4 nanorods are prepared by a simple hydrothermal method and compared to bulk Co_3O_4 prepared by thermal decomposition of cobalt nitrate [96]. Co_3O_4 nanorods show a higher activity for CH_4 combustion particularly for high GSHV (100 000 h^{-1}) tests due to the higher surface area and the advanced porous structure. Doping of cobalt oxide with other transition-metal oxides was also widely investigated. An example is given with the work of Li et al. who studied the methane combustion over manganese cobalt oxides with different Mn/Co ratios [97]. The T_{90} (the temperature needed to reach 90% CH_4 conversion) was used to rank the catalytic performances and the following descending order of activity was obtained: Co5Mn1 > Co3Mn1 > Co10Mno > > Co1Mn1 > Co1Mn3 ≈ CooMn10. Co/Mn molar ratio of 5 :1 was thus the optimum composition.

Mn doping into the cobalt spinel structure was supposed to generate disorders causing an enhancement of the activity of the reactive ions in the octahedral sites. Doping with ceria resulted for Li et al. [98] in two advantages: an increase of activity and stability. Indeed Co-Ce-O mixed oxide with a Co/Ce bulk atomic ratio of 3/1, shows the highest oxygen vacancies concentration, the strongest interface interaction between Ce and Co at the origin of the best activity and stability. Single manganese oxide is also reported as active catalyst for methane catalytic combustion following a Mars-van Krevelen mechanism even if Han et al. suggested with a kinetic study that CH_4 combustion is mainly through a Langmuir–Hinshelwood mechanism over α-Mn_2O_3 [99]. Mn_3O_4 will oxidize methane under the formation of water, carbon dioxide and MnO. Subsequently MnO will be regenerated, with air to Mn_3O_4. Only negligible carbon deposition was observed. This carbon laydown can be prevented completely by adding small amounts of water to the feed [82]. Doping MnO_x with Ce also promotes the catalytic activity and stability as compared to CeO_2 and Mn_2O_3 [100].

6.4.2 Perovskite catalysts

As seen for carbon monoxide oxidation, cobaltites and manganites are the most active perovskite catalyts in methane combustion and the catalytic performances can be widely tuned either by changing the A cation or by substituting partially the manganese or cobalt element which gives rise to an infinite number of compositions[23,94]. Contrary to CO oxidation, methane combustion occurs over perovskite catalysts at higher temperature and implies the participation of the bulk oxygen atoms via an intrafacial mechanism in a Mars-van Krevelen catalytic cycle. In $La_{1-x}M_xMnO_{3+\delta}$ (M = Ce, Sr) substituted manganese perovskite catalysts, methane catalytic combustion was correlated to the formation of -Mn^{3+}-O-Mn^{4+}- chains, favoring the double exchange

electron delocalization and hence the Mars van Krevelen mechanism [101]. The best activity was obtained for x = 1 Sr-doped perovskite which also has the higher concentration of Mn^{4+} ions, favoring the electron delocalization through the -Mn3+-O-Mn4+- chains. To study the effect of the synthesis conditions of $LaCoO_3$ on the redox properties and the catalytic activity for the CH_4 catalytic combustion, Royer et al. compared five $LaCoO_3$ samples prepared by different methods: solid state (SS), coprecipitation (COP), citrate complexation (CIT) and reactive grinding of the single oxides (RG) and of an amorphous precursor (COPRG) [102]. In the CH_4 oxidation reaction not all samples presented the same specific activity per unit surface area (Figure 6.7). These differences are explained by some different behaviour in oxygen mobility in the bulk of the solid samples. Neither TPD-O_2 nor TPR-H_2 results could however be simply and uniquely related to the rates of oxidation reactions. $LaCoO_3$ prepared with these different methods was investigated by Royer et al. in terms of oxygen mobility using the oxygen isotopic exchange (OIE) technique and compared with the results obtained for the methane oxidation reaction [103]. The two processes present similar activation energies (92 kJ mol^{-1} for the CH_4 oxidation reaction). In contrast to the OIE reaction, an effect of the BET surface area on the CH_4 oxidation reaction is observed, but the mobility of the bulk oxygen remains of great importance.

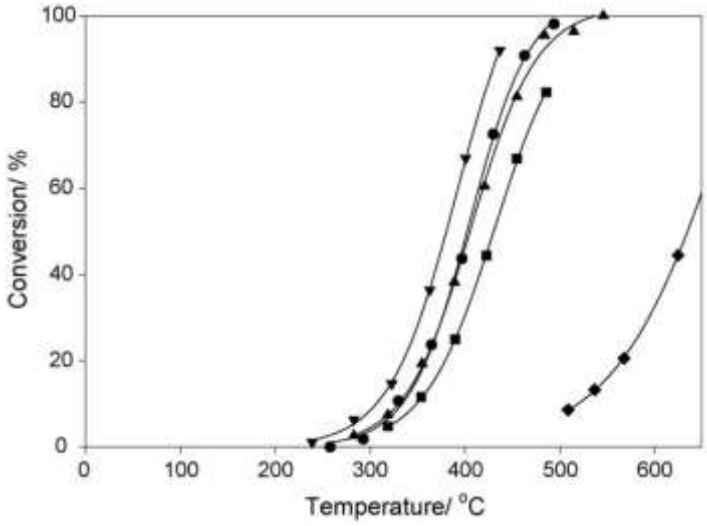

Figure 6.7 : Steady state conversions obtained for the oxidation reaction of 0.25% CH_4 as a function of the reaction temperature for: (▼) COPRG; (●)RG; (▲) CIT; (■) COP; (♦) SS $LaCoO_3$.Taken from [102]

$LaFeO_3$ was less studied because of its lower stability compared with manganites and cobaltites perovskites. For ferrite perovskite the oxygen mobility was evidenced as a crucial parameter. For example, substitution of La^{3+} by Sr^{2+} induces a generation of oxygen vacancies favoring the diffusion of lattice oxygen from the bulk to the surface and decreases significantly the T50 to lower temperature [104]. The increasing of oxygen transport properties is also at the origin of the promotion of catalytic activity for Ce doping at A-site of $LaFeO_3$ [105].

6.4.3 Hexaaluminate catalysts

Hexaaluminate (HA) mixed oxides with general formula of $AB_xAl_{12-x}O_{19-\delta}$ (A_{x+} and B_{y+} being respectively a lanthanide a transition/noble metal cations) consist of alternate layer of alumina spinel blocks and mirror planes

in which a large A cation is located [106]. Despite their lower performances compared with noble metal or perovskite catalysts, HA gained an increased attention in oxidation reaction at high temperature for their exceptional resistance to sintering [107]. Series of cation-substituted barium HA, $BaMAl_{11}O_{19-\delta}$ (M = Cr, Mn, Fe, Co, and Ni), was tested in methane combustion by Machida et al.[108] Among the substituted HA which exhibit higher activity than non-substituted one, Mn-substituted HA provided the best catalytic performances. The catalytic activity was related to the reversible redox cycle between di- and tri-valent states of manganese element in HA structure. During methane combustion over HA materials, methane is oxidized by surface active oxygen resulting in the formation of CO_2, H_2O and oxygen vacancies sites which are regenerated by the gaseous phase oxygen. The catalytic performances of HA are then significantly influenced by oxygen mobility and diffusion. In their study, Laassiri *et al.* confirmed the crucial role of oxygen mobility for methane combustion over HA materials prepared by Activated Reactive Synthesis (ARS) even if multiple factors like transition metal reducibility and concentration can also determine the catalytic activity as it can be seen in Figure 6.8. They also demonstrated that manganese containing HA were more active than the iron and cobalt containing materials. In another work the same authors compared the activity of perovskite and HA materials prepared by solvent free two steps (high energy – low energy) ARS method which results in an improvement of the solid surface area [33]. They concluded that the catalytic activity of these materials does not directly depend on the accessible surface area but is strongly related to the oxygen mobility. The higher activity of Mn-substituted perovskite originates from its higher oxygen mobility properties.

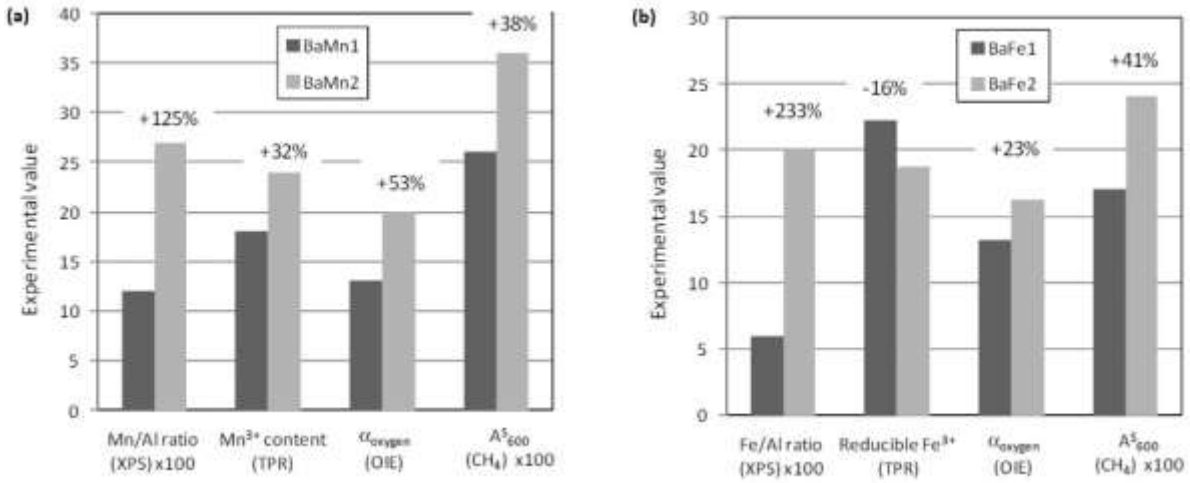

Figure 6.8: Impact of the degree of substitution on: transition metal surface content determined by XPS; reducible metal content as evaluated by TPR-H2; oxygen mobility measured by oxygen isotopic exchange (OIE); specific activity for the CH_4 oxidation reaction (A°_{600} : mmol of CH_4 converted at 600°C per unit of surface) for (a) Mn- and (b)Fe-substituted hexaaluminates. Taken from [33]

6.5. Other hydrocarbons and oxygenates

These molecules are classically referred to as Volatile Organic Compounds (VOC) in the literature. Oxidation of VOC over perovskites was reviewed by Royer et al. up to 2013 [23] while two recent papers give insights on VOC oxidation over oxides (compared to metals) up to 2015-16 [109,110]. As for CO and CH_4 oxidation, copper, manganese, cobalt and iron oxides are mainly used in VOC oxidation. Rare earth oxides (La_2O_3, CeO_2 or CeO_2-

ZrO_2) are often added as dopant to improve surface area, oxygen storage properties and stability of the single oxides [111,112,113,114,115]. Catalytic oxidation of hydrocarbon VOCs (including oxide as catalysts) was recently reviewed by Garcia et al. [116] while special properties of the interaction between copper and ceria and their implication in catalysis was overviewed by Konsolakis [117].

6.5.1. Hydrocarbons

Light alkanes. *Propane* oxidation has been widely used as model reaction of light alkane oxidation. It is often carried out for testing three-way catalysts (TWC) or Diesel Oxidation Catalysts (DOC). Noble metals (NM) are currently used in these tests but oxide catalysts have been considered as alternatives of NM catalysts [23]. Compared to CO whose oxidation occurs below 200°C, propane is fully oxidized in the 200-400°C temperature range on many oxide catalysts. Faure and Alphonse have compared the oxidation of CO and of propane on a series of $Co_xMn_{3-x}O_4$ spinel oxides [118]. Figure 6.9 represents their results for $0<x<3$.

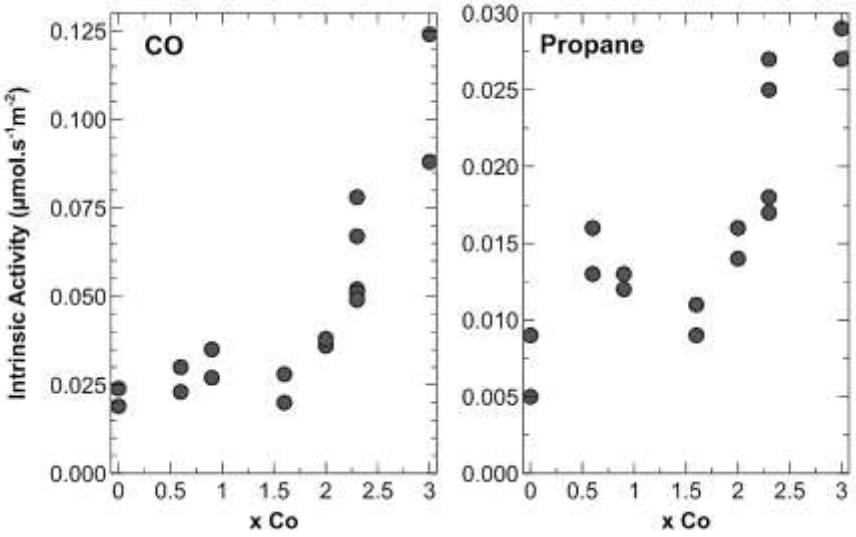

Figure 6.9. Intrinsic activity per m^2 of $Co_xMn_{3-x}O_4$ spinel oxides for CO oxidation at 60°C (left) and for propane oxidation at 200°C (right). From ref. [118].

Catalytic activity significantly increases with the faction x of cobalt in the spinel. Co^{2+} ions replace first Mn^{2+} ions in tetrahedral position. For higher values of x, Co^{3+} replaces Mn in octahedral position, which is more favorable to activity in oxidation. BET area being maximal for x=2.3, the $Co_{2.3}Mn_{0.7}O_4$ sample has the highest specific activity per gramme of catalyst. The activity ratio between CO and C_3H_8 oxidation can be calculated at 60°C on the basis of activation energy of 60 kJ mol^{-1} for the propane oxidation reaction. This ratio is close to 2500 for the pure cobalt spinel (Co_3O_4) and 1200 for $CoMn_2O_4$, which shows that Co accelerates more CO than propane oxidation. Propane oxidation was investigated over mesoporous Co_3O_4 by Garcia et al. [119] and over Ni doped-Co_3O_4 nano-arrays deposited on cordierite honeycomb by Ren et al. [120].Mesoporous Co_3O_4 was synthetized by a nanocasting route using KIT-6 silica as template. Depending on the aging temperature during the synthesis of the silica template (from 40 to 100°C) and the calcination temperature of the cobalt oxide (after silica elimination), unimodal, bimodal and partially ordered Co_3O_4 were obtained. The last oxide was the most active catalyst for C_3H_8 oxidation with a T50 at 200°C. It was proven that a certain degree of disorder favors the

formation of surface O vacancies together with a higher Co^{2+}/Co^{3+} ratio, beneficial for a higher oxidation activity [119]. SEM and TEM pictures of the Co_3O_4 nano-array prepared by Ren et al. [120] are shown in Figure 6.10.

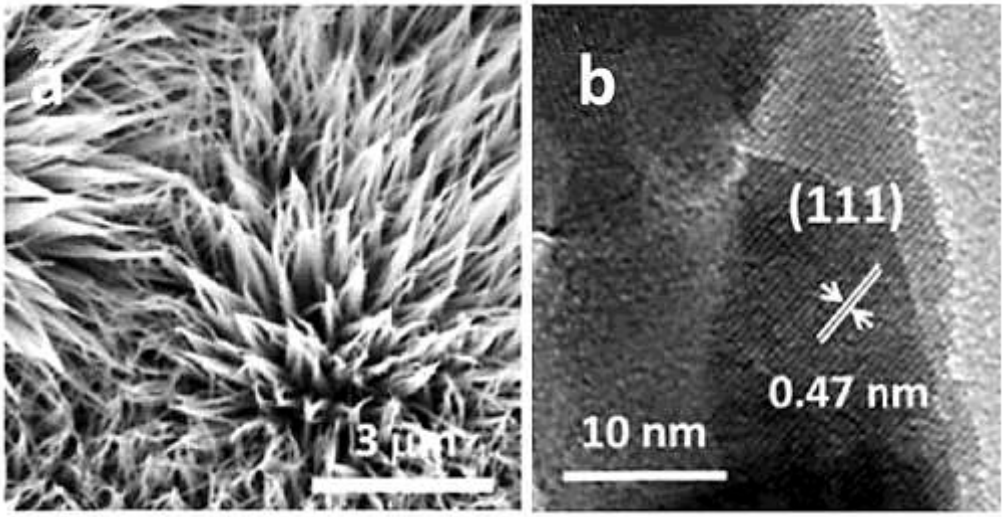

Figure 6.10. SEM (a) and HRTEM (b) image of the Co_3O_4 nano-arrays deposited on honeycomb cordierite. The cordierite was suspended in a Co nitrate aqueous solution, and then treated in urea. From ref. [120].

Similar pictures were obtained with Ni-doped cobalt oxide ($Ni_{0.27}Co_{2.73}O_4$). In spite of a high surface area of these nano-arrays (close to 150 $m^2\ g^{-1}$ after "scratching" from the honeycomb monolith) , activities for propane oxidation are relatively modest (T50 close to 350°C).

The nanocasting route used for Co_3O_4 was extended by Solsona et al. to the fabrication of mesoporous α-Fe_2O_3 for oxidation reaction [121]. The resulting materials were compared to a mesoporous oxide prepared by particle aggregation. This non-ordered oxide (71 $m^2\ g^{-1}$) was shown to be more active than the ordered-mesoporous Fe_2O_3 (208 $m^2\ g^{-1}$) in propane oxidation. The dominant parameter for this reaction would be the redox properties of iron oxide. H2-TPR of Fe_2O_3 shows two main peaks, at 300-370°C ($Fe_2O_3 \rightarrow Fe_3O_4$) and at 400-600°C ($Fe_3O_4 \rightarrow FeO \rightarrow Fe^0$). The non-ordered iron oxide reduces at the lowest temperature.

Total oxidation of isobutane was investigated by Almukhlifi and Burns on a variety of oxides [122] and ceria-supported oxide catalysts (doped or not with gold) [123]. β-MnO_2, α-Fe_2O_3, Co_3O_4 and NiO are active for the complete oxidation of *i*-C_4H_{10}. Cobalt oxide is the most active catalysts which can be ranked according to their T50 : Co_3O_4 (218°C) > β-MnO_2 (233°C) > α-Fe_2O_3 (345°C). Reaction on NiO starts at low temperature but, compared to other oxides, *i*-C_4H_{10} conversion increases slowly with the temperature (T50 = 319°C). Full conversion is not reached before 450°C on NiO compared to 220°C on Co_3O_4 [122]. High surface area ceria is a good support for these oxides. Ceria has a significant oxidation activity when alone and it changes the ranking of the oxides whose activity on ceria becomes: β-MnO_2 > Co_3O_4 > NiO > α-Fe_2O_3 [123].

Alkenes and Alkynes. Certain oxides used as supports (TiO_2, CeO_2) show a relatively good performance in propene oxidation (T50 around 350°C). Cobalt oxides significantly improve the activity of these oxides lowering the light-off temperature down to 210°C. The best catalyst is Co_3O_4/CeO_2 with ethylenediamine added during the impregnation of cobalt nitrate [124]. Oxidation of propene and acetylene was studied by Assebban et al.

on cordierite or clay monoliths coated with Co_3O_4 [125]. Monoliths were coated with cobalt oxide by chemical vapor deposition of cobalt acetylacetonate as precursor. Clay monolith is a better support than cordierite: it possesses a non-negligible intrinsic activity due to a high content of Fe_2O_3 (11%). Acetylene (T50 ≈ 280°C) oxidizes at lower temperature than propene (T50 ≈ 310°C). On clay monolith, cobalt oxide has little impact on acetylene oxidation while it decreases by 35°C the light-off temperature of propene.

Aromatics. *Benzene* combustion was recently investigated over Mn-based mixed oxides: CeO_2-MnO_x composites [126], mesoporous Cu-Mn (221 $m^2\ g^{-1}$) [127], mesoporous CoMnAl oxides prepared from hydrotalcites [128] and $NiMnO_3$-CeO_2 supported on cordierite [129]. In most cases, benzene oxidation starts around 120-140°C with T50 ranging from 180 to 240°C. Best compositions are $Ce_{0.3}Mn_{0.7}$ [126], $Cu_{0.6}Mn$ [127] and $CoMn_2Al$ [128]. A detailed kinetic analysis performed on the $NiMnO_3/CeO_2$/cordierite catalyst reveals that the apparent kinetic order with respect to benzene is close to 0.2 but the MvK mechanism best fits the kinetic results with a reaction rate expression analogous to Eq. 6.4 [129]. All the studies showed that O_2 adsorption and availability for oxidizing adsorbed benzene is a key step of the reaction.

Toluene oxidation was in-depth investigated on oxide catalysts as a model compound for removal of aromatics from gases. $LaMnO_3$ perovskites present interesting properties for the total oxidation of toluene [130,131,132]. Zhang et al. have prepared a series of $LaMnO_3$ by different ways. The perovskite prepared by the citrate sol-gel route (LMO-SG) has the highest BET area (35 $m^2\ g^{-1}$), the highest amount of O_α (desorbing at 250°C) and the best performance in oxidation (1000 ppm TOL in air) with a T50 at 193°C [130]. $LaMnO_3$ may also be supported on TiO_2 or yttrium-stabilized zirconia (YSZ) for a better practical use in dynamic reactor. Again, O adsorption and exchange properties seem to correlate the catalytic activity [131]. Morphological control of $LaMnO_3$ was performed by Wang et al. who succeeded in preparing isolated cubes of perovskites [132]. These cubes (T50 = 170°C) are about ten times more active than porous spherical particles in toluene oxidation. An interesting improvement of the performance of LaMnO3 was realized by eliminating La from the surface layer of $LaMnO_3$. $MnO_2/LaMnO_3$ can thus be prepared which has a much surface area (144 $m^2\ g^{-1}$) than the untreated perovskite (3 $m^2\ g^{-1}$) [133]. The Mn^{4+}/Mn^{3+} ratio and the catalytic activity are also significantly greater than in $LaMnO_3$. Non-perovskitic Mn oxides are also active in oxidation reactions. $Cu_{1.5}Mn_{1.5}O_4$ spinels synthetized via an alginate route are more active than the simple Mn_3O_4 oxide [134]. Total oxidation of toluene is achieved below 240°C, most probably following a MvK mechanism. OMS-2 ($KMn_8O_{16}.nH_2O$) is a tunnel-structured manganese oxide with excellent properties in oxidation reaction. Sun et al. have demonstrated the decisive role of lattice oxygen on the activity of OMS-2 for the total oxidation of toluene [135]. Even in absence of gaseous oxygen, OMS-2 is able to oxidize toluene via benzoyl and benzoate intermediate species (Figure 6.11).

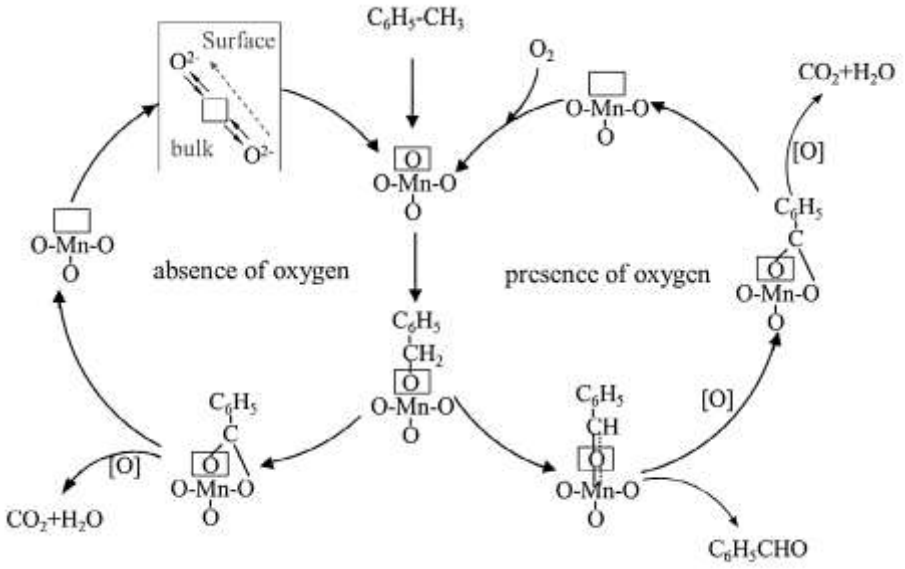

Figure 6.11 Mechanism of toluene oxidation over OMS-2 catalyst. Effect of the presence or not of O_2 in gas phase on the initial steps of reaction. From ref. [135].

Mn oxides are more stable and better dispersed when they are deposited on adequate supports. Hydroxyapatite $Ca_{10}(PO_4)_6(OH)_2$ was shown to be a good support of MnOx for toluene oxidation [136]. Good performances were obtained with Ca^{2+} enriched apatites and with nitrate precursors of Mn. Although they were less studied than Mn-containing catalysts, cobalt oxides show interesting properties in toluene oxidation. Co_6Al_2HT hydrotalcite-like compounds are excellent precursors of catalysts [137]. There is a good relationship between the surface concentration of Co^{2+}, the oxide reducibility and the catalytic activity, suggesting a MvK mechanism for these Co-catalysts. CoMgAl hydrotalcites were also developed by Pérez et al. who showed that doping these materials by ceria led to very active catalysts [138]. The use of EDTA for chelating Ce before impregnation gives more efficient catalysts. Ce-Co and La-Co mixed oxides were investigated by Carabineiro et al. [139] Mixed oxides prepared by the exotemplating method (using carbon as template) are more active than the solids prepared by evaporation of oxalate precursors. Interestingly, the authors propose a MvK mechanism in which oxygen mobility could be linked to the acidity of oxide, as already proposed by Soylu et al. for zeolite-supported oxides [140]. Copper oxide catalysts were less studied than those based on Mn and Co. The investigation of the reaction network performed by Menon et al. in 2011 deserves citation [141]. The reaction was studied by TAP using labeled molecules (^{13}C, D and ^{18}O). The MvK mechanism was confirmed (preliminary formation of $C^{16}O_2$ upon a pulse of C_6H_5-CH_3/$^{18}O_2$) together with a deep insight into the reaction intermediates. More recently, Zabihi et al. have compared the total oxidation of toluene and cyclohexane over Cu-Co mixed oxides supported on carbons [142]. Cu-Co oxide alloys are slightly more active than CuO covered with CoO or the reverse, CoO covered with CuO. Copper oxides supported on ceria-alumina supports were also used to oxidize *p*-xylene and xylene-CO mixtures [143]. Interestingly, these authors showed that small amounts of xylene can inhibit CO oxidation. This is due to competitive adsorption phenomenon but also to formation of new intermediates of reaction in the simultaneous oxidation of xylene and CO.

Naphthalene is generally chosen as model compound of bicyclic aromatics and, more generally, of PAH, polycyclic aromatic hydrocarbons. The following order of reactivity was reported by Garcia et al.: CeO_2 > MnOx > CoOx > CuOx > Fe_2O_3 [144]. These authors have compared the performances of various oxides for propane and naphthalene oxidation (Table 6.1)

Table 6.1. Total oxidation of propane and naphthalene over various oxides. T_{90} is the temperature for a 90% conversion of hydrocarbon. All the oxides are prepared by precipitation of nitrates by sodium carbonate, except CeO_2-U which is prepared by urea precipitation. Reaction conditions: 0.5 % C_3H_8 in air (propane) at a gas hourly space velocity (GHSV) of 15000 h^{-1} or 100 vpm $C_{10}H_8$ in air (naphthalene) at a GHSV of 60000 h^{-1}. Adapted from ref. [144].

Oxide	BET area (m^2 g^{-1})	Main phase	T_{90} Propane (°C)	T_{90} Naphthalene (°C)
Al_2O_3	180	γ-Al_2O_3	-	38% conv. @ 350
CeO_2	86	CeO_2	-	315
CeO_2-U	171	CeO_2	360	210
CoOx	69	Co_3O_4	180	270
CuOx	20	CuO	350	270
CuOx-ZnOx	29	CuO, ZnO	335	250
Fe_2O_3	51	Fe_2O_3 (haematite)	-	295
MnOx	76	Mn_2O_3	320	240
TiO_2	50	Anatase + rutile	-	66% conv. @ 350
ZnO	19	ZnO	-	335

Except CoOx, the oxides investigated by Garcia et al. are more active for naphthalene than for propane oxidation. Worthy of note is the behavior of CeO_2-U much more active than the solid prepared by sodium carbonate precipitation. The factor 2 on the BET area is obviously not the only reason of the superiority of CeO_2-U. A detailed study performed on CeO_2-U showed that activity of this oxide was clearly related to the number of surface defects measured by the full width at half maximum of the Raman band at 464 cm^{-1} [145]. Mesoporous cerias prepared by a nanocasting route (using KIT-6 as template) were also tested in naphthalene oxidation [146]. These materials are not more active than the precipitated CeO_2-U but they show excellent stability. Further refinement of the catalysis by ceria includes: shape-selective preparation of ceria (nanocubes, nanorods, nanoparticles) [147] and addition of copper [148]. Ceria nanoparticles are more active than nanocubes and nanorods, in line with the higher concentration of surface defects in the materials [147]. Copper is a good promoter of ceria for naphthalene oxidation. Optimum is obtained for the composition $Ce_{0.984}Cu_{0.016}O_X$; the intrinsic activity at 200°C (per m^2) is then 20 times greater than that of pure ceria [148].

6.5.2. Oxygenates

Oxides may be good oxidation catalysts for oxygenated VOC, still better than for hydrocarbons. However, significant amounts of intermediates (most often, other oxygenates) are currently observed before complete oxidation [149]. Moreover, the reactivity depends very much on the chemical structure, ethers and esters being generally more difficult to oxidize than alcohols, aldehydes and ketones of the same number of carbons [23,150]. Assebban et al. have compared the reactivity of VOCs, including hydrocarbons, oxygenates and chlorinated compounds, on an extruded clay honeycomb monolith [151]. The chemical composition of the clay is SiO_2 (58.50 wt.%), Al_2O_3 (23.90%), Fe_2O_3 (11.11%), K_2O (2.29%), MgO (1.55%), Na_2O (1.46%), TiO_2 (0.63%),

CaO (0.22%), ZrO_2 (0.02%), and MnO_2 (0.02%). Iron oxide is the active compound of the clay for oxidation reactions. The light-off temperatures recorded for the VOC studied by Assebban et al. are reported in Table 6.2

Table 6.2. Reactivity of various VOC compounds on a extruded clay honeycomb monolith (11.1 % Fe_2O_3). Reaction conditions: 1% VOC + 10%O_2 at a GHSV (gas hourly space velocity) of 2300 h^{-1} with respect to the volume of monolith. Variable amounts of CO are observed in addition to CO2 for all the VOC. Aldehydes are the main reaction intermediate of alcohol oxidation (formaldehyde, acetaldehyde, propanal, butanal in oxidation of methanol, ethanol, propanol, butanol, respectively). From ref. [151].

VOC compounds (CO & HC)	T50 (°C)	VOC compounds (Oxygenates & Cl-compounds)	T50 (°C)
CO	295	Methanol	261
Methane	512	Ethanol	272
Propane	420	n-Propanol	271
Propene	355	n-Butanol	278
Acetylene	299	Acetone	228
Benzene	345	Dimethylether (DME)	286
Toluene	329	Chlorobenzene	395
o-Xylene	321	1,2-Dichlorobenzene	414

The reactivity sequence on iron oxides of the clay mineral was found to be as follows: ketone > alcohol > ether > CO > alkyne > aromatic > alkene > chlorinated aromatic > alkane. As iron oxide is not the most active catalyst for VOC oxidation, T50 of the clay are shifted to higher temperatures if compared to Mn or Co oxides. However, it is confirmed that the reactivity of oxygenates is higher than that of any hydrocarbons, saturated or not.

Acetone. Among the oxygenates, appears as very reactive with a T50 of 228°C, that is 33°C lower than the light-off temperature of the alcohols tested by Assebban et al. [151]. Acetone combustion was studied over spinels ($CuFe_2O_4$, $MgFe_2O_4$, $Ni_{0.5}Co_{0.5}Fe_2O_4$) and perovskites catalysts ($SrMnO_3$, $FeMnO_3$, $La_{0.6}Pb_{0.2}Ca_{0.2}MnO_3$) by Rezlescu et al.[152]. $SrMnO_3$ (2.2 m^2 g^{-1}) is the most active catalyst with T50 at 185°C. Presence of ceria in the materials allows obtaining very good performances for acetone oxidation. M-Ce/Al-SiO2 composites (M = Mn, Co, Cu, Ni, Fe) were developed by Lin and Bai [153] while Qin et al. focused their attention on CuCeOx nanofibers prepared by an electrospinning method [154]. In every case, cerium ions play a decisive role by creating numerous O vacancies in the materials. Light-off temperatures are below 200°C with an exceptional behavior of the $Mn_{0.5}Ce_{0.5}O_x$/Al-SiO_2 catalyst of Lin and Bai (T50 = 110°C).

Ethanol. In the last decades, great efforts were made to produce hydrogen by ethanol steam reforming [155]. The reaction being endothermic, the most practical way is to heat the reformer by combustion of ethanol. Steam reforming or oxidation of ethanol can lead to ethylene, acetaldehyde and acetone as intermediates [156]. Total oxidation thus requires a good performance of the catalysts for alkene, aldehyde and ketone oxidation. Acetaldehyde is the main oxidation intermediate on basic oxides such as ceria [157]. Minor amounts of acetic acid and ethyl acetate are also observed. Total conversion of ethanol is reached on ceria nanorods at 235°C but complete selectivity to CO_2 requires much higher temperatures to oxidize all the intermediates, acetic acid being the most refractory compound. Mn-based oxides are more active catalysts for ethanol oxidation. Nanorods (1D-MnO_2) and mesostructured MnO_2 using SBA-15 (2D-MnO_2) or KIT-6 (3D-MnO_2) as templates were synthetized by Bai et al. [158]. These materials were tested in ethanol and acetaldehyde oxidation. The turnover frequency per mol of Mn^{4+} was the highest for 3D-MnO2 (0.17 h^{-1} at 110◦C instead of 0.14 h-1 for 2D-

MnO2 and only 0.03 h-1 for 1D-MnO2). This is clearly linked to the higher reducibility and to more surface adsorbed oxygen species and Mn^{4+} ions on 3D-MnO_2 [158]. Ethanol oxidation was also investigated over Mn-cryptomelane OMS-2 [159,160]. Cryptomelanes KMn_8O_{16} prepared by a sol-gel technique ($KMnO_4$ in fumaric acid) or by a reflux method ($KMnO_4$ added to a boiling solution of Mn acetate in acetic acid) show the best performance in ethanol oxidation (T50 at 120°C) [159]. Sulfate-doped OMS-2 are more active than undoped catalysts. A suitable amount of SO_4^{2-} species into the OMS-2 catalyst could decrease the Mn-O bond strength and also enhance the lattice oxygen concentration and number of acid sites, which then effectively promoted the catalytic activity of OMS-2 [160]. Co-Mn-Al mixed oxides of spinel structure were prepared by Kovanda et al. by calcination of layered double hydroxides (LDH) precursors deposited on anodized aluminum [161].They are more active in ethanol oxidation (T50 = 123 °C) than mixed oxides formed from coprecipitated salts (T50 ranging from 150 to 190°C). However, acetaldehyde being less oxidizable than ethanol, there is a shift between the light-off temperature of ethanol consumption and the T50 observed on the production of CO_2. The preparation by calcination of LDH was extended by Jirátová et al. to different mixed oxides containing Mn, Co, Cu and Ni [162]. Catalysts containing Mn are very active with T50 below 150°C. The best system was a ternary oxides containing Cu-Ni-Mn. Addition of Ni to a perovskite $LaMnO_3$ is also an excellent way to improve the performance of the perovskite $LaMnO_3$ [163]. The optimum is reached for the perovskite $LaMn_{0.9}Ni_{0.1}O_3$ which converts ethanol and acetaldehyde at the lowest temperature. Incorporating Ni generates Ni–O–Mn sites, assumed to play a key role in enhancing catalytic activity. Very few studies were devoted to Mn-free catalysts. $CoFe_2O_4$ spinels (119 $m^2\ g^{-1}$) were investigated by Hammiche-Bellal et al. with good performance above 200°C [164]. It is necessary to reach 300°C to avoid formation of acetaldehyde and acetic acid. Motak et al. have studied ethanol oxidation (1000 ppm) in the presence of NOx (500 ppm) over clays minerals (vermicullite, bentonite or montmorillonite) doped with copper or silver [165]. Relatively high temperatures (> 350°C) are required to reach a 50% conversion. Ag-doped clays give better performances than those doped with Cu. They are also less sensitive to the presence of NOx.

Ethyl acetate. Oxidation of this compound was investigated as a model of esters and also because it is widely used in industry as solvent. Copper-ceria or cobalt-ceria oxides are quite effective catalysts for ethyl acetate abatement below 200°C [166,167]. Cu-Ce oxides were supported on SBA-15 or KIT-6 by Tsoncheva et al. to give catalysts of 600-700 $m^2\ g^{-1}$ (SBA-15) or 300-500 $m^2\ g^{-1}$ (KIT-6) but Cu-Ce/KIT-6 are more active than Cu-Ce on SBA-15 [166]. Unsupported oxides were prepared by Chen et al. by an exotemplating or an evaporation method [167]. Catalytic activity seems linked to the onset temperature of reduction suggesting that a MvK mechanism is taking place [167]. The Cu/Ce or the Co/Ce ratio of 1 gives the best performances (467 ppm ethyl acetate in air, GHSV of 53 000 h^{-1}) with virtually no production of CO. Iron oxides may be used for ethyl acetate oxidation provided that iron be stabilized by another oxide. In this respect, Tsoncheva et al. have developed a new catalytic system based on iron modified titanium–hafnium binary oxides [168]. Small amount of Hf in titania (typically 1.8%) facilitates the formation of substituted $Fe_xTi_{1-x}O_2$ and finely dispersed hematite particles. In spite of the low Fe loading (0.14%), light-off temperature of 300°C can be obtained with these catalysts (1.2% EA in air). Ethyl acetate being generally mixed with hydrocarbons in air, several studies were devoted to purification of VOC comprising ethyl acetate and toluene (oxidized separately or mixed together) [169,170,171].

In most cases, toluene is converted at higher temperatures than ethyl acetate, but with a better selectivity to CO_2. The Cu-Ce system gives excellent performances, with a significant effect of the support: SBA-15 [169] or ZSM-5 [171]. MnMgOx oxides prepared by autocombustion are a good alternative to CuCeOx oxides [170]. Interestingly, these catalysts were compared to a 1%Pt-Al_2O_3, a reference noble metal catalyst for VOC abatement. It was shown that Pt is a better catalyst for toluene oxidation but less good than MnMgOx for ethyl acetate oxidation, which confirms the superiority of oxide catalysts (with respect to noble metals) for ester oxidation. Oxidation of ethyl acetate and n-hexane was studied by Tang et al. over Mn-Co oxide nanorods (105 $m^2\ g^{-1}$) [172]. Hexane being more reactive than toluene, the ester and the hydrocarbon are oxidized at the same temperature (190-210°C) and total oxidation is achieved below 230°C.

Other oxygenates. Formaldehyde is a toxic VOC emitted indoor by resins and glues of furniture and floor coverings. Most active catalysts can oxidize formaldehyde at room temperature but they contain generally noble metals. Attempts at replacing noble metals by transition metal oxides were made recently. Cobalt oxide encapsulated in cyclodextrin is a promising catalyst based on Co^{3+}/Co^{2+} redox sites [173]. Nevertheless, temperatures close to 170°C are required for a good oxidation activity. Nanosheets of $NiCo_2O_4$ spinels doped with NaOH (48-71 $m^2\ g^{-1}$) are more active since they are able to convert formaldehyde at room temperature while total oxidation is achieved over untreated $NiCoO_4$ at 150°C only [174]. Mn-substituted ferrites (general formula: $Fe_{3-x}Mn_x)_{1-\delta}V_{3\delta}O_4$, V being a vacant position of the spinel ferrite) are a good alternative to noble metal catalysts but the best catalysts (x=0.1) has a T50 of 126°C and requires temperatures close to 200°C for a complete conversion of HCHO [175]. Total oxidation of isopropanol was also investigated, in most case over Mn-based catalysts [176], sometimes assisted by plasma discharge to get oxidation at room temperature [177]. Though oxidation of acetic acid in water was extensively studied by wet air oxidation techniques [178], oxidation of acetic acid in gas phase was more rarely studied. Melang Me Nze et al. have investigated this reaction over MgAlCe mixed oxides [179]. Cooperation between redox sites for O_2 activation and basic sites for CH_3COOH adsorption is beneficial to catalytic activity. However, strength of basic sites should be moderated to avoid carbonate formation and catalyst deactivation.

6.6. Oxidation of chlorine- and sulfur-containing compounds

6.6.1. **Chlorinated VOCs**

Chlorinated compounds are toxic VOCs. They also contribute to the depletion of the ozone layer. Therefore, drastic rules regulate their use, some of them (CFC, chloroflurorocarbons) being prohibited. Several reviews or book chapters were devoted to the oxidation of chlorinated hydrocarbons by the group of Bilbao [180,181] while the specific use of zeolites for the abatement of persistent organic pollutants (including PCDD/Fs, polychlorinated dibenzo-dioxins/furans) was reviewed by Marie-Rose et al. [182]. Only the most recent works on some chlorinated hydrocarbons (methane, ethane, ethylene, benzene) will be reviewed.

Dichloromethane (DCM). The oxidative dechloration of DCM can lead to the following reactions:

$$CH_2Cl_2 + O_2 \rightarrow CO_2 + 2HCl \quad (6.8)$$

$$CH_2Cl_2 + 3/2\ O_2 \rightarrow CO_2 + Cl_2 + H_2O \quad (6.9)$$

Hydrochloric acid is the desired product since it can be easily eliminated by washing of the gases with alkaline solutions. Chlorine may be formed directly by Cl recombination or by the Deacon reaction (Eq. 6.10):

$$2HCl + ½\ O_2 \rightarrow Cl_2 + H_2O \quad (6.10)$$

Formaldehyde and formic acid may also be produced by DCM hydrolysis over acid sites (Eq. 6.11):

$$CH_2Cl_2 + H_2O \rightarrow HCHO + 2HCl \quad (6.11)$$

Total oxidation of DCM (1000 ppm in 10%O_2) was investigated over CeOx-doped titania by Cao et al. [183]. Titania has Lewis acid sites responsible for the adsorption and the rupture of C–Cl bonds. But titania is rapidly poisoned by accumulation of chlorinated species. The role of ceria would be to allow a fast desorption of Cl species (as Cl_2 or HCl). The reaction starts below 200°C and total conversion of DCM is achieved at 350°C. Significant amounts of reaction intermediates are observed in the 200-350°C temperature range on undoped titania: CO, CH_3Cl, formic acid, methyl formate,... The presence of ceria drastically reduces the formation of these intermediates.

1,2-Dichloroethane (DCE). DCE oxidation was studied by Yang et al. over CeO2-CrOx mixed oxides supported on carbon [184]. They showed that CeCrOx catalysts could be improved by supporting them over certain acidic supports [185]. Niobia gives the best promotion: the intrinsic activity is slightly higher and is associated with a better selectivity to HCl. DCE oxidation can also give rise to the formation of chloroethylene C_2H_3Cl which is significantly reduced over CeCrOx/Nb_2O_5 than on unsupported CeCrOx. The promotion of the catalysts by niobia is linked to the increase of Ce^{3+} and Cr^{6+} species at the surface of CeCrOx. The simple association of ceria with zeolitic support may give good performances in DCE oxidation. De Rivas showed that impregnation of H-ZSM5 with cerium (III) nitrate in ethanol gives a solid able to totally oxidize DCE below 250°C (T50 = 195°C) [186]. Al-substituted $LaMnO_3$ perovskites were also studied for DCE oxidation [187]. The most active system is $Al_{0.2}La_{0.8}MnO_3$ with a T50 of 295°C (1000ppm DCE in wet air, VVH of 20000 h^{-1}). Surface analysis revealed that the optimal catalyst has the highest $Mn^{4+}/(Mn^{3+}+Mn^{4+})$ ratio.

Cobalt-based catalysts were also developed for DCE oxidation by the Group of Bilbao [188,189]. Co_3O_4 supported on Ca-deficient hydroxyapatite are active for DCE oxidation but high selectivity to CO2 requires a high cobalt loading [188]. Catalysts with low-loading of cobalt tend to form CO and vinylchloride. SBA-15 is also a good support of cobalt with T50 around 330°C [189]. Cobalt oxide loadings higher than 30 wt% present an adequate activity for the deep DCE oxidation. An optimum equilibrium between acidic properties (weak Brønsted acidity of the silica support and Lewis acidity of the cobalt oxide particles) and redox properties should be reached in order to favour HCl formation.

Trichloroethylene (TCE). Oxidation of TCE was studied by Yang et al. over ceria-MOx mixed oxides with a Ce/M ratio of 4 (M = V, Cr, Mn, Fe, Co, Ni and Cu) [190]. CeO_2-CrOx and CeO_2-CuO are the most active catalysts for TCE oxidation. Final chlorinated products are HCl and Cl_2. Tetrachloroethylene (C_2Cl_4) is an intermediate of reaction. However CeO_2-CrOx has the highest selectivity to HCl and the lowest to Cl_2 and C_2Cl_4, which makes this catalyst more attractive for Cl-VOC abatement. BEA zeolite is a good support of Cu and Co for TCE oxidation [191]. Catalysts prepared by ion exchange of the zeolite beta give the best performance and Cu-BEA is much

more active than Co-BEA. When Cu or Co salt are incorporated during the zeolite synthesis, activity are relatively modest, probably because this method tends to produce non-acidic catalysts. As for many VOC compounds, association of plasma and catalysis is a good way to oxidize TCE at low temperature [192,193]. However, the control of selectivity is not total (a lot of CO may be produced) and the nature of the oxidant species (ozone, oxygen reactive species, NO issuing from air, ...) is not clarified.

6.6.2. **Sulfur compounds**

Oxidation of sulfur compounds (SVOC) has not been as much studied as that of other VOC. Partial oxidation by H_2O_2 or hydroperoxides can be used to transform organic sulfides of gasoils or gasolines into oxidized products (sulfoxides, sulfones) more easily eliminated by extraction. This process is known as "Oxidative desulfurization process" (ODP) developed for the ultimate purification of gasoline or gasoils [194,195]. H2O2 or hydroperoxides being expensive, attempts were made to oxidize sulfur compounds directly by O_2 [196]. Elimination of the SOx produced in SCOV oxidation is not a facile task. It is advantageous to produce selectively SO_2 instead of SO_3 which tends to form sulfuric acid in the presence of moisture. Another problem with SVOC is their strong odor at the ppb level, which imposes a severe elimination very close to 100%. While there are numerous reviews on VOC abatement, very few of them deal with the treatment of SVOC. In this respect, the review by Ojala et al. deserves special attention [197]. Methyl mercaptan CH_3S (MM), dimethyl sulfide CH_3-S-CH_3 (DMS), dimethyl disulfide CH_3-S-S-CH_3 (DMDS), thiophene C_4H_4S (T), benzothiophene C_8H_6S (BT) or dibenzothiophene $C_8H_{12}S$ (DBT) were generally taken as model compounds of SVOC. DMS is the major product of SCOV present in atmosphere. It can be oxidized by OH radicals according to the following sequence of reactions (eq. 6.12 and eq. 6.13) [198]:

$$OH + CH_3SCH_3 \rightarrow CH_3S(OH)CH_3 \quad (6.12)$$

$$CH_3S(OH)CH_3 + O2 \rightarrow \text{products (COx, SOx, H2O)} \quad (6.13)$$

Catalytic ozonation of dimethyl sulfide and other VOC was investigated by Devulapelli and Sahle-Demessie over CuO-MoO_3 [199] or V_2O_5-TiO_2 catalysts [200] and, more recently, by Chand Soni et al. over Fe/ZrO2 catalysts [201]. H_2O does not affect SVOC conversion [200]. Ozone acts as a strong Lewis base having a great affinity with O vacancies of Fe_2O_3-ZrO_2 [201]. It is supposed that Fe^{3+}-O-Zr^{4+} structures are formed, very active in the C-S bond splitting. A possible mechanism is depicted in Figure 6.12.

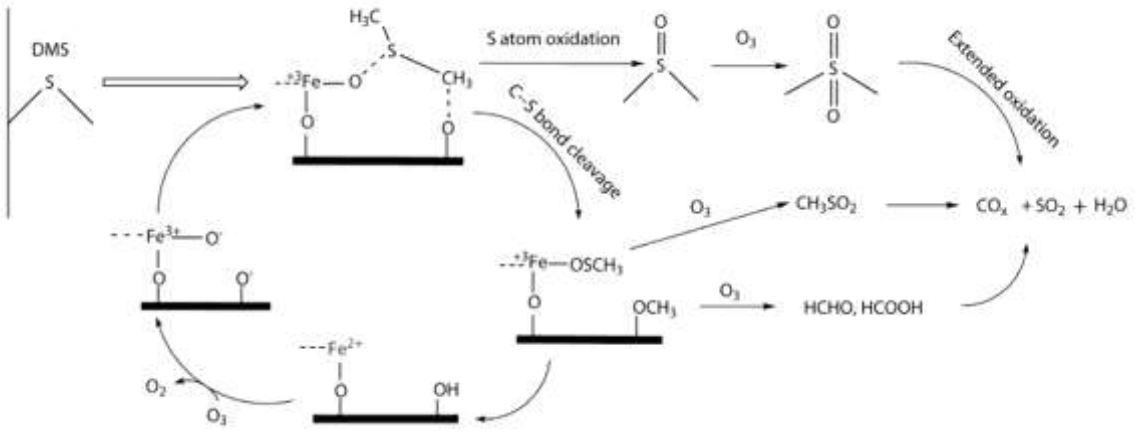

Figure 6.12. Possible reaction mechanism for the catalytic oxidation of DMS in presence of ozone over Fe catalysts. Taken from ref. [201].

Adsorption of SVOC on oxides of high oxidation state can lead to partial oxidation. DMS and ethyl mercaptan can thus be treated over MnO_2 [202]. A further desorption in oxidative medium can lead to total oxidation products.

6.7. Oxidation of automotive soots

Automotive converters were implanted in Europe after 1990. The first regulation for soot particle emissions (EURO 1) specified that Diesel cars could not emit more than 140 mg particles/km. Drastic improvements of the Diesel engines such as direct injection at very high pressure allow the car makers to meet the European standards up to 2008. EURO 4 imposing less than 5 mg/km after 2009, followed by EURO 5 and 6 restricting the emissions at 4.5 mg/km, could not be respected by the most sophisticated, modern engines which emitted 20-30 mg particles in the best conditions. It was then necessary to implement Diesel particulates filters (DPF) on Diesel cars. These filters should be regenerated to avoid anomalous pressure drops in the exhaust pipe and defective engine operation. This involves burning the soots regularly, in the presence of a catalyst to lower the ignition temperature. The catalyst may be added to the fuel (fuel-borne catalyst, some ppm of a Ce or a Fe compound) or wash-coated on the filter walls. Catalysts added to the filter are generally composed of noble metals (mainly Pt). However, a great number of studies have been made to replace these NPs by oxide catalysts, much less expensive. Most studies are carried out by mixing carbon powder representative of soots with the catalysts. The catalytic activity is evaluated by a temperature-programmed oxidation in air. Single oxides were first evaluated. The study of Neeft et al. gives a good overview of the performance of 14 oxides and 4 alkali metal carbonates [203]. The main results of this study (Table 6.3) are: (i) Co_3O_4 is a very performing oxide, combining high combustion rate and quasi-total selectivity to CO_2 (ii) oxides commonly used in oxidation may be ranked as follows: Co_3O_4 >> MnO_2 > CuO > Fe_2O_3 > Cr_2O_3 ; (iii) alkali metal carbonates are excellent combustion agents, their activity increasing with the basicity (Cs > K > Na > Li).

Table 6.3 Combustion rates at 60% conversion of carbon and mean CO_2/CO ratio in the 40-80% range of conversion. Tight contact between carbon (U-printex Degussa) and catalyst (ratio 1:1). Measurements are made at 383°C for oxides and 279°C for carbonates. From ref [203].

Oxide	Reaction rate @ 383°C ($\mu g\ g_{carbon\ initial}^{-1}\ s^{-1}$)	Mean CO_2/CO ratio	Carbonate	Reaction rate @ 279°C ($\mu g\ g_{carbon\ initial}^{-1}\ s^{-1}$)	Mean CO_2/CO ratio
PbO	> 240	20	Cs_2CO_3	182	15
Co_3O_4	233	500	K_2CO_3	101	14
V_2O_5	203	6	Na_2CO_3	65	18
Ag_2O	95	15	Li_2CO_3	6	17
MoO_3	66	5	none	0.003	*nd*
CuO	27	6			
Bi_2O_3	22	8			
MnO_2	21	150			
Sb_2O_3	20	8			
CaO	16	7			
La_2O_3	13	8			
Cr_2O_3	12	3			
Fe_2O_3	7	6			
NiO	1	5			
none	0.9	2			

Promotion of oxides (Mn, Fe, Co) by potassium was investigated by Jakubek et al. who showed that the promotion is due to the formation of bulk compounds between K and metal oxides [204]. This also allows formation of tunneled or layered structures, which enable very high potassium mobility. Another classical feature of the soot combustion is the specific reactivity of NO_2/O_2 mixtures allowing oxidation at much lower temperature than in O_2 alone. This effect was studied in detail by Wasalathanthri et al. over mesoporous Mn oxides [205]. NO_2 allows decreasing the ignition temperature and is particularly efficient on the less active oxides: while T50 in O_2 varies between 300 and 400°C for the different Mn oxides, oxidation profiles are much closer with T50 varying from 270 to 300°C in NO_2+O_2 mixtures.

To-day, there is a so huge flow of publications mixtures.ver mixed oxides that it is not possible to be exhaustive. As several recent reviews were published on the subject, analysis of the literature will be restricted to the very most recent publications. Mixed oxide catalysts used in DPF are most often made of perovskites, of spinels or of cerium-based oxides (other than perovskites).

Perovskites for soot combustion. The use of perovskites for soot combustion was reviewed by Royer et al. [23], Mishra and Prasad [206] and Labhasetwar et al. [207]. Co_3O_4 being one of the most active oxide, Co-based perovskites were widely investigated. Sun et al. have synthetized core–shell Co NPs socketed on oxygen-deficient layered perovskite composed of $Pr_{0.5}Ba_{0.5}MnO_3$ (PBMO) partially substituted with cobalt [208]. The PBMO perovskite was impregnated with 10%Co and treated in H2 at 500-850°C. Part of Mn substitutes for Co (PBMCo) while Co° nanoparticles are formed at the surface of the layered perovskite. The system is very active for soot combustion with T50 below 460°C. PBMCo acts as O donor (superoxides species) which are spillovered to Co NP. During soot combustion, CoNP are covered by a layer of Co oxide, forming probably the active sites of oxidation. Lee et al. have prepared nanofibers of $La_{1-x}Sr_xCo_{0.2}Fe_{0.8}O_{3-\delta}$ perovskite by electrospinning, which increases the high-contact area by trapping soot in the unique pore structure of the fibers [209]. Temperatures

of soot oxidation are shifted down of 30-40°C with respect to a bulk perovskite of the same composition. Alkali metals being good promoters of soot oxidation, K promotion of Mg-substituted $La_{0.8}Ce_{0.2}CoO_3$(LCCM) perovskite was investigated by Wang et al. [210] while Shao et al. focused their attention on the promotion of $LaCoO_3$ by Cs [211]. 10%K added to Mg-LCCM shift down the temperature of maximal rate of combustion from 450 to 380°C [210]. Comparatively, promotion of $LaCoO_3$ by Cs seems modest and more marked in $NO+O_2$ ($\Delta T50$ = 19°C) than in O_2 ($\Delta T50$ = 9°C), which suggests that the alkali metal has a strong effect on NO activation [211]. In fact, Cs rather inhibits NO oxidation but significantly increases NOx adsorption. Silver can also be used as a promoter of soot oxidation. Dinamarca et al. have shown that the temperature of the maximal oxidation rate was shifted from 458°C for $LaMn_{0.9}Co_{0.1}O_3$ to 371°C for $La_{0.7}Ag_{0.3}Mn_{0.9}Co_{0.1}O_3$ perovskite [212].

Spinels and other structures. Spinel chromites were investigated for soot combustion. Wang et al. have prepared three-dimensionally ordered macroporous (3DOM) spinel-type MCr_2O_4 (M = Co, Ni, Zn, Mn) catalysts by a citrate route in the presence of polymethyl methacrylate (PMMA) microspheres [213]. After dissolution of PMMA microspheres, open structures of 3DOM spinel are formed that allows a good contact of carbon soots with the catalyst and a higher oxidation rate (Figure 6.13).

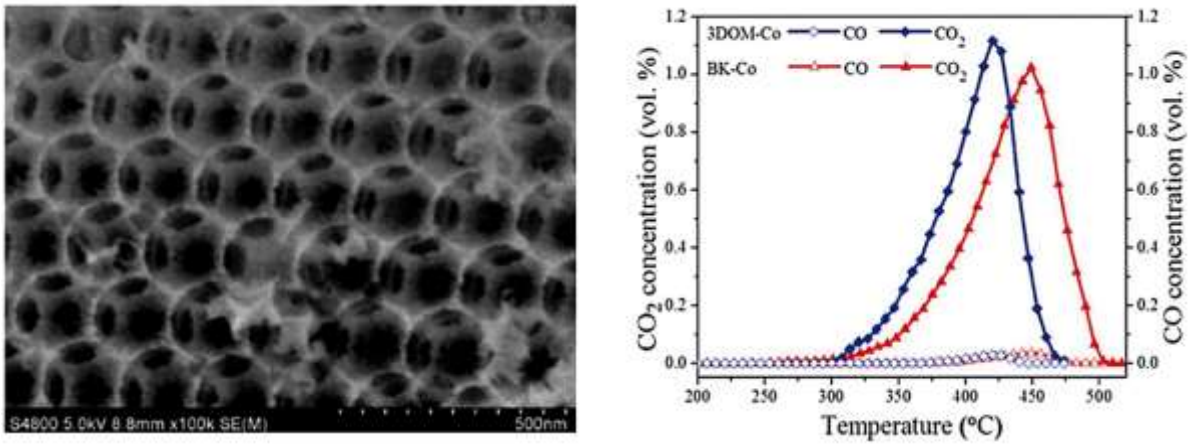

Figure 6.13. SEM image of 3D-$CoCr_2O_4$ spinel (left) and soot oxidation on this catalyst (right). The 3DOM $CoCr_2O_4$ catalyst (3DOM-Co, 40 $m^2\ g^{-1}$) is prepared using monodisperse polymethyl methacrylate (PMMA) microspheres with an average size of 360 nm as the colloidal crystal template. For the soot oxidation (5%O_2+2500ppm NO), 100mg of catalyst is intimately mixed with 10mg of soot (MA100 Mitsubishi); temperature ramp of 2°C min^{-1}. Oxidation profile of BK-Co (bulk $CoCr_2O_4$, 62 $m^2\ g^{-1}$) is given for comparison. From ref. [213].

Chromite of cobalt can also be improved by substituting a part of the cobalt by cerium. Niu et al. have shown that mesoporous $Ce_{0.1}Co_{0.9}Cr_2O_4$ spinels (165 $m^2\ g^{-1}$) were much more active than the non-substituted $CoCr_2O_4$ spinel with a decrease of the oxidation temperature of soot of 59°C [214]. Pyrochlores are also promising catalysts for soot oxidation. Wang investigated $Ln_2Sn_2O_7$ pyrochlores (Ln = La, Nd and Sm) and showed that $La_2Sn_2O_7$ possessed the most interesting properties [215]. However, these materials seemed not better than the perovskites and spinels reviewed above.

Ceria-based catalysts. A considerable number of studies were published on these catalysts probably because cerium species were originally used as fuel-borne catalyst, which prompted authors to consider that small amounts of cerium oxides could be very active for soot combustion. Moreover, the extraordinary redox

properties of ceria-based oxides allowed to imagine that O transfer from gaseous phase to soot could be facilitated on these materials [216]. Ceria-based catalysts for soot oxidation were reviewed by Bueno-López in 2014 [217] and by Montini et al. in 2016 [218]. Accordingly, only papers published after this date will be examined. Voskanyan et al. have prepared mesoporous ceria by utilizing colloidal SiO_2 as a template [219]. The procedure is similar to the one used by Wang et al. [213] illustrated in Figure 6.7A, except that PMMA polymer microspheres are replaced by colloidal silica nanoparticles of about 20 nm. A shift of 70°C on the temperature of soot oxidation was observed on the mesoporous ceria with respect to a conventional sol-gel ceria. The role of ceria morphology (nanorods, nanocubes,…) was investigated by Aneggi et al. [220] et by Zhang et al. [221]. Aneggi et al. conclude that higher activity is observed over nanocubes and nanorods as compared with polycrystalline ceria octahedral particles [220]. Thermal aging at T> 500°C markedly affects the crystal shape by truncation of the edges and corners (Figure 6.14). Finally thermal aging tends to give materials having similar soot oxidation activity.

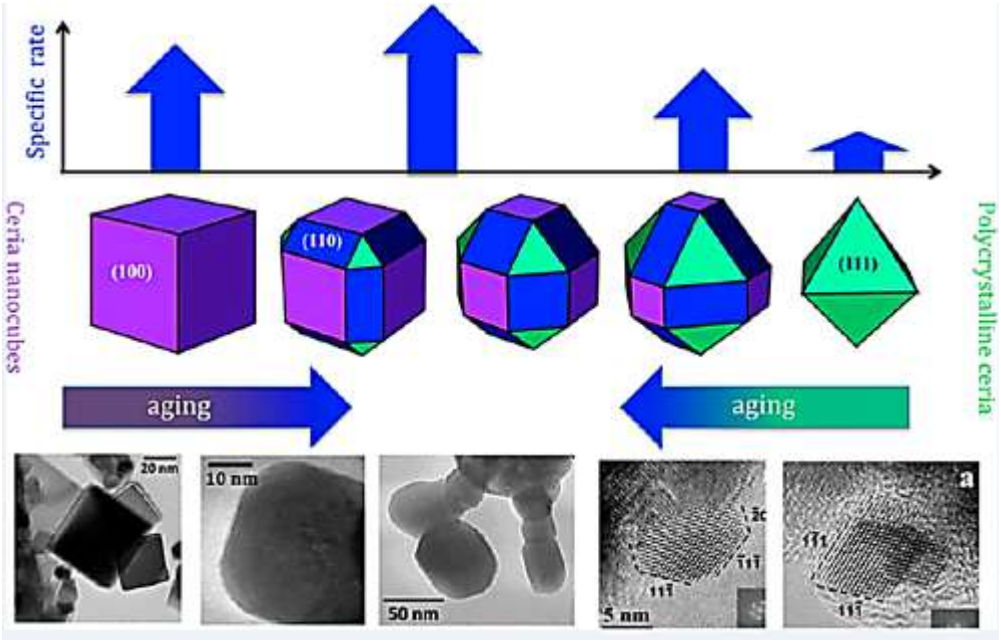

Figure 6.14 Role of crystal shape of ceria on the relative rate of soot oxidation. Nanocubes and nanorods are initially more active. But thermal aging creates edge and corners on polycrystalline particles, which tends to make them similar to cubes and rods in term of catalytic activity. From ref. [220].

Similar conclusions were reported by Zhang et al. with a very good activity of nanorods, compared to nanoparticles and nanoflakes [221]. The intimate mechanism of soot oxidation was investigated by means of ambient pressure photoemission spectroscopy [222]. It appears that carbon is consumed in two cooperative steps: (i) reaction of O_2 at the ceria-soot interface forming O vacancies and reduced Ce(III) species; (ii) direct reaction of O_2 on soot by active superoxides species which result from the reaction of gaseous O_2 on O vacancies. This result is in line with the formation of Ce_6O_{11} nanodomains during soot combustion [223]. There is strong indication that the contact between ceria or ceria-ziconia and soot plays a decisive role on carbon oxidation. Aneggi et al. demonstrated that a 2D layer of carbon wrapping CeZrOx particles could be oxidized at very low temperature (onset oxidation at 70-100°c and maximum rate between 250 and 270°C) [224]. Activity

of ceria can be improved by addition of praseodymium, $Ce_{0.5}Pr_{0.5}O_2$ being more active than ceria [225] or $Ce_{0.5}Zr_{0.5}O_2$ catalysts [226]. Combining Pr and Zr in $Ce_{0.8}Zr_{0.1}Pr_{0.1}$ is also a possibility to improve activity of pure ceria [227]. Finally, addition of Fe [228] or Cu [229,230] can give promising performances in soot oxidation, particularly in $NO+O_2$.

6.8. Nitrogen-containing compounds

Nitrogen compounds, including nitrogen oxides (NO and NO_2) and nitrous oxide (N_2O) are currently considered as dangerous air pollutants involved in acid rains, photochemical smog, ozone depletion, greenhouse effect and can have direct harmful effects on human health. Consequently, standards are applicable for major sources of air pollution to limit discharge of nitrogen compounds.

6.8.1. Scope of the section

Worldwide, the selective catalytic reduction (SCR) technology is well established as an emissions control system for stationary and mobile source. Lean NOx trap (LNT), also called NOx storage-reduction (NSR), is another deNOx after-treatment process to control NOx emissions of direct injection gasoline and Diesel engines of vehicles.The NSR (or LNT) system operates in transient conditions. It works mainly in lean condition. NOx are then oxidized on precious metals and stored on basic compounds, mainly as nitrates. Periodically, the catalyst is submitted to rich conditions for a few seconds and the previously stored NOx are reduced into N_2 on the precious metals. To the opposite, the SCR system aimed to reduce NOx in continuous in an oxygen-rich environment and requires a reductant agent to convert NOx to nitrogen. To this purpose, the typical on-boarded reductant is an aqueous solution of urea. Ammonia is then obtained by two consecutive reactions: the "urea thermolysis" (Eq. 6.14) leading to NH_3 and HNCO, and the "HNCO hydrolysis" (Eq. 6.15), leading to the second NH_3 molecule to provide the expected amount of reductant. The deNOx reactions are then assumed to occur via the so-called NH_3-SCR process.

$$(NH_2)CO(NH_2) \rightarrow NH_3 + HNCO \quad (6.14)$$

$$HNCO + H_2O \rightarrow NH_3 + CO_2 \quad (6.15)$$

Higher deNOx performances are obtained in both system (SCR and LNT) when the NO_2 concentration to the input of deNOx technology is boosted. Usually, a Diesel Oxidation Catalyst (DOC) is placed upstream the deNOx converter to partially convert NO into NO_2. The exhaust gas enriched with NO_2 allows the onset of the SCR reaction by ammonia at lower temperature. It enables to achieve the fast-SCR stoichiometry. NO_2 is also more appropriate for the storage step of the NSR process. As a consequence, the oxidation reaction of NO to NO_2 remains from a great interest for the efficiency of NOx emissions control system. NO_2 also presents a powerful oxidizing ability thereby participates to the soots combustion trapped in the Diesel particulate filter (DPF). The deNOx after-treatment technology, either SCR or LNT, also provide NH_3 emissions that need to be contained to limit the ammonia slip.

At present, the NH_3-SCR process is the preferred technology for NOx abatement in Diesel exhausts. The WO_3-V_2O_5-TiO_2 catalyst developed for stationary deNOx applications is now replaced by Cu or Fe-exchanged zeolites (mainly stabilized ferrierite, chabazite, SAPO or SSZ-13). Extensive reviews [231, 232, 233] and

outstanding studies, both on vanadium-based oxides [234,235] or zeolite catalysts [236,237,238] were devoted to this technology which is not detailed in this section mainly focused on oxidation reactions, important steps of the deNOx processes. In this respect, great efforts were made by industry and academia researchers to promote oxidation activities of NO, urea and NH_3 in the framework of Urea-SCR, NH_3-SCR and LNT processes. This section is focused on reference oxide materials for these reactions.

6.8.2. NO oxidation

The control of soot/particulate matter (PM) and NOx ($NO+NO_2$) emissions from Diesel vehicles is one of the most important and challenging problem since last few decades. Presently, the most effective technology to regulate PM emissions is the Diesel particulate Filter (DPF), in which the collected soot can be oxidized by NO_2 (passive regeneration). The NOx selective catalytic reduction (SCR) by NH_3 is worldwide well-established to control NOx emissions from stationary and mobile source urea (in this later case, urea is then used as NH_3 carrier). The NOx conversion is assumed to be strongly dependant of the NO_2 concentration to reach the so-called fast-SCR stoichiometry, *i.e.* when NO, NO_2 and NH_3 are present in a 1:1:2 stoichiometry. NOx reduction can also be reached by the NOx storage-reduction (NSR) process. In this method, which alternates lean phase (storage) and rich phase (reduction), the adsorption step is largely enhanced when NOx are available as NO_2.

Thus, the NO oxidation into NO_2 remains from a great interest for the efficiency of both Diesel particulate filter and deNOx exhaust gas post-treatments. Catalysts from platinum group metals (PGM) are well-known to find practical applications for this reaction, but they have high cost and limited availability. Noble metals catalysts are also deactivated by high temperature or by poisoning due to the presence of numerous elements of the exhaust gas feed such as sulfur or alkaline metals. Consequently, great efforts were devoted to develop highly efficient noble metal-free catalysts for NO oxidation to NO_2. Commonly, the catalyst supports are oxides such as alumina, silica, ceria (and derived oxides) and zeolites. The specific surface area and porosity, the surface properties and the interactions with active phase are also important factors that determine the activities of catalysts [239]. Considering that the NO oxidation into NO2 is mainly crucial for Diesel exhaust gas treatment and that the exhaust gas temperature is then quite low, the aim is to be able to oxidize NO to NO_2 from the 150–300°C temperature range.

The elementary steps of NO oxidation are thought to involve either Langmuir–Hinshelwood or Eley–Rideal mechanisms, which can be depicted by the following reactions (where □ denotes an oxygen vacancy and O* an active oxygen on oxide material). The oxidation reaction (Eq. 6.16) is assumed to be rapid and equilibrated and dissociative adsorption (Eq. 6.17) is assumed to be rate limiting step [240].

$$O_2 + 2\square \rightarrow 2O^* \quad (6.16)$$

$$NO_{(gas\ or\ adsorbed)} + O^* \rightarrow NO_2 + \square \quad (6.17)$$

The next parts of this section aims to report an overview of recent works published for NO oxidation over oxide based catalysts, organized by type of oxides, (ceria, cobalt, manganese, copper, perovskites, and finally zeolite microporous-based samples), considering the main active site (for instance, Cu/CeO-ZrO2 and Cu/zeolite catalysts are depicted in *copper-based samples* section).

Ceria-based samples. For ceria bulk oxide, the maximum of NO oxidation to NO_2 is observed around 450°C, and above this temperature, the NO conversion is thermodynamically limited [241]. Consequently, great efforts were devoted to understand and improve the redox properties of noble metal-free ceria in the last years [242].

$Ce_xZr_{1-x}O_2$ mixed oxides with different Ce/Zr ratio were evaluated in NO oxidation by several authors. For instance, Lopez et al. [243] studied the NO oxidation of ceria-zirconia catalysts by catalytic tests performed in a fixed-bed reactor under a 500 ppm NOx + 5%O_2 gas flow (500 ml/min; GHSV 30000 h^{-1}). It appears that all the cerium containing catalysts accelerate the oxidation of NO to NO_2 to the opposite of ZrO_2 sample, accordingly to [244,245]. However, $Ce_{0.76}Zr_{0.24}O_2$ and CeO_2 present the same NO_2 profile, with NO_2 formation starting from approximately 275°C and a maximum NO_2 level at 450°C (30% of NO_2 yield).

The addition of lanthanide cations with variable oxidation state (+3/+4), such as praseodymium, also deserves particular interest to enhance the ceria redox behavior. The corresponding $Ce_xPr_{1-x}O_{2-\delta}$ mixed oxides allows the oxygen exchange at a lower temperature compared with pure ceria. The kinetic and structural studies of oxygen availability of the mixed $Pr_{1-x}M_xO_y$ (M=Ce or Zr) oxides was studied by Sinev [246]. Addition of either Ce or Zr to pure Pr oxide affects both the total amount of oxygen that can be reversibly exchanged between oxide and gas phase and the kinetics of the redox processes. The addition of praseodymium in the ceria network increases the creation of oxygen vacancies and induces more labile oxygen species. It results that Ce promotion dramatically increases the oxygen exchange ability (per Pr atom) and lowers the temperature of exchange, while speed up the rate of $Pr_{1-x}Ce_xO_y$ mixed oxides in oxygen exchange reaction. These results are supported by the lower binding energy values for Ce–O bond than for Pr–O bond, and also because the Ce^{3+} ionization energy which is 2.22 eV lower than for Pr^{3+}.

Giménez-Mañogil et al. [247] analyzed the trends in catalytic activities toward the NO oxidation to NO_2 of various ceria-praseodymia mixed oxides. Catalytic tests were performed in a fixed-bed reactor under a 500 ppm NO + 5 %O_2/N_2 gas flow (500 mL min^{-1}; GHSV 30,000 h^{-1}) from 25 to 750°C at 10°C min^{-1}. It is reported that increasing the praseodymium content in $Ce_xPr_{1-x}O_{2-\delta}$ formulation led to higher NO_2 production. Additionally, the maximum NO_2 production was shifted to lower temperatures. For instance, the ceria doping with only 20 mol % Pr ($Ce_{0.8}Pr_{0.2}O_{2-\delta}$) led to an increase of the NO conversion from 24 to 39% at 375°C. Increase Pr amount in $Ce_xPr_{1-x}O_{2-\delta}$ mixed oxide ($Ce_{0.5}Pr_{0.5}O_{2-\delta}$ and $Ce_{0.2}Pr_{0.8}O_{2-\delta}$) led to a supplementary improvement of the maximum NO_2 production. It also results that the BET surface area is not a determining parameter in the NO_2 production. In fact, pure praseodymia presented the highest NO_2 production (48 % at 375°C), therefore indicating that Pr-based oxides are very active for the NO oxidation to NO_2. TG-MS experiments revealed that pure ceria is not able to release O_2 under inert atmosphere, but ceria-praseodymia mixed oxides and pure praseodymia presented different O_2 evolution profiles. In addition, the recorded CO_2 profiles show that the surface carbonates amount increases with the Pr content. These carbonates do not seem to inhibit the NO oxidation reaction. The Lewis acid character of NO and NO_2, which tend to react with basic oxygen sites, was proposed to displace the surface carbonate species [243]. Interestingly, H_2-TPR results were correlated to NO oxidation to NO_2 trends. It is reported that the reduction temperature decreases together with the increase of the overall hydrogen consumption, with respect to the Pr amount in the $Ce_xPr_{1-x}O_{2-\delta}$ mixed oxide.

Copper-based samples. Cerium-based oxides have been extensively studied in the framework of automotive emission control of pollutants from the exhaust gases of gasoline engines in the three-way catalysts (TWC). For instance, copper-doped ceria-zirconia mixed oxides ($Ce_{0.8}Zr_{0.2}O_2$) with different amounts of copper (0.5, 1, 2, 4 and 6 wt-%) were evaluated for NO oxidation to NO_2 by Giménez-Mañogil et al.[248]. Characterizations revealed that copper was well-dispersed onto the ceria-zirconia support for the catalysts with low copper loading. To the opposite, CuO particles were identified by XRD and XPS in samples with 4 and 6 $_{wt}$% of copper. Additionally, both specific surface area and pore volume concurrently diminished for catalysts with more than 1 wt-% copper loading, due to the blocking of porosity. Catalysts with copper drastically decreased the reduction temperature of CuO/ceria-zirconia samples in H_2-TPR experiments, due to the synergistic effect conferred by the copper–ceria interfacial interactions. The maximum of activity was found for the 4%CuO/ceria-zirconia composition, with 54% of NO conversion in NO_2 at 348 °C. Note that a very low loading of copper significantly increased the activity for the NO oxidation to NO_2 with regard to the ceria-zirconia support. Similarly, Wang et al. [249] reported that the dispersion of CuO species on the small crystallite size of $Ce_{0.8}Zr_{0.2}O_2$ support was favorable for NO adsorption. The Cu–Ce–Zr solid solution provided the sites of oxygen vacancies, leading to the formation of active oxygen to improve the oxidation activity of NO. Interestingly, ternary oxides-base samples as Ba-Cu-Ce catalysts enabled to maintain higher activity for NO oxidation than with CuO_x-CeO_2 mixed oxides after aging. In fact, Ba restrains the sintering of $(Cu,Ce)O_x$, resulting in relatively more favorable redox properties and thus higher activity for NO oxidation [250].

Copper exchanged zeolites are commonly used for the selective catalytic reduction (SCR) of NOx (NO and NO_2) with NH_3, especially for mobile sources. This process is strongly dependent to the NO_2/NOx ratio, and it is generally admitted that NO is first oxidized by O_2 to form some types of surface complexes on the zeolite catalysts, which subsequently react with NH_3 to form N_2. The comparative activities of a small-pore Cu-CHA (chabazite) and a large-pore Cu-BEA (Beta) catalyst for the oxidation of NO to NO_2 and the subsequent formation of surface nitrates were investigated by Chen et al.[251]. Both catalysts presented a limited NO oxidation activity with around 20% of NO conversion into NO_2 at 500°C. In addition, the stability of surface nitrates compounds were investigated by TPD experiments following the adsorption of (NO_2 + NO + O_2). Authors reported that the poor NO oxidation activity is not due to the formation of stable surface nitrates on the catalyst. On the contrary, NO was found to reduce and decompose surface nitrates, with different pathway in regard on Cu-CHA or Cu-BEA sample. Interestingly, NO oxidation is favored by Cu ion dimers over exchanged copper zeolite and increasing the copper loading beyond the saturation point of the zeolite leads to a relatively higher proportion of Cu ions [252]. In addition, the site requirements and mechanism of dry NO oxidation were examined on a series of Cu-SSZ-13 catalysts by Ribeiro et al. [253]. Combined experimental and computational kinetic studies revealed at least two Cu ion configurations within hydrated SSZ-13, namely hydrated isolated Cu^{2+} ion (as $[Cu(H_2O)_6]^{2+}$) and Cu_xO_y species (clustered Cu^{2+} ions $x \geq 2$, $y \geq 1$) for low (Cu/Al_{tot}<0.2) and high (Cu/Al_{tot}>0.2) copper atomic ratio, respectively. It was reported that the hydrated isolated Cu^{2+} ions are quantitatively converted to dehydrated isolated Cu^{2+} ions under NO oxidation conditions and do not contribute to the rate of NO oxidation. To the opposite, the Cu_xO_y species remain present under NO oxidation conditions

and only the Cu dimers (Cu_2O_y) with local Cu-O_y-Cu bonds can accommodate adsorption and dissociation of O_2 necessary to catalyze NO oxidation. Complementary information about zeolites are available thereafter in the *Zeolite and microporous-based materials* section.

NO oxidation can be also performed over Cu doped $LaCoO_3$ perovskite oxides. Various $LaCo_{1-x}Cu_xO_3$ (x = 0.1, 0.2, 0.3), synthesized using a modified sol–gel method, were studied by Zhou et al.[254]. $LaCo_{0.9}Cu_{0.1}O_3$ sample exhibited the best performance and achieved a NO conversion of 82% at 310°C. The following sequence was proposed for the catalytic activities: $LaCo_{0.9}Cu_{0.1}O_3$ > $LaCoO_3$ > $LaCo_{0.8}Cu_{0.2}O_3$ > $LaCo_{0.7}Cu_{0.3}O_3$. It appeared that high copper loading was not favorable for the NO oxidation. It was showed by means of structural characterizations (XRD, BET, FTIR and TEM) that increasing the Cu doping content results in the formation of isolated CuO on the surface of the oxides. It was proposed that the interaction between Co and Cu promoted the conversion of NO to NO_2. It was also advanced that Cu doping would facilitate the reaction by decreasing the energy of oxygen vacancy formation and the NO_2 desorption barrier from nitrites species.

As expected, numerous other copper supported catalysts are able to catalyze the NO oxidation reaction. For instance, Cu/TiO2 catalysts was found active for the oxidation of NO to NO_2 in oxygen-rich atmosphere, with an optimum temperature at about 350-400°C for around 60% of conversion [255]. However, the specific nature of active copper species was not addressed in this study.

Cobalt-based samples. Considering their high catalytic activity for oxidation reactions, Co_3O_4 based catalysts deserve particular attention. Irfan et al. [256] compared various transition metal oxides with cobalt-supported catalysts for the NO oxidation reaction. Experiments were performed in a fixed bed quartz reactor. The powder catalysts were loaded with an aid of quartz wool and heated to the desired reaction temperature. The reaction mixture consisted of 150 ppm NO, 8% H_2O, 10% O_2 balanced in N_2 for a total gas flow rate of 1500 cc/min. The following activities order was reported: Co_3O_4/SiO_2 > Pt-WO_3/TiO_2 > Pt/TiO_2 > Pt/SiO_2 > CuO_x/TiO_2 > Co_3O_4/TiO_2 > MnO_x/TiO_2 > Pt-V_2O_5/TiO_2. TiO_2 and especially SiO_2 (from low surface area) supported Co_3O_4 (20 wt-%) exhibited high activities. A maximum of 69% NO conversion was reported at 300°C on Co_3O_4/SiO_2 (4 $m^2\ g^{-1}$) with this high space velocity condition. Note that the activities of unsupported metal oxide catalysts for NO oxidation were also determined. Among the oxides tested (Mn, Co, Cu), Co_3O_4 (35 $m^2\ g^{-1}$) is the most active catalyst (66% of NOx converted at 300°C, compared to 59% conversion for MnO_x sample of 8 $m^2\ g^{-1}$). Authors concluded that the more oxidizing ability towards NO is the major reason for better activity of Co based catalysts, compared to MnO_x and CuO_x sample.

Huang et al. [257] studied cobalt oxide supported on mesoporous silica (1119 $m^2\ g^{-1}$) for NO oxidation, and achieved about 82% NO conversion at 300°C, which was very good activity and quite comparable to noble metal catalysts. However, the use of mesoporous silica is still not considered for practical application due to thermal stability requirements. They also observed that high temperature calcination led to rapid decrease in catalytic activity, and sintering occurs at a temperature as low as about 300°C.

Recently, Kim et al. [258] studied NO oxidation on supported cobalt oxide synthesized by conventional wet impregnation method using various supports including CeO_2, SiO_2, ZrO_2, TiO_2 and SiO_2. Among tested

catalysts, they reported that Co_3O_4 supported on high surface area ceria (230 m^2 g^{-1}) showed the highest catalytic activity with approximately 70% conversion at about 270°C using a weight-to-flow ratio of 0.045 $g.s.mL^{-1}$. It resulted that the catalytic activity of cobalt oxide can be substantially improved by using high surface area supports with good thermal stability. Megarajan et al. [259] synthesized ceria supported cobalt oxide by the incipient wetness impregnation method. They obtained high catalytic activity for NO oxidation at moderate temperature (80% of NO oxidized at 300°C for 10 wt% Co incorporated in CeO_2 sample of 61 m^2 g^{-1}). The catalytic activity in NO oxidation was even comparable with those reported with noble metal based catalysts. It could be mainly due to the high dispersion of Co_3O_4 nanoparticles on ceria support with enhanced catalyst support interaction, also associated with an improvement of the redox properties of Co_3O_4-ceria catalyst.

Manganite-based samples. MnO_x is widely used in NO oxidation due to their high catalytic efficiency and fairly cost-effective. Effects of Mn precursors [260] and preparation methods [261] on NO oxidation over Mn/TiO_2 were studied. Chen et al. [262] indicated that adding Fe on MnO_x could increase the activity for NO oxidation into NO_2. This result is supported by Zhao et al. [263] that also showed that the addition of Fe (Fe–La–Mn/Al_2O_3) increased both NO conversion and resistance to H_2O and SO_2. Consequently, $FeMnO_x$-based catalysts were expected to perform well for NO oxidation. The effect of loading sequences on the structure and activity of $FeMnO_x/TiO_2$ catalyst was studied in [264].The better catalytic activity was obtained from one-step impregnation method. For instance, $Fe_{0.15}$–$Mn_{0.3}/TiO_2$ exhibited the highest catalytic activity, with a maximum NO conversion of 70% at 320°C (space velocity of 15 000 h^{-1}). The excellent activity was attributed to higher surface area, lower crystalline of manganese oxides, abundant Mn^{3+}, Fe^{3+} and chemisorbed oxygen species (O_α) on the surface.

Perovskite-based samples. Cobalt based perovskite type catalysts are well known to exhibit good activity for NO oxidation and therefore show a potential as substitute for Pt based NO oxidation catalysts. Wen et al. [265] studied series of $La_{1-x}Ce_xCoO_3$ perovskite oxide catalysts for nitrogen monoxide oxidation, and reported approximately 80% conversion on $La_{0.8}Ce_{0.2}CoO_3$ at 300°C under the W/F ratio of 0.096 $g.s.mL^{-1}$. Kim et al. [266] also investigated the perovskite supported honeycomb catalysts for NO oxidation using 400 ppm NO and at space velocity of 30 000 h^{-1}, and reports remarkable NO conversion of 86% at about 300°C on $La_{0.9}Sr_{0.1}CoO_3$. Under realistic conditions, $La_{1-x}Sr_xCoO_3$ catalysts achieved higher NO conversion into NO_2 than a commercial platinum-based DOC catalyst, constituting a promising way for a considerably lower-cost diesel exhaust treatment system.

Zeolite and microporous-based materials. Kim et al.[267] studied three different types of acid form zeolites, namely chabazite (H-CHA), beta (H-BEA), and mordenite (H-MOR) for the NO oxidation reaction. The corresponding catalysts presented a very low activity, with NO conversion below 2%. However, authors reported that the acid form H-CHA showed the highest activity due to the small pore cavity, which enhances the stability of the transition complex, assumed as N_xO_y surface species (NO_2, N_2O_4, N_2O_3, ...). Similar results were previously reported by Lobo et al. [268]. By evaluating the NO oxidation activity over microporous materials, it was shown that NO oxidation is catalyzed by chabazite zeolites in the proton (H^+), sodium (Na^+) and siliceous forms, and by microporous carbons. The catalytic properties of the samples were attributed to

their ability to stabilize a $[N_2O_4]^{2+}$ transition state within the micropores through van der Waals forces. Electrostatic effects from extra-framework cations within SSZ-13 samples (a CHA zeolite type) were shown to provide additional stabilization of the transition state and further enhanced reaction rates. SSZ-13 is favored for SCR processes because of its small-pore structure that enables to resist to dealumination effect from hydrothermal aging and to avoid structure collapse. The confinement effects from the framework that accelerate the gas-phase reaction were also proposed by Artioli et al. [269] to explain the NO oxidation activity of silicalite-1 (siliceous ZSM-5) and siliceous samples of zeolite beta (BEA) and chabazite (CHA). These results stated that no specific catalytic sites were present and that NO oxidation reaction proceeds via elementary steps. The obtained NO oxidation rates are much higher (by factors of 10^4) than homogeneous reaction rates.

Active sites of H-ZSM5 catalysts for the oxidation of nitric oxide by oxygen was studied by Halasz et al. [270]. Authors concluded that Lewis acidic lattice (aluminium ions and silanol hydroxyls) are probably not the active sites in the catalytic oxidation of NO. To the contrary, the oxidation of NO to NO_2 would be catalyzed above 200°C by Brønsted acidic bridging hydroxyls. Harold et al.[271] focused on the comparison of iron and copper exchanged ZSM-5 catalysts for the NO oxidation reaction. Combining comprehensive experimental and kinetic modeling studies, it was demonstrated that Fe-zeolite was more active in NO oxidation than Cu-zeolite. The presence of water in the gas mixture strongly inhibits the NO oxidation. Additionally, the instability of nitrates in the presence of NO was also reported and the surface reaction between adsorbed O atoms and gaseous NO was proposed as the rate determining step. It was also related that the NO_2 is more strongly bound on Cu-chabazite compared with Fe-ZSM-5.

6.8.3. Ammonia oxidation

The removal of ammonia from air or water is environmentally important. Currently, ammonia is removed from industrial flue gases via biological treatment by absorption, or by thermal combustion. An attractive alternative process is the selective catalytic oxidation (SCO) to nitrogen and water. Such technology may also find application in combination with the selective catalytic reduction (SCR) process, in which NOx is reduced to nitrogen using ammonia, to avoid NH_3 slip. It can proceed in the following three principal ways below (Eq. 6.18-20):

$$2NH_3 + 3/2O_2 \rightarrow N_2 + 3H_2O \quad (6.18)$$

$$2NH_3 + 2O_2 \rightarrow N_2O + 3H_2O \quad (6.19)$$

$$2NH_3 + 3/2O_2 \rightarrow 2NO + 3H_2O \quad (6.20)$$

With many practical catalysts, N_2, N_2O and NO are formed simultaneously at 400-500°C in various proportions [272], but the N-compounds selectivity may be tune with appropriate materials. For instance, the main product is nitric oxide in the presence of platinum or cobalt oxide catalysts at 750-900°C. With manganese oxide, nitrous oxide is formed at 300-400°C. Ammonia can be oxidized into N_2 over vanadium pentoxide at 500-600°C. Overall, the oxidation of ammonia results in the formation of N_2 at low temperature. N_2O is observed by raising the temperature of reaction, its yield passing through a maximum. Ammonia is oxidized to a greater extent (NO) for higher temperatures.

Mechanisms of the Langmuir-Hinshelwood type were proved to be unsuitable for the interpretation of the experimental data. It was proposed that the first step of the process involves the chemisorption of oxygen with the formation of the O_2^- anion, followed by the reaction of NH_3 with surface oxygen to form adsorbed (NH) species, subsequently converted into surface nitroxyl (HNO). The final reaction products are N_2 from (NH) and (HNO) and/or N_2O from two nitroxyl species.

Simple oxide-based samples. Catalytic behaviors of simple oxide for NH_3 oxidation was studied by several authors. Lanthanide (La, Ce, Pr) oxides exhibit a low activity, while Al_2O_3 and SiO_2 show activities even lower. The activity of barium peroxide tends to that of Fe_2O_3. Finally, according to Il'chenko et al. [272] the activities of the single oxides decrease as follows:

$$Co_3O_4, Mn_2O_3 > Cr_2O_3 > Fe_2O_3 > CuO > NiO > V_2O_5 > MoO_3 > ThO_2 > WO_3 > SnO_2 > ZrO_2 > ZnO > Nb_2O_5 > Bi_2O_3 > Sb_2o_4 > Ta_2O_5$$

It appears that transition metal oxides such as Co_3O_4, MnO_2 (Mn_2O_3), Cr_2O_3 and CuO present the highest activities in the NH_3 oxidation. NiO, Fe_2O_3, and V_2O_5 oxides are moderately active, whereas the activities of the La_2O_3, Pr_6O_{11} CeO_2, TiO_2, ZrO_2, ThO_2, Nb_2O_5, T_2O_5, MoO_3 and WO_3 are low. The higher selectivity regarding N_2O is obtained with the most active oxides.

Complex and promoted oxide-based samples. Concerning the reaction involving the oxidation of NH_3 to N_2O at 200-300°C, it was reported that MnO_2 with addition of Bi_2O_3 is extremely efficient [272]. Sazonova et al. [273] studied a wide range of various catalytic systems from ordinary oxides to multi-component supported and unsupported catalysts, including perovskites and zeolites, with a particular attention paid to vanadium supported catalysts (V_2O_5/MeO, MeO = TiO_2, SiO_2, MgO). They concluded that the most active in ammonia oxidation to molecular nitrogen are vanadium-titanium, copper-titanium and copper-substituted zeolites (ZSM-5) catalysts. Promotion by MoO_3 and WO_3 of vanadium-titanium catalysts changed the temperature dependence of the nitrogen formation rate: at low temperatures (250°C), N2 formation decreased with the increase of MoO_3 and WO_3 content.

The selective catalytic oxidation (SCO) of ammonia to nitrogen over Fe_2O_3–Al_2O_3, Fe_2O_3–TiO_2, Fe_2O_3–ZrO_2 and Fe_2O_3–SiO_2 was studied by Yang et al. [274]. The Fe_2O_3–TiO_2 catalysts prepared from iron sulfate yielded a higher selectivity for N_2 than those prepared from nitrate, with more than 92 % of N_2 yields at 400-450°C (GHSV = 2.0×10^5 h^{-1}). It was reported that lattice oxygen may participate in the SCO reaction. Authors assumed a two-step SCO mechanism in which NH_3 is first oxidized to NO and then NO is reduced to N_2 by unreacted NH_3 adsorbed species through a SCR reaction pathway.

Several alumina-supported (transition) metal (Cu, Mo, V, Pt, Ir, Rh, Pd) were evaluated by Gang et al. [275] in the NH_3 oxidation to nitrogen reaction. Authors showed that Cu/Al_2O_3 sample presented the higher activity of transient metal supported catalysts. However, noble-metal catalysts remained more active and metal-exchanged zeolite are proposed as promising materials for ammonia oxidation.

Zeolite-based samples. A screening study about ZSM-5 based sample reported promising performances of copper-substituted zeolite materials [273]. Cobalt exchanged ZSM-5 catalysts were studied by Li et al. [276]

which confirmed that ion exchanged zeolite are more active than the corresponding Al_2O_3 supported catalysts with the same metal loading. Higher N_2 selectivity was achieved with Y zeolite exchanged with transient metals. The oxidation of ammonia on Y zeolites containing Mn^{2+}, Fe^{3+}, Co^{2+}, Ni^{2+}, Cu^{2+}, Cr^{3+} or Ag^{+} cations was investigated and the following activity ranking was established:

Cu-Y > Cr-Y > Ag-Y > Co-Y > Fe-Y > Ni-Y, Mn-Y.

Gang et al. [275] reported that the activity of copper ion-exchanged Y zeolite catalysts for ammonia oxidation was shown to be comparable to that of noble metal catalysts at low temperatures, with even much higher N_2 selectivity for the zeolite catalysts.

6.8.4. Urea oxidation

Studies about urea reactivity are essentially devoted to SCR process, since $(NH_2)CO(NH_2)$ is recognized as a safe storable ammonia precursor. NH_3 is obtained by two consecutive reactions: the "urea thermolysis" (Eq.6.14) leading to NH_3 and HNCO, and the "HNCO hydrolysis" (Eq. 6.15). The overall reaction corresponds to the "direct urea hydrolysis" (Eq. 6.21).

$$(NH_2)CO(NH_2) + H_2O \rightarrow 2NH_3 + CO_2 \qquad (6.21)$$

Urea thermolysis (Eq. 6.14) is endothermic and thermally assisted compared to HNCO hydrolysis (Eq. 6.14) which is exothermic. With pure urea, Koebel *et al.* [277] observed the thermal decomposition according to (Eq. 6.14) and reported that isocyanic acid is stable in the gas phase. However, HNCO is easily hydrolyzed with water vapor on many solid oxides, such as SCR catalysts (Eq 6.15) [278]. It was proposed that the rate of HNCO hydrolysis is much higher than the rate of the SCR reaction at low to medium temperatures on usual SCR catalysts. Interestingly, it was reported that both (Eq. 6.14) and (Eq. 6.15) reactions can be catalyzed by transition metal materials and then the rate determining step depends on the temperature. For instance, over anatase TiO_2, Bernhard et al. [279] observed that the hydrolysis was somewhat slower than thermolysis below 150°C, whereas the hydrolysis was faster above 160°C. Unfortunately, during the urea decomposition process, undesired reactions can also occur. Schaber et al. [280] indicated that, at around 190°C, cyanuric acid ($C_3H_3N_3O_3$), ammelide and ammeline are produced primarily from biuret, which results itself from reaction of HNCO with urea. All these by-products may induce catalyst surface deactivation caused by deposit formation and also lead to imbalance in the NH_3-NOx stoichiometry, degrading the DeNOx efficiency.

Using an innovative experimental synthetic gas bench adjusted to powdered catalysts and allowing the use of urea or ammonia as reductant agent, the competitive reactivity of the HNCO intermediate species was recently evidenced by Seneque et al. over acidic zirconia-based catalyst [281,282].The expected HNCO hydrolysis to yield ammonia can compete with other reactions and possible divergences in terms of DeNO*x* efficiency were evidenced depending on the nature of the reductant (i.e. NH_3 or urea aqueous solution). It was demonstrated that HNCO appeared more reactive toward O_2 than NH_3. Selective catalytic oxidation (SCO) experiments showed a reductant oxidation of about 30% at 300°C for Urea-SCO, compared with 8% for NH_3-SCO. Oxidation of HNCO intermediate by NO_2 was also evidenced, even if these oxidation reactions appeared negligible over the studied catalyst under usual SCR mixtures.

Interestingly, this study also evidences a new "HNCO-SCR" route involving both NO and NO_2, probably *via* the formation of HONO, which is commonly proposed as intermediate species in NO_x reduction mechanisms. Finally, the various competitive reactions regarding HNCO in the urea SCR process are highlighted in Scheme 6.1.

Scheme 6.1. Competitive reactivity of HNCO for Urea-SCR with shortened urea residence time. From ref. 282.

6.8.5. NOx-trap systems (basic oxides)

Due to the high efficiency of noble metals for both NO oxidation in lean media and stored NOx reduction during short rich incursions, catalysts developed for Lean NOx trap process essentially deal with Platinum Group Metal (PGM) materials, usually based on a mix of Pt, Pd and Rh. However, catalysts without PGM were also investigated such as transient oxide catalysts, spinel type structures, zirconia and titania functionalized oxides, or perovskite-based samples. For instance, spinel-type oxide was studied by Fino et al. for NOx removal from Diesel engine [283]. Nanostructured spinel-type oxides catalysts AB_2O_4 (where A = Co and Mn, and B = Cr and Fe), prepared by the solution combustion method and characterized by BET, XRD, SEM and TEM, were evaluated by temperature programmed oxidation/reduction (TPO/TPR) for NOx removal. The following activity classification for NO_x reduction in the 350–450°C temperature range was obtained: $CoFe_2O_4$ > $CoCr_2O_4$ > $MnCr_2O_4$. Based on transient thermal analysis studies (TPD), authors proposed that the prevalent activity of the chromite catalysts could be explained by their higher concentration of weakly chemisorbed suprafacial oxygen, which contributed actively to the oxidation mechanism by *spillover*.

NOx storage and reduction pathways on zirconia and titania functionalized binary and ternary oxides (ZrO_2/TiO_2, $Al_2O_3/ZrO_2/TiO_2$) as NOx storage and reduction (NSR) systems was also studied [284]. NOx adsorption on the $Al_2O_3/ZrO_2/TiO_2$ (AZT) system was found to be significantly greater than that of ZrO_2/TiO_2 (ZT), due to specific surface area ten times higher (264 $m^2\ g^{-1}$ for AZT material compared with 26 $m^2\ g^{-1}$ for ZT system). It was reported that the thermal stability of nitrates species is higher over AZT compared with ZT, assigned to the defective structure and the presence of coordinative unsaturated sites (CUS) on the former surface. Nevertheless, Pt-functionalized counterparts facilitated the decomposition of nitrates together with an enhancement of the NOx reduction rate.

Supported YCeZrO ternary oxides using $LaCoO_3$ perovskite as active phase were also proposed as efficient Lean NOx-trap catalysts. A series of non-platinic ceria-based oxides supported catalysts $LaCoO_3/K_2CO_3$/S

(S=CeO_2, $Ce_{0.75}Zr_{0.25}O_2$ or 5%Y/$Ce_{0.75}Zr_{0.25}O_2$) revealed interesting behaviors [285]. It was reported that the doping of Zr or YZr into CeO_2 facilitates the formation of CeZrO binary or YCeZrO ternary solid solutions, increasing the specific surface area and improving the redox properties of ceria. Additionally, by means of EXAFS and H_2-TPR experiments it was found that $LaCoO_3$ supported over the solid solutions exhibited higher dispersion and better reducibility than that supported on CeO_2. Finally, the YCeZrO ternary solid solution supported catalyst containing 5 wt % K_2CO_3 exhibited the best performance for the NSR process at 350 °C: a high NO-to-NO_2 conversion (66.5%) was obtained in lean condition, and a very high NOx reduction percentage (98.2%), associated with an extremely high NOx-to-N_2 selectivity (98.8%), was recorded in rich condition in the absence of CO_2.

6.8.6. NOx direct decomposition

Nitrogen oxides (NOx) emitted from combustion facilities are harmful for human health and our environment. As a consequence, the NOx decomposition ($2NO \rightarrow N_2 + O_2$) is the most desirable but also the most challenging NOx abatement process. Therefore, the direct decomposition of NO is one of the candidate reactions for the high temperature deNOx applications. Numerous types of catalysts, such as supported noble metals [286,287,288], ion-exchanged zeolites [289] and metal oxides [290,291,292] are known to be possibly suitable for this purpose. The main elementary steps involved are:

$$NO_g \leftrightarrow NO_{ads.} \quad (6.22)$$

$$NO_{ads.} \rightarrow N_{ads.} + O_{ads.} \quad (6.23)$$

$$2N_{ads.} \rightarrow N_2 \quad (6.24)$$

$$2O_{ads.} \rightarrow O_2 \quad (6.25)$$

The poisoning of catalyst by oxygen resulting from NO decomposition (and/or coexisting component) was commonly admitted as the main reason for low catalytic performances. Consequently, perovskite-type oxides, which possess oxygen-deficient sites in their structure, exhibit relatively high catalytic activity in the high-temperature region. Brownmillerite-like compounds, as $Sr_2Fe_2O_5$ which has perovskite structure with randomly distributed oxygen vacancies, showed a remarkable NO decomposition activity at 700-900°C, whereas the calcium analogue ($Ca_2Fe_2O_5$) was almost inactive even at such a high temperature as 900°C [293]. It was reported that $Ca_2Fe_2O_5$ does not change its own crystal structure and remains in the orthorhombic brownmillerite-like structure, so-called an "ordered" oxygen deficient perovskite structure. To the opposite, an order-disorder transition was observed for $Sr_2Fe_2O_5$ at 700°C. As a result, $Sr_2Fe_2O_5$ possesses a statistically disordered oxygen-deficient perovskite structure at temperatures above 700°C, with the formation of anion-deficient perovskite phase. It implies that significant oxygen vacancies are necessary for NO decomposition. $Ba_2Cu_3O_{7-y}$ perovskite-like compounds also exhibited interesting behaviors [294]. MgO supported Y-Ba-Cu-O catalysts were studied in order to highlight the improvement of catalytic properties through a high dispersion. At 700 °C, the conversion was about 35%, similar to that of bulk $Ba_2Cu_3O_{7-y}$ catalyst. When the temperature is increased up to 800°C, the conversion reached approximately 73% for the supported catalyst, compared to 40% for the perovskite bulk compound. The following activity order was obtained at 800°C, in which a

commercial platinum sample was evaluated as a reference: Y-Ba-Cu-O/MgO > Pt/Al_2O_3 > $La_{0.85}Sr_{0.15}CoO_3$. It was advanced that (i) the decomposition of NO is likely to be facilitated by the redox cycle of Cu ($Cu^{2+} \leftrightarrow Cu^{+}$) and (ii) the NO adsorption sites are Cu ions adjacent to oxygen vacancies. The decomposition of NO required higher temperatures (700 to 800°C), because it implies the completion of the Cu redox cycle. The role of the copper valence in the direct decomposition of nitrogen monoxide was also advanced by Yasuda et al.[295] for $La_{2x}A'_xCu_{1-y}B'_yO_4$ (K_2NiF_4 type structure with A' = Sr, B' = Al, Zr, x = 0 - 1.0, y = 0, 0.2) catalysts. It was reported that the average oxidation number of copper in the catalyst samples increased from 2.00 for La_2CuO_4 up to 2.30 with Sr^{2+} substitution, and decreased with Al^{3+} or Zr^{4+} substitution. The highest oxidation state was observed for the Sr^{2+} substitution with x = 0.5. The composition became oxygen rich upon Al^{3+} and Zr^{4+} substitution and oxygen-deficient with Sr^{2+} substitution. It was observed that the catalytic activity increased with the increase of the average oxidation number of copper, resulting in the redox cycle of $Cu^{2+} \leftrightarrow Cu^{3+}$. Note that, contrary to Shimada et al. [294], the presence of Cu^{+} is unlikely because of its instability in the octahedral site of the K_2NiF_4-type structure.

Rare earth oxides (REOs)-based catalysts from C-type cubic structure were also reported as efficient NO decomposition catalysts [296,297,298]. High NO decomposition activity was achieved in the presence of oxygen-deficient sites, which may increase the probability of NO adsorption. Several alkaline earth oxides, which did not include oxygen-deficient sites in the lattice, such as Sr/La_2O_3 and Ba/MgO, were reported to effectively catalyze the NO decomposition reaction by Vannice et al. [299] and Lunsford et al. [300,301]. A barium–nitro phase was reported as an intermediate in the catalytic cycle. Nitro species at the surface apparently react with NO to form the decomposition products, N2 and O_2. The catalytic performance of supported alkaline earth metal oxides for NO decomposition decreased following the order: Ba/Y_2O_3 > Sr/Y_2O_3 > Ca/Y_2O_3 > Mg/Y_2O_3 > Y_2O_3. Finally, Ba containing metal oxide catalysts, as BaMnO-based perovskite [302], Ba/Ba–Y–O [303], Ba/Y_2O_3 [304] or $Ba_3Y_{3.4}Sc_{0.6}O_9$ samples [305], showed relatively high NO decomposition activity. Note that the additive effect of Ba into CeO_2-based mixed oxides such as CeO_2-MnO_x, CeO_2-FeO_x and rare earth oxides was also reported by Iwamoto et al. [306,307,308] and Haneda et al. [309].

The reaction mechanism of NO decomposition by Cu/zeolites highlighted the role of the Cu^{I} coordination and its localization in zeolites on the reaction profile. The improved coordination of the Cu^{I} cation with the framework resulted in the formation of less stable reaction intermediates and surprisingly in higher apparent energies of activation [289].

6.9. Wet air oxidation

Wet air oxidation (WAO) is a process of elimination of aqueous pollutants by oxidation with O_2 under pressure. Other oxidants can also be used: H_2O_2 in the wet peroxide oxidation (WPO) or ozone in ozonation processes. Oxide catalysts can be used but care should be taken to avoid leaching of metallic ions. Information about catalytic processes of WAO can be found in recent reviews by Arena et al. [310] and by Jing et al. [311]. WAO of dye wastewater was reviewed by Fu and Kyzas [312]. Due to its low biodegradability and high toxicity for activated sludges, phenol is often used as a model compound in WAO [313] or WPO [314,315]. H_2O_2 being a

oxidant stronger than O_2, WPO is generally carried out at low temperature with Cu or Fe catalysts. Figure 6.15 shows the unique role of the association of a catalyst (4%CuO-SBA-15) with H_2O_2 in WPO of phenol.

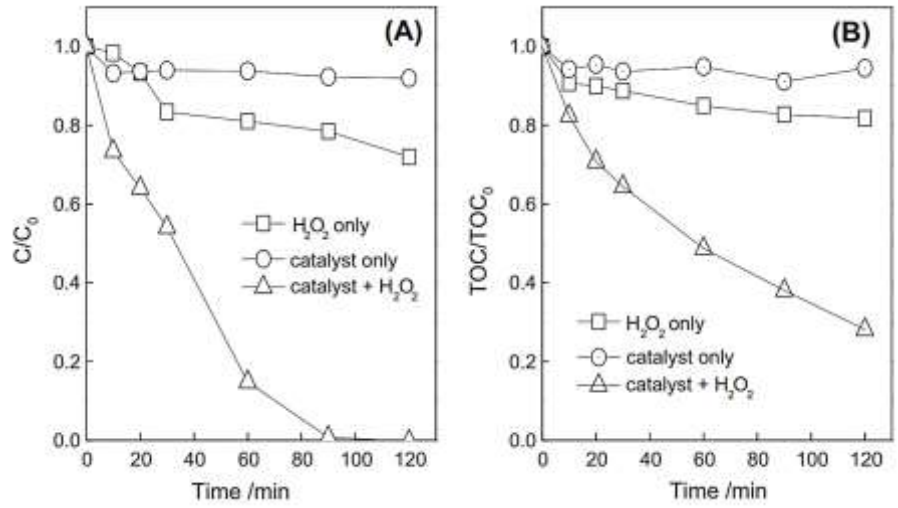

Figure 6.15 Phenol conversion and removal of TOC (total organic carbon) at 60°C with H_2O_2 alone, with catalyst alone and in CWPO (catalyst+H_2O_2). From ref. [314].

The high activity of the system CuO-H_2O_2 would be due to the formation of very reactive $HO_2^{\bullet}$ and $OH^{\bullet}$ radicals (eq. 6.26 and 6.27):

$$S–Cu^{2+} + H_2O_2 \rightarrow S–Cu^{1+} + HO_2^{\bullet} + H^+ \quad (6.26)$$

$$S–Cu^{1+} + H_2O_2 \rightarrow S–Cu^{2+} + OH^{\bullet} + OH^- \quad (6.27)$$

Phenol concentration decreases more rapidly than TOC, which means that organic intermediates are formed before total oxidation (first catechol, hydroquinone, resorcinol and then maleic, oxalic, formic and acetic acid). Cu, Mn, Fe oxides were used for CWAO processes: degradation of Acid Red over Cu-Mn/TiO_2 composites [316], oxidation of Rhodamine B over MnO_2 [317], oxidation of paper industry wastewater over $Ce_{0.4}Fe_{0.6}O_2$ [318] or $Ce_{1-x}Co_xO_y$ mixed oxides [319]. CWPO were mainly performed over Fe [320,321] or Cu catalysts [322], the systems Fe^{2+}/Fe^{3+} and Cu^{+}/Cu^{2+} being best able to generate active oxygen species from H_2O_2. Coupling CWPO with photons (photo-Fenton) allows to obtain decolorization of Orange II at ambient temperature over Fe-smectite [323]. Though noble metal catalysts are generally more active than oxide catalysts in CWAO, there are some exceptions to this rule. For instance, Pt catalysts are rapidly deactivated when the wastewater contains amines which form soluble complexes with noble metals. It was proven by Schmit et al. that β-MnO_2/CeO_2 catalysts could oxidize methylamine at 190°C without serious leaching of Mn ions (<0.1 ppm after a 24h-reaction) [324].

6.10. Conclusions and perspectives

If oxide catalysts are mainly used in selective oxidation processes, the progresses made in their synthesis allow to obtain efficient catalysts for combustion and depollution systems. Cobalt, manganese, iron and copper-based oxides can exhibit very high activity for CO, CH_4 and VOC oxidation. Mixed oxides (perovskites, spinels, hexaaluminates, ...) still show superior performances thanks to their high surface area and improved stability.

Redox supports, especially those based on ceria, reinforce the performance of oxide catalysts in oxidation reactions by stabilizing the proper $M^{n+}/M^{(n+1)+}$ balance required for a good activity. Copper or iron-exchanged zeolites are also used in DeNOx processes with zeolites stable above 900°C. Shape-structured oxides (nanocubes, nanowires, nanobelts,…) were widely investigated in the recent years. Not only the nature of the exposed faces but also crystals defects (vacancies, intersticial atoms, shear planes,…) can have a decisive effect on the catalyst performances. In most cases, oxygen mobility is a key-factor in oxidation processes. $^{18}O/^{16}O$ exchange between the gas phase and surface or bulk O species can give useful information about the mechanism of reaction. In the future, more and more sophisticated oxides (mesoporous and nanocasting, core-shell, shaped-structured,….), with a perfect control of the metal-metal and metal-oxygen interaction, should be developed for interesting applications provided that these new oxides have proven their stability at high temperature. Another way of improvement is to fractionate very stable oxides into nanoparticles of high surface area by reactive grinding. And finally, new activation processes (plasma, ultrasound, ….) may also be excellent ways of research for these materials.

References

[1] T. Exley in *Principles of Natural Philosophy*, Longman et al Publ. London, 1827.
[2] M. W. Roberts, Birth of the catalytic concept (1800-1900), Catal. Lett. 67 (2000) 1-4.
[3] R. K. Grasselli, Selective oxidation and ammoxidation catalysis: History of catalyst design, in *Surface Properties and Catalysis by Non-Metals*, Volume 105 , NATO ASI Series (J. P. Bonnelle, B. Delmon & E. Derouane, Eds), Springer,pp 273-288 (1983).
[4] S. D. Jackson, J. S. J. Hargreaves, *Metal Oxide Catalysis*, Wiley VCH (2009).
[5] J. C. Védrine, I. Fechete, Review: Heterogeneous partial oxidation catalysis on metal oxides, C. R. Chimie 19 (2016) 1203-1225.
[6] A. B. Lamb, W. C. Bray, J. C. W. Frazer, The removal of carbon monoxide from air, Ind. Eng. Chem. 12 (1920) 213-221.
[7] E. C. Pitzer, J. C. W. Frazer, The physical chemistry of hopcalite catalysts, J. Phys. Chem. 45 (1941) 761-776.
[8] Z.-R. Tang, S. A. Kondrat, C. Dickinson, J. K. Bartley, A. F. Carley, S. H. Taylor, T. E. Davies, M. Allix, M. J. Rosseinsky, J. B. Claridge, Z. Xu, S. Romani, M. J. Crudace, G. J. Hutchings, Synthesis of high surface area $CuMn_2O_4$ by supercritical anti-solvent precipitation for the oxidation of CO at ambient temperature, Catal. Sci. Technol. 1 (2011) 740-746.
[9] T. Biemelt, K. Wegner, J. Teichert, S. Kaskel, Microemulsion flame pyrolysis for hopcalite nanoparticle synthesis: a new concept for catalyst preparation, Chem. Commun. 51, 2015, 5872-5875.
[10] Z. Jaworska-Galas, W. Mista, J. Wrzyszcz, M. Zawadzki, Thermal stability improvement of hopcalite catalyst, Catal. Lett. 24 (1994) 133-139.
[11] E. C. Njagi, C.-H. Chen, H. Genuino, H. Galindo, H. Huang, S. L. Suib , Total oxidation of CO at ambient temperature using copper manganese oxide catalysts prepared by a redox method, Appl. Catal. B: Environmental 99 (2010) 103-110.
[12] H. C. Genuino, S.Dharmarathna, E. C. Njagi, M. C. Mei, S. L. Suib , Gas-phase total oxidation of benzene, toluene, ethylbenzene, and xylenes using shape-selective manganese oxide and copper manganese oxide catalysts, J. Phys. Chem. C 116 (2012) 12066-12078
[13] W. Tang, X. Wua, S. Li, X. Shan, G. Liu, Y. Chen, Co-nanocasting synthesis of mesoporous Cu-Mn composite oxides and their promoted catalytic activities for gaseous benzene removal, Appl. Catal. B: Environmental, 162 (2015) 110–121.
[14] X. Xie, Y. Li, Z.-Q. Liu, M. Haruta, W. Shen, Low-temperature oxidation of CO catalysed by Co_3O_4 nanorods, Nature, 458 (2009) 746-749.
[15] G. S. Parkinson, Iron oxide surfaces, Surf. Sci. Rep. 71 (2016) 272–365.

[16] S. Royer, D. Duprez, Catalytic oxidation of carbon monoxide on transition metal oxides, ChemCatChem 3 (2011) 24-65.
[17] G. Li, L. Li, B. Wu, J. Li, Y. Yuan, J. Shi , Controlled one-step synthesis of Pt decorated octahedral Fe3O4 and its excellent catalytic performance for CO oxidation, Nanoscale, 7 (2015) 17855–17860.
[18] L. Hu, Q. Peng, Y. Li, Selective Synthesis of Co_3O_4 nanocrystal with different shape and crystal plane effect on catalytic property for methane combustion, J. Am. Chem. Soc. 130 (2008) 16136–16137.
[19] G. Evans, I. V. Kozhevnikov, E. F. Kozhevnikova, J. B. Claridge, R. Vaidhyanathan, C. Dickinson, C. D. Wood, A. I. Cooper, M. J. Rosseinsky, Particle size–activity relationship for $CoFe_2O_4$nanoparticle CO oxidation catalysts, J. Mater. Chem. 18 (2008) 5518–5523.
[20] C. Shao, X. Liu, D. Meng, Q. Xu, Y. Guo, Y. Guo, W. Zhan, L. Wang, G. Lu, Catalytic performance of Co–Fe mixed oxide for NH3-SCR reaction and the promotional role of cobalt, RSC Adv. 6 (2016) 66169–66179.
[21] K. Rida, A.López Cámara, M.A. Peña, C.L. Bolívar-Díaz, A. Martínez-Arias, Bimetallic Co-Fe and Co-Cr oxide systems supported on CeO2: Characterization and CO oxidation catalytic behavior, Int. J. Hydrogen Energy 40 (2015) 11267-11278.
[22] M. A. Peña, J. L. G. Fierro, Chemical Structures and Performance of Perovskite Oxides, Chem. Rev. 101 (2001) 1981-2017.
[23] S. Royer, D. Duprez, F. Can, X. Courtois, C. Batiot-Dupeyrat, S. Laassiri, H. Alamdari , Perovskites as substitutes of noble metals for heterogeneous catalysis: dream or reality, Chem. Rev. 114 (2014) 10292−10368.
[24] H. Najjar, H. Batis, Development of Mn-based perovskite materials: Chemical structure and applications, Catal. Rev.-Sci. Eng. 58 (2016) 371-438.
[25] J. A. Bennett, K. Wilson, A. F. Lee, Catalytic applications of waste derived materials, J. Mater. Chem. A 4 (2016) 3617–3637.
[26] R. Burch, M. J. Hayes, C-H bond activation in hydrocarbon oxidation on solid catalysts, J. Mol. Cata. A: Chemicals, 100 (1995) 13-33.
[27] F. Diehl, J. Barbier Jr, D. Duprez, I. Guibard, G. Mabilon, Catalytic oxidation of heavy hydrocarbons over Pt/Al_2O_3. Influence of the structure of the molecule on its reactivity. Appl. Catal. B: Environmental 95 (2010) 217–227.
[28] D. Duprez, Study of surface reaction mechanisms by $^{16}O/^{18}O$ and H/D isotopic exchange, Catal. Today 112 (2006) 17-22.
[29] P. Mars, D. W. van Krevelen, Oxidations carried out by means of vanadium oxide catalysts, Chem. Eng. Sci., Special Suppl. 3 (1954) 41-57.
[30] G. K. Boreskov, V. S. Muzykantov,Investigation of oxide-type oxidation catalysts by reaction of oxygen isotopic exchange, Ann. N. Y. Acad. Sci. 213 (1973) 137-160.
[31] W. Yang, R. Zhang, B. Chen, N. Bion, D. Duprez, L. Hou, H. Zhang, S. Royer, Design of nanocrystalline mixed oxides with improved oxygen mobility: a simple non-aqueous route to nano-LaFeO3 and the consequences on the catalytic oxidation performances, Chem. Comm. 49 (2013) 4923-4925.
[32] S. Laassiri, N. Bion, D. Duprez, H. Alamdari, S. Royer, Role of M^{n+} cations in the redox and oxygen transfer properties of $BaM_xAl_{12-x}O_{19-\delta}$ (M = Mn, Fe, Co) nanomaterials for high temperature methane oxidation, Catal. Sci. Technol. 3 (2013) 2259-2269.
[33] S. Laassiri, N. Bion, D. Duprez, S. Royer, H. Alamdari, Clear microstructure–performance relationships in Mn-containing perovskite and hexaaluminate compounds prepared by activated reactive synthesis, Phys. Chem. Chem. Phys. 16 (2014) 4050-4060.
[34] M. Richard, F. Can, D. Duprez, S. Gil, A. Giroir-Fendler, N. Bion, Remarkable enhancement of O_2 activation on yttrium-stabilized zirconia surface in a dual catalyst bed, Angew. Chem. Int. Ed. 53 (2014) 11342-11345.
[35] M. Richard, F. Can, S. Gil, A. Giroir-Fendler , D. Duprez, N. Bion, Study of lanthanum manganate and yttrium-stabilized zirconia-supported palladium dual-bed catalyst system for the total oxidation of methane :A study by $^{18}O_2/^{16}O_2$ isotopic exchange, ChemCatChem 8 (2016) 1921 –1928.
[36] C.-J. Liang, J. W. Fang, Predicting the kinetics of catalytic oxidation of multicomponent organic waste gases, Chem. Eng. Sci. 144 (2016) 101–107.
[37] M. A. Vannice, An analysis of the Mars–van Krevelen rate expression, Catal. Today, 123 (2007) 18–22.
[38] S. Keav, S. Kumar Matam, D. Ferri, A. Weidenkaff, Structured Perovskite-Based Catalysts and Their Application as Three-Way Catalytic Converters-A Review, Catalysts 4 (2014) 226-255.
[39] F. S. Toniolo, M. Schmal, Improvement of Catalytic Performance of Perovskites by Partial Substitution of Cations and Supporting on HighSurface Area Materials, in *Perovskite Materials - Synthesis, Characterisation, Properties, and Applications* (Likun Pan and Guang Zhu, Eds), InTech publ. Rijeka, Croatia (2016).
[40] A. Ladavos, P. Pomonis, Methane Combustion on Perovskites, in *Perovskites and Related Mixed Oxides: Concepts and Applications* (P. Granger, V. I. Parvulescu, S. Kaliaguine, W. Prellier, Eds) Wiley VCH Publ. (2016).

[41] Y. Yu, T. Takei, H. Ohashi, H. He, X. Zhang, M. Haruta, Pretreatments of Co_3O_4 at moderate temperature for CO oxidation at -80°C, J. Catal. 267 (2009) 121-128.
[42] P. Broqvist, I. Panas, H. Persson, A DFT Study on CO Oxidation over Co_3O_4 , J. Catal. 210 (2002) 198-206.
[43] A. K. Kandalam, B. Chatterjee, S.N. Khanna, B.K. Rao, P. Jena, B.V. Reddy, Oxidation of CO on Fe_2O_3 model surfaces, Surf. Sci. 601 (2007) 4873-4880.
[44] S. Wagloehner, D. Reichert, D. Leon-Sorzano, P. Balle, B. Geiger, S. Kureti, Kinetic modeling of the oxidation of CO on Fe_2O_3 catalyst in excess of O2, J. Catal. 260 (2008) 305-314.
[45] D. Ciuparu, M. R. Lyubovsky, E. Altman, L. D. Pfefferle, A. Datye, Catalytic combustion of methane over palladium-based catalysts, Catal. Rev.-Sci. Eng. 44 (2002) 593-649.
[46] P. Gélin, M. Primet, Complete oxidation of methane at low temperature over noble metal based catalysts: a review, Appl. Catal. B: Environmental, 39 (2002) 1-37.
[47] S. Royer, C. Ayrault, C. Carnevillier, F. Epron, P. Marécot, D. Duprez, Enthalpy recovery of gases issued from H2 production processes: Activity and stability of oxide and noble metal catalysts in oxidation reaction under highly severe conditions, Catal. Today 117 (2006) 543–548.
[48] S. Pengpanich, V. Meeyoo, T. Rirksomboon, K. Bunyakiat, Catalytic oxidation of methane over CeO_2-ZrO_2 mixed oxide solid solution catalysts prepared via urea hydrolysis, Appl. Catal. A General 234 (2002) 221-233.
[49] V. C. Belessi, A. K. Ladavos, G. S. Armatas and P. J. Pomonis , Kinetics of methane oxidation over La-Sr-Ce-Fe-O mixed oxide solids, Phys. Chem. Chem. Phys. 3 (2001) 3856-3862.
[50] F. Zasada, W. Piskorz, J. Janas, J. Gryboś , P. Indyka, Z. Sojka, Reactive Oxygen Species on the (100) Facet of Cobalt Spinel Nanocatalyst and their Relevance in $^{16}O_2/^{18}O_2$ Isotopic Exchange, *de*N2O,and *de*CH_4 Processes. A Theoretical and Experimental Account, ACS Catal. 5 (2015) 6879–6892.
[51] C. Liu, H. Xian, Z. Jiang, L. Wang, J. Zhang, L. Zheng, Y. Tan, X. Li, Insight into the improvement effect of the Ce doping into the SnO2 catalyst for the catalytic combustion of methane, Appl. Catal. B: Environmental 176-177 (2015) 542-552.
[52] I. Popescu, Y. Wu, P. Granger, I.-C. Marcu, An *in situ* electrical conductivity study of LaCoFe perovskite-based catalysts in correlation with the total oxidation of methane, Appl. Catal. A: General 485 (2014) 20-27.
[53] Y.-F.Y. Yao, The oxidation of hydrocarbons and CO over metal oxides: III. Co3O4, J. Catal. 33 (1974) 108–122.
[54] D. H. Cunningham, T. Kobayashi, N. Kamijo, M. Haruta, Influence of dry operating conditions: observation of oscillations and low temperature CO oxidation over Co3O4 and Au/Co3O4 catalysts, Catal. Lett. 25 (1994) 257–264.
[55] J. Jansson, A.E.C. Palmqvist, E. Fridell, M. Skoglundh, L. Osterlund, P. Thormahlen, V. Langer, On the catalytic activity of Co3O4 in low-temperature CO oxidation, J. Catal. 211 (2002) 387–397.
[56] Y. Zhou, Y. Li, W. Shen, Shape Engineering of Oxide Nanoparticles for Heterogeneous Catalysis, Chem. – Asian J. 11 (2016) 1470–1488.
[57] L.F. Liotta, H. Wu, G. Pantaleo, A.M. Venezia, Co3O4 nanocrystals and Co3O4–MOx binary oxides for CO, CH_4 and VOC oxidation at low temperatures: a review, Catal. Sci. Technol. 3 (2013) 3085–3102.
[58] J. Pal, T. Pal, Faceted metal and metal oxide nanoparticles: design, fabrication and catalysis, Nanoscale. 7 (2015) 14159–14190.
[59] X. Xie, Y. Li, Z.-Q. Liu, M. Haruta, W. Shen, Low-temperature oxidation of CO catalysed by Co_3O_4 nanorods, Nature. 458 (2009) 746-749.
[60] P. Broqvist, I. Panas, H. Persson, A DFT Study on CO Oxidation over Co3O4, J. Catal. 210 (2002) 198–206.
[61] L. Hu, K. Sun, Q. Peng, B. Xu, Y. Li, Surface active sites on Co_3O_4 nanobelt and nanocube model catalysts for CO oxidation, Nano Res. 3 (2010) 363-368.
[62] V. Iablokov, R. Barbosa, G. Pollefeyt, I. Van Driessche, S. Chenakin, N. Kruse, Catalytic CO Oxidation over Well-Defined Cobalt Oxide Nanoparticles: Size-Reactivity Correlation, ACS Catal. 5 (2015) 5714-5718.
[63] Y. Yu, T. Takei, H. Ohashi, H. He, X. Zhang, M. Haruta, Pretreatments of Co3O4 at moderate temperature for CO oxidation at −80 °C, J. Catal. 267 (2009) 121–128.
[64] A. Trovarelli, P. Fornasiero, World Scientific (Firm), Catalysis by ceria and related materials, Imperial College Press; Distributed by World Scientific Pub. Co., London; Singapore, 2013.
[65] H.C. Yao, Y.F.Y. Yao, Ceria in automotive exhaust catalysts: I. Oxygen storage, J. Catal. 86 (1984) 254–265.
[66] A. Trovarelli, Catalytic properties of ceria and CeO_2-containing materials, Catal. Rev.-Sci. Eng. 38 (1996) 439–520.
[67] S. Bedrane, C. Descorme, D. Duprez, $^{16}O/^{18}O$ isotopic exchange: A powerful tool to investigate oxygen activation on $M/Ce_xZr_{1-x}O_2$ catalysts, Appl. Catal. Gen. 289 (2005) 90-96.

[68] Y. Madier, C. Descorme, A.M. Le Govic, D. Duprez, Oxygen Mobility in CeO_2 and $Ce_xZr_{(1-x)}O_2$ Compounds: Study by CO Transient Oxidation and $^{18}O/^{16}O$ Isotopic Exchange, J. Phys. Chem. B. 103 (1999) 10999-11006.
[69] A. Galdikas, C. Descorme, D. Duprez, F. Dong, H. Shinjoh, Study of the oxygen diffusion on three-way catalysts: a kinetic model, Top. Catal. 30–31 (2004) 405-409.
[70] C. Descorme, Y. Madier, D. Duprez, Infrared Study of Oxygen Adsorption and Activation on Cerium–Zirconium Mixed Oxides, J. Catal. 196 (2000) 167-173.
[71] T. Montini, M. Melchionna, M. Monai, P. Fornasiero, Fundamentals and Catalytic Applications of CeO_2-Based Materials, Chem. Rev. 116 (2016) 5987-6041.
[72] Z. Wu, M. Li, S.H. Overbury, On the structure dependence of CO oxidation over CeO_2 nanocrystals with well-defined surface planes, J. Catal. 285 (2012) 61-73.
[73] K. Wu, L.-D. Sun, C.-H. Yan, Recent Progress in Well-Controlled Synthesis of Ceria-Based Nanocatalysts towards Enhanced Catalytic Performance, Adv. Energy Mater. 6 (2016) 1600501.
[74] E. Aneggi, J. Llorca, M. Boaro, A. Trovarelli, Surface-structure sensitivity of CO oxidation over polycrystalline ceria powders, J. Catal. 234 (2005) 88-95.
[75] X. Liu, K. Zhou, L. Wang, B. Wang, Y. Li, Oxygen Vacancy Clusters Promoting Reducibility and Activity of Ceria Nanorods, J. Am. Chem. Soc. 131 (2009) 3140-3141.
[76] F. Esch, S. Fabris, L. Zhou, T. Montini, C. Africh, P. Fornasiero, G. Comelli, R. Rosei, Electron localization determines defect formation on ceria substrates, Science. 309 (2005) 752-755.
[77] Y. Gao, R. Li, S. Chen, L. Luo, T. Cao, W. Huang, Morphology-dependent interplay of reduction behaviors, oxygen vacancies and hydroxyl reactivity of CeO_2 nanocrystals, Phys. Chem. Chem. Phys. 17 (2015) 31862-31871.
[78] Y. Sun, Q. Liu, S. Gao, H. Cheng, F. Lei, Z. Sun, Y. Jiang, H. Su, S. Wei, Y. Xie, Pits confined in ultrathin cerium(IV) oxide for studying catalytic centers in carbon monoxide oxidation, Nat. Commun. 4 (2013) 2899.
[79] Y. Sun, S. Gao, F. Lei, Y. Xie, Atomically-thin two-dimensional sheets for understanding active sites in catalysis, Chem. Soc. Rev. 44 (2015) 623–636.
[80] J. Gao, C. Jia, L. Zhang, H. Wang, Y. Yang, S.-F. Hung, Y.-Y. Hsu, B. Liu, Tuning chemical bonding of MnO_2 through transition-metal doping for enhanced CO oxidation, J. Catal. 341 (2016) 82–90.
[81] S. Liang, F. Teng, G. Bulgan, R. Zong, Y. Zhu, Effect of Phase Structure of MnO_2 Nanorod Catalyst on the Activity for CO Oxidation, J. Phys. Chem. C. 112 (2008) 5307–5315.
[82] E.R. Stobbe, B.A. de Boer, J.W. Geus, The reduction and oxidation behaviour of manganese oxides, Catal. Today. 47 (1999) 161–167.
[83] J. Xu, Y.-Q. Deng, Y. Luo, W. Mao, X.-J. Yang, Y.-F. Han, Operando Raman spectroscopy and kinetic study of low-temperature CO oxidation on an α-Mn_2O_3 nanocatalyst, J. Catal. 300 (2013) 225–234.
[84] P. Venkataswamy, K.N. Rao, D. Jampaiah, B.M. Reddy, Nanostructured manganese doped ceria solid solutions for CO oxidation at lower temperatures, Appl. Catal. B Environ. 162 (2015) 122–132.
[85] K.R. Barnard, K. Foger, T.W. Turney, R.D. Williams, Lanthanum cobalt oxide oxidation catalysts derived from mixed hydroxide precursors, J. Catal. 125 (1990) 265–275.
[86] J. Shu, S. Kaliaguine, Well-dispersed perovskite-type oxidation catalysts, Appl. Catal. B Environ. 16 (1998) L303–L308.
[87] B. Levasseur, S. Kaliaguine, Effects of iron and cerium in La1−yCeyCo1−xFexO3 perovskites as catalysts for VOC oxidation, Appl. Catal. B Environ. 88 (2009) 305–314.
[88] L.A. Isupova, G.M. Alikina, S.V. Tsybulya, N.N. Boldyreva, G.N. Kryukova, I.S. Yakovleva, V.P. Isupov, V.A. Sadykov, Real structure and catalytic activity of La1−xSrxCoO3 perovskites, Int. J. Inorg. Mater. 3 (2001) 559–562.
[89] K.S. Chan, J. Ma, S. Jaenicke, G.K. Chuah, J.Y. Lee, Catalytic carbon monoxide oxidation over strontium, cerium and copper-substituted lanthanum manganates and cobaltates, Appl. Catal. Gen. 107 (1994) 201–227.
[90] W. Yang, R. Zhang, B. Chen, N. Bion, D. Duprez, S. Royer, Activity of perovskite-type mixed oxides for the low-temperature CO oxidation: Evidence of oxygen species participation from the solid, J. Catal. 295 (2012) 45–58.
[91] R.W. Howarth, R. Santoro, A. Ingraffea, Methane and the greenhouse-gas footprint of natural gas from shale formations, Clim. Change. 106 (2011) 679.
[92] P. Gélin, M. Primet, Complete oxidation of methane at low temperature over noble metal based catalysts: a review, Appl. Catal. B Environ. 39 (2002) 1–37.
[93] D. Ciuparu, M.R. Lyubovsky, E. Altman, L.D. Pfefferle, A. Datye, Catalytic combustion of methane over palladium-based catalysts, Catal. Rev. 44 (2002) 593–649.
[94] J. Chen, H. Arandiyan, X. Gao, J. Li, Recent Advances in Catalysts for Methane Combustion, Catal. Surv. Asia. 19 (2015) 140–171.

[95] L. Hu, Q. Peng, Y. Li, Selective Synthesis of Co_3O_4 Nanocrystal with Different Shape and Crystal Plane Effect on Catalytic Property for Methane Combustion, J. Am. Chem. Soc. 130 (2008) 16136–16137.
[96] F. Teng, M. Chen, G. Li, Y. Teng, T. Xu, Y. Hang, W. Yao, S. Santhanagopalan, D.D. Meng, Y. Zhu, High combustion activity of CH_4 and cataluminescence properties of CO oxidation over porous Co_3O_4 nanorods, Appl. Catal. B Environ. 110 (2011) 133–140.
[97] J. Li, X. Liang, S. Xu, J. Hao, Catalytic performance of manganese cobalt oxides on methane combustion at low temperature, Appl. Catal. B Environ. 90 (2009) 307–312.
[98] H. Li, G. Lu, D. Qiao, Y. Wang, Y. Guo, Y. Guo, Catalytic Methane Combustion over Co_3O_4/CeO_2 Composite Oxides Prepared by Modified Citrate Sol–Gel Method, Catal. Lett. 141 (2011) 452–458.
[99] Y.-F. Han, L. Chen, K. Ramesh, E. Widjaja, S. Chilukoti, I. Kesumawinata Surjami, J. Chen, Kinetic and spectroscopic study of methane combustion over α-Mn_2O_3 nanocrystal catalysts, J. Catal. 253 (2008) 261–268.
[100] G. Zhou, P.R. Shah, R.J. Gorte, A Study of Cerium–Manganese Mixed Oxides for Oxidation Catalysis, Catal. Lett. 120 (2008) 191–197.
[101] C. Oliva, M. Allieta, M. Scavini, C. Biffi, I. Rossetti, L. Forni, Electron Paramagnetic Resonance Analysis of $La_{1-x}M_xMnO_{3+\delta}$ (M = Ce, Sr) Perovskite-Like Nanostructured Catalysts, Inorg. Chem. 51 (2012) 8433–8440.
[102] S. Royer, F. Bérubé, S. Kaliaguine, Effect of the synthesis conditions on the redox and catalytic properties in oxidation reactions of $LaCo_{1-x}Fe_xO_3$, Appl. Catal. Gen. 282 (2005) 273–284.
[103] S. Royer, D. Duprez, S. Kaliaguine, Role of bulk and grain boundary oxygen mobility in the catalytic oxidation activity of $LaCo_{1-x}Fe_xO_3$, J. Catal. 234 (2005) 364–375.
[104] X. Zhang, H. Li, Y. Li, W. Shen, Structural Properties and Catalytic Activity of Sr-Substituted $LaFeO_3$ Perovskite, Chin. J. Catal. 33 (2012) 1109–1114.
[105] E. Campagnoli, A.C. Tavares, L. Fabbrini, I. Rossetti, Y.A. Dubitsky, A. Zaopo, L. Forni, $La_{1-x}A_xCo_{1-y}Fe_yO_{3\pm\delta}$ (A = Ce,Sr) catalysts for the flameless combustion of methane, J. Mater. Sci. 41 (2006) 4713–4719.
[106] N. Iyi, S. Takekawa, S. Kimura, Crystal chemistry of hexaaluminates: β-alumina and magnetoplumbite structures, J. Solid State Chem. 83 (1989) 8–19.
[107] M. Tian, X.D. Wang, T. Zhang, Hexaaluminates: a review of the structure, synthesis and catalytic performance, Catal. Sci. Technol. 6 (2016) 1984–2004.
[108] M. Machida, K. Eguchi, H. Arai, Catalytic properties of $BaMAl_{11}O_{19-\alpha}$ (M = Cr, Mn, Fe, Co, and Ni) for high-temperature catalytic combustion, J. Catal. 120 (1989) 377–386.
[109] H. Huang, Y. Xu, Q. Feng, D. Y. C. Leung, Low temperature catalytic oxidation of volatile organic compounds: a review, Catal. Sci. Technol. 5 (2015) 2649-2669.
[110] Z. Zhang, Z. Jiang, W. Shangguan, Low-temperature catalysis for VOCs removal in technology and application: A state-of-the-art review, Catal. Today 264 (2016) 270-278
[111] D. Delimaris, T. Ioannides, VOC oxidation over MnO_x–CeO_2 catalysts prepared by a combustion method, Appl. Catal. B: Environmental 84 (2008) 303-312.
[112] D. Delimaris, T. Ioannides, VOC oxidation over CuO-CeO_2 catalysts prepared by a combustion method, Appl. Catal. B: Environmental 89 (2009) 295-302.
[113] C. Hu, Catalytic combustion kinetics of acetone and toluene over $Cu_{0.13}Ce_{0.87}O_y$ catalyst, Chem. Eng. J. 168 (2011) 1185-1192.
[114] S. A. C. Carabineiro, X. Chen, M. Konsolakis, A. C. Psarras, P. B. Tavares, J. J. M. Órfão, M. F. R. Pereira, J. L. Figueiredo, Catalytic oxidation of toluene on Ce-Co and La-Co mixed oxides synthesized by exotemplating and evaporation methods, Catal. Today 244 (2015) 161-171.
[115] E. Colman-Lerner, M. A. Peluso, J. Sambeth, H. Thomas, Cerium, manganese and cerium/manganese ceramic monolithic catalysts. Study of VOCs and PM removal , J. Rare Earths 34 (2016) 675-682.
[116] T. Garcia, B. Solsona, S. H. Taylor, The catalytic oxidation of hydrocarbon volatile organic compounds, in *"Handbook of advanced methods and processes in oxidation catalysis"* (D. Duprez, F. Cavani, Eds) Imperial College Press, London, 2014. Chapter 3, pp 51-90.
[117] M. Konsolakis, The role of Copper-Ceria interactions in catalysis science: Recent theoretical and experimental advances, Appl. Catal. B: Environmental 198 (2016) 49-66.
[118] B. Faure, P. Alphonse, Co-Mn-oxide spinel catalysts for CO and propane oxidation at mild temperature, Appl. Catal. B: Environmental 180 (2016) 715-725.
[119] T. Garcia, S. Agouram, J. F. Sánchez-Royo, R. Murillo, A. M. Mastral, A. Aranda, I. Vázquez, A. Dejoz, B. Solsona, Deep oxidation of volatile organic compounds using ordered cobalt oxides prepared by a nanocasting route, Appl. Catal. A: General 386 (2010) 16-27.

[120] Z. Ren, Z.Wu, W. Song, W. Xiao, Y. Guo, J. Ding, S. L. Suib, P.-X. Gao, Low temperature propane oxidation over Co_3O_4 based nano-array catalysts: Ni dopant effect, reaction mechanism and structural stability, Appl. Catal. B: Environmental 180 (2016) 150-160.
[121] B. Solsona, T. García, R. Sanchis, M. D. Soriano, M. Moreno, E. Rodríguez-Castellón, S. Agouram, A. Dejoz, J. M. López Nieto, Total oxidation of VOCs on mesoporous iron oxide catalysts: Soft chemistry route versus hard template method, Chem. Eng. J. 290 (2016) 273-281.
[122] H. A. Almukhlifi, R. C. Burns, The effects of gold nanoparticles obtained from the thermolysis of n-hexanethiolate-stabilized gold nanoparticles on isobutane oxidation over metal oxide catalysts, J. Molec. Catal. A: Chemical 411 (2016) 349-363.
[123] H. A. Almukhlifi, R. C. Burns, The complete oxidation of isobutane over CeO_2 and Au/CeO_2, and the composite catalysts MOx/CeO_2 and $Au/MOx/CeO_2$ (M^{n+} = Mn, Fe, Co and Ni): the effects of gold nanoparticles obtained from n-hexanethiolate-stabilized gold nanoparticles, J. Molec. Catal. A: Chemical 415 (2016) 131-143.
[124] F.Wyrwalski, J.-M. Giraudon, J.-F. Lamonier, Synergistic Coupling of the Redox Properties of Supports and Cobalt Oxide Co_3O_4 for the Complete Oxidation of Volatile Organic Compounds, Catal. Lett. 137 (2010) 141-149.
[125] M. Assebban, Z.-Y. Tian, A. El Kasmi, N. Bahlawane, S. Harti, T. Chafik, Catalytic complete oxidation of acetylene and propene over clay versus cordierite honeycomb monoliths without and with chemical vapor deposited cobalt oxide, Chem. Eng. J. 262 (2015) 1252-1259.
[126] Z. Wang, G. Shen, J. Li, H. Liu, Q. Wang, Y. Chen, Catalytic removal of benzene over CeO_2-MnO_x composite oxides prepared by hydrothermal method, Appl. Catal. B: Environmental 138-139 (2013) 253-259.
[127] W. Tang, X. Wua, S. Li, X. Shan, G. Liu, Y. Chen, Co-nanocasting synthesis of mesoporous Cu-Mn composite oxides and their promoted catalytic activities for gaseous benzene removal, Appl. Catal. B: Environmental 162 (2015) 110-121.
[128] S. Mo, S. Li, W. Li, J. Li, J. Chen, Y. Chen, Excellent low temperature performance for total benzene oxidation over mesoporous CoMnAl composited oxides from hydrotalcites, J. Mater. Chem. A, 4 (2016) 8113-8122.
[129] B. Li, Y. Chen, L. Li, J. Kan, S. Hea, B. Yang, S. Shen, S. Zhu, Reaction kinetics and mechanism of benzene combustion over the $NiMnO_3/CeO_2$/Cordierite catalyst, J. Mol. Catal. A: Chemical, 415 (2016) 160-167.
[130] C. Zhang, Y. Guo, Y. Guo, G. Lu, A. Boreave, L. Retailleau, A. Baylet, A. Giroir-Fendler, $LaMnO_3$ perovskite oxides prepared by different methods for catalytic oxidation of toluene, Appl. Catal. B: Environmental 148–149 (2014) 490–498.
[131] A. Giroir-Fendler, M. Alves-Fortunato, M. Richard, C. Wang, J. Antonio Díaz, S. Gil, C. Zhang, F. Can, N. Bion, Y. Guo, Synthesis of oxide supported LaMnO3 perovskites to enhance yields in toluene combustion, Appl. Catal. B: Environmental 180 (2016) 29-37.
[132] Y. Wang, S. Xie, J. Deng, S. Deng, H. Wang, H. Yan, H. Dai, Morphologically Controlled Synthesis of Porous Spherical and Cubic LaMnO3 with High Activity for the Catalytic Removal of Toluene, ACS Appl. Mater. Interfaces, 6 (2014) 17394–17401.
[133] W. Si, Y. Wang, S. Zhao, F. Hu, J. Li, A Facile Method for in Situ Preparation of the $MnO_2/LaMnO_3$ Catalyst for the Removal of Toluene, Environ. Sci. Technol., 50 (2016) 4572-4578.
[134] S. Behar, N.-A. Gómez-Mendoza, M.-Á. Gómez-García, D. Świerczyński, F. Quignard, N. Tanchoux, Study and modelling of kinetics of the oxidation of VOC catalyzed by nanosized Cu–Mn spinels prepared via an alginate route, Appl. Catal. A: General 504 (2015) 203-210.
[135] H. Sun, Z. Liu, S. Chen, X. Quan, The role of lattice oxygen on the activity and selectivity of the OMS-2 catalyst for the total oxidation of toluene, Chem. Eng. J. 270 (2015) 58-65.
[136] D. Chlala, J.-M. Giraudon, N. Nuns, C. Lancelot, Rose-Noëlle Vannier, M. Labaki, J.-F. Lamonier, Active Mn species well dispersed on Ca^{2+} enriched apatite for total oxidation of toluene, Appl. Catal. B: Environmental 184 (2016) 87-95.
[137] E. Genty, J. Brunet, C. Poupin, S. Casale, S. Capelle, P. Massiani, S. Siffert, R. Cousin, Co-Al mixed oxides prepared via LDH route using microwaves or ultrasound: Application for catalytic toluene total oxidation, Catalysts 5 (2015) 851-867.
[138] A. Pérez, R. Molina, S. Moreno, Enhanced VOC oxidation over Ce/CoMgAl mixed oxides using a reconstruction method with EDTA precursors, Appl. Catal. A: General 477 (2014) 109-116.
[139] S. A. C. Carabineiro, X. Chen, M. Konsolakis, A. C. Psarras, P. B. Tavares, J. J. M. Órfãoa, M. F. R. Pereira, J.L. Figueiredo, Catalytic oxidation of toluene on Ce–Co and La–Co mixed oxides synthesized by exotemplating and evaporation methods, Catal. Today 244 (2015) 161-171.

[140] G. S. P. Soylu, Z. Özçelik, I. Boz, Total oxidation of toluene over metal oxides supported on a natural clinoptilolite-type zeolite, Chem. Eng. J. 162 (2010) 380-387.
[141] U. Menon, V. V. Galvita, G. B. Marin, Reaction network for the total oxidation of toluene over CuO–CeO2/Al2O3, J. Catal. 283 (2011) 1-9.
[142] M. Zabihi, F. Khorasheh, J. Shayegan, Supported copper and cobalt oxides on activated carbon for simultaneous oxidation of toluene and cyclohexane in air, RSC Adv. 5 (2015) 5107-5122.
[143] L. C. Loc, N. Tri, H. T. Cuong, H. S. Thoang, Yu. A. Agafonov, N. A. Gaidaib, N. V. Nekrasov, A. L. Lapidus, Kinetics of the total oxidation of *para*-xylene and its mixtures with carbon monoxide over supported copper catalysts, Kinet. Catal. 55 (2014) 611-619.
[144] T. García, B. Solsona, S. H. Taylor, Naphthalene total oxidation over metal oxide catalysts, Appl. Catal. B: Environmental 66 (2006) 92-99.
[145] E. N. Ndifor, T. García, B. Solsona, S. H. Taylor, Influence of preparation conditions of nano-crystalline ceria catalysts on the total oxidation of naphthalene, a model polycyclic aromatic hydrocarbon, Appl. Catal. B: Environmental 76 (2007) 248-256.
[146] B. Puertolas, B. Solsona, S. Agouram, R. Murillo, A. M. Mastral, A. Aranda, S. H. Taylor, T. García, The catalytic performance of mesoporous cerium oxides prepared through a nanocasting route for the total oxidation of naphthalene, Appl. Catal. B: Environmental 93 (2010) 395-405.
[147] L. Torrente-Murciano, A. Gilbanka, B. Puertolas, T. García, B. Solsona, D. Chadwick, Shape-dependency activity of nanostructured CeO_2 in the total oxidation of polycyclic aromatic hydrocarbons, Appl. Catal. B: Environmental 132-133 (2013) 116-122.
[148] A. Aranda, E. Aylón, B. Solsona, R. Murillo, A. M. Mastral, D. R. Sellick, S. Agouram, T. García, S. H. Taylor, High activity mesoporous copper doped cerium oxide catalysts for the total oxidation of polyaromatic hydrocarbon pollutants, Chem. Comm. 48 (2012) 4704-4706.
[149] M. Baldi, E. Finocchio, F. Milella, G. Busca, Catalytic combustion of C3 hydrocarbons and oxygenates over Mn_3O_4, Appl. Catal. B: Environmental 16 (1998) 43-51.
[150] V. Blasin-Aubé, J. Belkouch, L. Monceaux, General study of catalytic oxidation of various VOCs over $La_{0.8}Sr_{0.2}MnO_{3+x}$ perovskite catalyst-influence of mixture, Appl. Catal. B: Environmental 43 (2003) 175–186.
[151] M. Assebban, A. El Kasmi, S. Harti, T. Chafik, Intrinsic catalytic properties of extruded clay honeycomb monolith toward complete oxidation of air pollutants, J. Hazard. Mater. 300 (2015) 590-597.
[152] N. Rezlescu, E. Rezlescu, P. Dorin Popa, C. Doroftei, M. Ignat, Some nanograined ferrites and perovskites for catalytic combustion of acetone at low temperature, Ceram. Intern. 41 (2015) 4430-4437.
[153] L.-Y. Lin, H. Bai, Promotional effects of manganese on the structure and activity of Ce–Al–Si based catalysts for low-temperature oxidation of acetone, Chem. Eng. J. 291 (2016) 94-105.
[154] R. Qin, J. Chen, X. Gao, X. Zhu, X. Yu, K. Cen, Catalytic oxidation of acetone over CuCeOx nanofibers prepared by an electrospinning method, RSC Adv. 4 (2014) 43874–43881.
[155] N. Bion, D. Duprez, F. Epron, Design of nanocatalysts for green hydrogen production from bioethanol, ChemSusChem, 5 (2012) 76-84.
[156] L. V. Mattos, G. Jacobs, B. H. Davis, F. B. Noronha, Production of hydrogen from ethanol: review of reaction mechanism and catalyst deactivation, Chem. Rev. 112 (2012) 4094-4123.
[157] G. Zhou, B. Gui, H. Xie, F. Yang, Y. Chen, S. Chen, X.Zheng, Influence of CeO_2 morphology on the catalytic oxidation of ethanol in air, J. Ind. Eng. Chem. 20 (2014) 160-165.
[158] B. Bai, J. Li, J. Hao, 1D-MnO_2, 2D-MnO_2 and 3D-MnO_2 for low-temperature oxidation of ethanol, Appl. Catal. B: Environmental 164 (2015) 241-250.
[159] C. Almquist, M. Krekeler, L. Jiang, An investigation on the structure and catalytic activity of cryptomelane-type manganese oxide materials prepared by different synthesis routes, Chem. Eng. J. 252 (2014) 249–262.
[160] J. Zhang, C. Zhang, H.He, Remarkable promotion effect of trace sulfation on OMS-2 nanorod catalysts for the catalytic combustion of ethanol, J. Environ. Sci. 35 (2015) 69-75.
[161] F. Kovanda, K. Jirátová, J. Ludvíková, H. Raabová, Co–Mn–Al mixed oxides on anodized aluminum supports and their use as catalysts in the total oxidation of ethanol, Appl. Catal. A: General 464-465 (2013) 181-190.
[162] K. Jirátová, F. Kovanda, J. Ludvíková, J. Balabánová, J. Klempa, Total oxidation of ethanol over layered double hydroxide-related mixed oxide catalysts: Effect of cation composition, Catal. Today 277 (2016) 61–67.
[163] Y.-C. Hou, M.-W. Ding, S.-K. Liu, S.-K. Wu, Y.-C. Lin, Ni-substituted $LaMnO_3$ perovskites for ethanol oxidation, RSC Adv. 4 (2014) 5329–5338.

[164] Y. Hammiche-Bellal, A. Djadoun, L. Meddour-Boukhobza, A.Benadda, A. Auroux, M.-H. Berger, F. Mernache, Effect of the preparation method on the structural and catalytic properties of spinel cobalt-iron oxide, Mater. Chem. Phys. 177 (2016) 384-397.
[165] M. Motak, Ł. Kuterasiński, P. Da Costa, B. Samojeden, Catalytic activity of layered aluminosilicates for VOC oxidation in the presence of NOx, C. R. Chimie 18 (2015) 1106-1113.
[166] T. Tsoncheva, G. Issa, J. M. López Nieto, T. Blasco, P. Concepcion, M. Dimitrova, G. Atanasova, D. Kovacheva, Pore topology control of supported on mesoporous silicas copper and cerium oxide catalysts for ethyl acetate oxidation, Micropor. Mesopor. Mater. 180 (2013) 156–161.
[167] X. Chen, S. A. C. Carabineiro, S. S. T. Bastos, P. B. Tavares, J. J. M. Órfãoa, M. F. R. Pereira, J. L. Figueiredo, Catalytic oxidation of ethyl acetate on cerium-containing mixed oxides, Appl. Catal. A: General 472 (2014) 101-112
[168] T. Tsoncheva, R. Ivanova, J. Henych, N. Velinov, M. Kormunda, M. Dimitrova, D. Paneva, M. Slušná, I. Mitov, V. Štengl, Iron modified titanium–hafnium binary oxides as catalysts in total oxidation of ethyl acetate, Catal. Comm. 81 (2016) 14-19.
[169] T. Tsoncheva, G. Issa, T. Blasco, M. Dimitrova, M. Popova, S. Hernández, D. Kovacheva, G. Atanasova, J. M. López Nieto, Catalytic VOCs elimination over copper and cerium oxide modified mesoporous SBA-15 silica, Appl. Catal. A: General 453 (2013) 1-12.
[170] M. Haidy Castaño, R. Molina, S. Moreno, Catalytic oxidation of VOCs on MnMgAlOx mixed oxides obtained by auto-combustion, J. Mol. Catal. A: Chemical 398 (2015) 358-367.
[171] D. Baojuan, L. Shumin, L. Deliang, Z. Ruozhu, L. Jingge, H. Qinglan, B. Feng, Catalytic oxidation of ethyl acetate and toluene over Cu–Ce–Zr supported ZSM-5/TiO_2 catalysts, RSC Adv. 6 (2016) 53852–53859.
[172] W. Tang, X.Wu, S. Li, W. Li, Y. Chen, Porous Mn–Co mixed oxide nanorod as a novel catalyst with enhanced catalytic activity for removal of VOCs, Catal. Comm. 56 (2014) 134-138.
[173] L. Bai, F. Wyrwalski, M. Safariamin, R. Bleta, J.-F. Lamonier, C. Przybylski, E. Monflier, A. Ponchel, Cyclodextrin-cobalt (II) molecule-ion pairs as precursors to active Co_3O_4/ZrO_2 catalysts for the complete oxidation of formaldehyde: Influence of the cobalt source, J. Catal. 341 (2016) 191-204.
[174] Y. Huang, W. Fan, B. Long, H. Li, W. Qiu, F. Zhao, Y. Tong, H. Ji, Alkali-modified non-precious metal 3D-$NiCo_2O_4$ nanosheets for efficient formaldehyde oxidation at low temperature, J. Mater. Chem. A 4 (2016) 3648-3654.
[175] P. Liu, H. He, G. Wei, X. Liang, F. Qia, F.Tan, W. Tan, J. Zhu, R. Zhu, Effect of Mn substitution on the promoted formaldehyde oxidation over spinel ferrite: Catalyst characterization, performance and reaction mechanism, Appl. Catal. B: Environmental 182 (2016) 476-484.
[176] W. Ling, Z. Huiping, Y. Ying, Z. Xinya, Total oxidation of isopropanol over manganese oxide modified ZSM-5 zeolite membrane catalysts, RSC Adv. 5 (2015) 29482–29490.
[177] L. Sivachandiran, F. Thevenet, A. Rousseau, Isopropanol removal using MnXOYpacked bed non-thermal plasma reactor: Comparison between continuous treatment and sequential sorption/regeneration, Chem. Eng. J. 270 (2015) 327-335.
[178] G. Lafaye, J. Barbier Jr., D. Duprez, Impact of cerium-based support oxides in catalytic wet air oxidation: Conflicting role of redox and acid-base properties, Catal. Today, 253 (2015) 89-98.
[179] V. Melang Me Nze, C. Fontaine, J. Barbier Jr, Preparation and characterization of MgAlCe mixed oxides for catalytic oxidation of acetic acid (in French), CR Chimie 20 (2017) 67-77.
[180] A. Aranzabal, B. Pereda-Ayo, M. Pilar González-Marcos, J. A. González-Marcos, R. López-Fonseca, J. R. González-Velasco, State of the art in catalytic oxidation of chlorinated volatile organic compounds, Chem. Papers 68 (2014) 1169–1186.
[181] J. R. González-Velasco, A. Aranzabal, B. Pereda-Ayo, M. Pilar González-Marcos, J. A. González-Marcos, Catalytic oxidation of volatile organic compounds: chlorinated hydrocarbons, in *"Handbook of advanced methods and processes in oxidation catalysis"* (D. Duprez, F. Cavani, Eds) Imperial College Press, London, 2014. Chapter 4, pp 91-131.
[182] S. Marie-Rose, M. Taralunga, X. Chaucherie, F. Nicol, E. Fiani, T. Belin, P. Magnoux, J. Mijoin, Zeolites as alternative catalysts for the oxidation of persistent organic pollutants, in *"Handbook of advanced methods and processes in oxidation catalysis"* (D. Duprez, F. Cavani, Eds) Imperial College Press, London, 2014. Chapter 5, pp 132-154.
[183] S.Cao, H. Wang, F. Yu, M. Shi, S. Chen, X. Weng, Y. Liu, Z. Wu, Catalyst performance and mechanism of catalytic combustion of dichloromethane (CH_2Cl_2) over Ce doped TiO_2, J. Colloid Interface Sci. 463 (2016) 233-241.
[184] P. Yang, Z. Meng, S. Yang, Z. Shi, R. Zhou, Highly active behaviors of CeO2-CrOx mixed oxide catalysts in deep oxidation of 1,2-dichloroethane, J. Mol. Catal. A: Chemical 393 (2014) 75-83.

[185] P. Yang, S. Zuo, Z. Shi, F. Tao, R. Zhou, Elimination of 1,2-dichloroethane over $(Ce,Cr)_xO_2/MO_y$ catalysts (M = Ti, V, Nb, Mo, W and La), Appl. Catal. B: Environmental 191 (2016) 53-61.
[186] B. de Rivas, C. Sampedro, E. V. Ramos-Fernández, R. López-Fonseca, J. Gascon, M. Makkee, J. I. Gutiérrez-Ortiz, Influence of the synthesis route on the catalytic oxidation of 1,2-dichloroethane over CeO_2/H-ZSM5 catalysts, Appl. Catal. A: General 456 (2013) 96-104.
[187] S.-X. Chen, Y. Wang, A.-P. Jia, H.-H. Liu, M.-F. Luo, J.-Q. Lu, Enhanced activity for catalytic oxidation of 1,2-dichloroethane over Al-substituted $LaMnO_3$ perovskite catalysts, Appl. Surf. Sci. 307 (2014) 178-188.
[188] Z. Boukha, J. González-Prior, B.de Rivas, J. R. González-Velasco, R. López-Fonseca, J. I. Gutiérrez-Ortiz, Synthesis, characterisation and behaviour of Co/hydroxyapatite catalysts in the oxidation of 1,2-dichloroethane, Appl. Catal. B: Environmental 190 (2016) 125-136.
[189] J. Gonzalez-Prior, J. I. Gutierrez-Ortiz, R. Lopez-Fonseca, G. Busca, E. Finocchio, B. de Rivas, Oxidation of chlorinated alkanes over Co_3O_4/SBA-15 catalysts. Structural characterization and reaction mechanism, Catal. Sci. Technol. 6 (2016) 5618-5630.
[190] P. Yang, S. Yang, Z. Shi, Z. Meng, R. Zhou, Deep oxidation of chlorinated VOCs over CeO_2-based transition metal mixed oxide catalysts, Appl. Catal. B: Environmental 162 (2015) 227-235.
[191] N. Blanch-Raga, A. E. Palomares, J. Martínez-Triguero, S. Valencia, Cu and Co modified beta zeolite catalysts for the trichloroethylene oxidation, Appl. Catal. B: Environmental 187 (2016) 90-97.
[192] M. T. Nguyen Dinh, J.-M. Giraudon, J.-F. Lamonier, A. Vandenbroucke, N. De Geyter, C. Leys, R. Morent, Plasma-catalysis of low TCE concentration in air using $LaMnO_{3+\delta}$ as catalyst, Appl. Catal. B: Environmental 147 (2014) 904– 911
[193] A. M. Vandenbroucke, M. Mora, C. Jiménez-Sanchidrián, F.J. Romero-Salguero, N. De Geyter, C. Leys, R. Morent, TCE abatement with a plasma-catalytic combined system using MnO_2 as catalyst, Appl. Catal. B: Environmental 156-157 (2014) 94-100.
[194] B. Zapata, F. Pedraza, M. A. Valenzuela, Catalyst screening for oxidative desulfurization using hydrogen peroxide, Catal. Today, 106 (2005) 219–221.
[195] N. D. McNamara, G. T. Neumann, E. T. Masko, J. A. Urban, J. C. Hicks, Catalytic performance and stability of (V) MIL-47 and (Ti) MIL-125 in the oxidative desulfurization of heterocyclic aromatic sulfur compounds, J. Catal. 305 (2013) 217–226.
[196] L. Gao, Y. Tang, Q. Xue, Y. Liu, Y. Lu, Hydrotalcite-like compounds derived CuZnAl oxide catalysts for aerobic oxidative removal of gasoline-range organosulfur compounds, Energy Fuels, 23 (2009) 624-630.
[197] S. Ojala, S. Pitkäaho, T. Laitinen, N. Niskala Koivikko, R. Brahmi, J. Gaálová, L. Matejova, A. Kucherov, S. Päivärinta, C. Hirschmann, T. Nevanperä, M. Riihimäki, M. Pirilä, R. L. Keiski, Catalysis in VOC Abatement, Top. Catal. 54 (2011) 1224-1256.
[198] I. Barnes, J. Hjorth, N. Mihalopoulos, Dimethyl sulfide and dimethyl sulfoxide and their oxidation in the atmosphere, Chem. Rev. 106 (2006) 940-975.
[199] V. G. Devulapelli, E. Sahle-Demessie, Catalytic oxidation of dimethyl sulfide with ozone: Effects of promoter and physico-chemical properties of metal oxide catalysts, Appl. Catal. A: General 348 (2008) 86–93.
[200] E. Sahle-Demessie, V. G. Devulapelli, Oxidation of methanol and total reduced sulfur compounds with ozone over V2O5/TiO2catalyst: Effect of humidity, Appl. Catal. A: General 361 (2009) 72–80.
[201] K. Chand Soni, S. Chandra Shekar, B. Singh, T. Gopi, Catalytic activity of Fe/ZrO2 nanoparticles for dimethyl sulfide oxidation, J. Colloid Interface Sci. 446 (2015) 226–236.
[202] J. He, . Liu, L. Li, B. Wang, J. Hu, Experimental investigation of the interaction of dimethyl sulfide/ethyl mercaptan with nano-manganese dioxide, Ind. Eng. Chem. Res. 51 (2012) 15912−15917.
[203] J. P. A. Neeft, M. Makkee, J. A. Moulijn, Catalytic oxidation of carbon black - 1. Activity of catalysts and classification of oxidation profiles, Fuels 77 (1998) 11-118.
[204] T. Jakubek, W. Kaspera, P. Legutko, P. Stelmachowski, A. Kotarba, How to efficiently promote transition metal oxides by alkali towards catalytic soot oxidation, Top. Catal. 59 (2016) 1083–1089.
[205] N. D. Wasalathanthri, T. M. SantaMaria, D. A. Kriz, S. L. Dissanayake, C.-H. Kuo, S. Biswas, S. L. Suib, Mesoporous manganese oxides for NO2 assisted catalytic soot oxidation, Appl. Catal. B: Environmental 201 (2017) 543–551.
[206] A. Mishra, R. Prasad, Preparation and application of perovskite catalysts for diesel soot emissions control: An overview, Catal. Rev. 56 (2014) 57-81.
[207] N. Labhasetwar, G. Saravanan, S. K. Megarajan, N. Manwar, R. Khobragade, P. Doggali, F. Grasset, Perovskite-type catalytic materials for environmental applications, Sci. Technol. Adv. Mater. 16 (2015) 036002.
[208] Y.-F. Sun, J.-H. Li, Y.-Q. Zhang, B. Hua, J.-L. Luo, Bifunctional catalyst of core−shell nanoparticles socketed on oxygen-deficient layered perovskite for soot combustion: In situ observation of synergistic dual active sites, ACS Catal. 6 (2016) 2710−2714.

[209] C. Lee, Y. Jeon, S. Hata, J.-I. Park, R. Akiyoshi, H. Saito, Y. Teraoka, Y.-G. Shul, H. Einaga, Three-dimensional arrangements of perovskite-type oxide nano-fiber webs for effective soot oxidation, Appl. Catal. B: Environmental 191 (2016) 157-164.
[210] L. Wang, S. Fang, N. Feng, H. Wan, G. Guan, Efficient catalytic removal of diesel soot over Mg substituted $K/La_{0.8}Ce_{0.2}CoO_3$ perovskites with large surface areas, Chem. Eng. J. 293 (2016) 68-74.
[211] W. Shao, Z. Wang, X. Zhang, L. Wang, Z. Ma, Q. Li, Z. Zhang, Promotion effects of cesium on perovskite oxides for catalytic soot combustion, Catal. Lett. 146 (2016) 1397–1407.
[212] R. Dinamarca, X. Garcia, R. Jimenez, J. L. G. Fierro, G. Pecchi, Effect of A-site deficiency in $LaMn_{0.9}Co_{0.1}O_3$ perovskites on their catalytic performance for soot combustion, Mater. Res. Bull. 81 (2016) 134-141.
[213] J. Wang, G. Yang, L. Cheng, E. Woo Shin, Y. Men, Three-dimensionally ordered macroporous spinel type MCr2O4(M = Co, Ni, Zn, Mn) catalysts with highly enhanced catalytic performance for soot combustion, Catal. Sci. Technol. 5 (2015) 4594-4601.
[214] X.Niu, L. Zhou, X. Hu, W. Han, Mesoporous $Ce_xCo_{1-x}Cr_2O_4$ spinels: synthesis, characterization and catalytic application in simultaneous removal of soot particulate and NO, RSC Adv. 5 (2015) 52595-52601.
[215] Z. Wang, H. Zhu, L. Ai, X. Liu, M. Lv, L. Wang, Z. Ma, Z. Zhang, Catalytic combustion of soot particulates over rare-earth substituted $Ln_2Sn_2O_7$ pyrochlores (Ln = La, Nd and Sm), J. Colloid Interface Sci. 478 (2016) 209-216.
[216] B. Bassou, N. Guilhaume, K. Lombaert, C. Mirodatos, D. Bianchi, Experimental microkinetic approach of the catalytic oxidation of diesel soot by ceria using temperature-programmed experiments. Part 1: Impact and evolution of the ceria/soot contacts during soot oxidation, Energy Fuels 24 (2010) 4766–4780.
[217] A. Bueno-Lopez, Diesel soot combustion ceria catalysts, Appl. Catal. B: Environmental 146 (2014) 1-11.
[218] T. Montini, M. Melchionna, M. Monai, P. Fornasiero, Fundamentals and Catalytic Applications of CeO_2-Based Materials, Chem. Rev. 116 (2016) 5987-6041.
[219] A. A. Voskanyan, K.-Y. Chan, C.-Y. Vanessa Li, Colloidal solution combustion synthesis: Toward mass production of a crystalline uniform mesoporous CeO_2 catalyst with tunable porosity, Chem. Mater. 28 (2016) 2768-2775.
[220] E. Aneggi, D. Wiater, C. de Leitenburg, J. Llorca, A. Trovarelli, Shape-Dependent Activity of Ceria in Soot Combustion, ACS Cat. 4 (2014) 172-181.
[221] W. Zhang, X. Niu, L. Chen, F. Yuan, Y. Zhu, Soot combustion over nanostructured ceria with different morphologies, Sci. Rep. 6 (2016) 29062.
[222] L. Soler, A.Casanovas, C. Escudero, V. Pérez-Dieste, E. Aneggi, A. Trovarelli, J.Llorca, Ambient Pressure Photoemission Spectroscopy Reveals the Mechanism of Carbon Soot Oxidation in Ceria-Based Catalysts, ChemCatChem 8 (2016) 2748-2751.
[223] E. Aneggi, N. J. Divins, C. de Leitenburg, J. Llorca, A. Trovarelli, The formation of nanodomains of Ce_6O_{11} in ceria catalyzed soot combustion, J. Catal. 312 (2014) 191-194.
[224] E. Aneggi, V. Rico-Perez, C. de Leitenburg, S. Maschio, L. Soler, J. Llorca, A. Trovarelli, Ceria–zirconia particles wrapped in a 2D carbon envelope : Improved low-temperature oxygen transfer and oxidation activity, Angew. Chem. Int. Ed. 54 (2015) 14040-14043.
[225] T. Andana, M. Piumetti, S. Bensaid, N. Russo, D. Fino, R. Pirone, Nanostructured ceria-praseodymia catalysts for diesel soot combustion, Appl. Catal. B: Environmental 197 (2016) 125-137.
[226] N. Guillén-Hurtado, A. García-García, A. Bueno-López, Active oxygen by Ce-Pr mixed oxide nanoparticles outperform diesel soot combustion Pt catalysts, Appl. Catal. B: Environmental 174-175 (2015) 60-66.
[227] T. Andana, M. Piumetti, S. Bensaid, N. Russo, D. Fino, R. Pirone, CO and Soot Oxidation over Ce-Zr-Pr Oxide Catalysts, Nanoscale Res. Lett. 11 (2016) 278.
[228] H. Li, K. Li, H. Wang, X. Zhu, Y. Wei, D. Yan, X. Cheng, K. Zhai, Soot combustion over $Ce_{1-x}Fe_xO_{2-\delta}$ and CeO_2/Fe_2O_3 catalysts: Roles of solid solution and interfacial interactions in the mixed oxides, Appl. Surf. Sci. 390 (2016) 513-525.
[229] V. Rico-Pérez, E. Aneggi, A. Bueno-López, A. Trovarelli, Synergic effect of $Cu/Ce_{0.5}Pr_{0.5}O_{2-\delta}$ and $Ce_{0.5}Pr_{0.5}O_{2-\delta}$ in soot combustion, Appl. Catal. B: Environmental 197 (2016) 95-104.
[230] A. Bueno-López, D. Lozano-Castelló, A. J. McCueb, J. A. Anderson, NOx storage and reduction over copper-based catalysts. Part 3: Simultaneous NOx and soot removal, Appl. Catal. B: Environmental 198 (2016) 266-275.
[231] J. Li, H. Chang, L. Ma, J. Hao, R. T. Yang, Low-temperature selective catalytic reduction of NOx with NH_3 over metal oxide and zeolite catalysts-A review, Catal. Today 175 (2011) 147-156.

[232] F. Gao, J. H. Kwak, J. Szanyi, C. H. F. Peden, Current understanding of Cu-exchanged chabazite molecular sieves for use as commercial diesel engine deNOx catalysts, Top. Catal. 56 (2013) 1441-1459.
[233] B. Guan, R. Zhan, H. Lin, Z. Huang, Review of state of the art technologies of selective catalytic reduction of NOx from diesel engine exhaust, Appl. Therm. Eng. 66 (2014) 395-414.
[234] P. G.W.A. Kompio, A. Brückner, F. Hipler, G. Auer, E. Löffler, W. Grünert, A new view on the relations between tungsten and vanadium in $V_2O_5AWO_3/TiO_2$ catalysts for the selective reduction of NO with NH_3, J. Catal. 286 (2012) 237-247.
[235] A. Marberger, D. Ferri, M. Elsener, O. Kröcher, The significance of Lewis acid sites for the selective catalytic reduction of nitric oxide on vanadium-based catalysts, Angew. Chem. Intern. Ed. 55 (2016) 11989-11994.
[236] J. Xue, X. Wang, G. Qi, J. Wang, M. Shen, W. Li, Characterization of copper species over Cu/SAPO-34 in selective catalytic reduction of NOxwith ammonia: Relationships between active Cu sites and de-NOx performance at low temperature, J. Catal. 297 (2013) 56-64.
[237] S. A. Bates, A. A. Verma, C. Paolucci, A. A. Parekh, T. Anggara, A. Yezerets, W. F. Schneider, J. T. Miller, W. N. Delgass, F. H. Ribeiro, Identification of the active Cu site in standard selective catalytic reduction with ammonia on Cu-SSZ-13, J. Catal. 312 (2014) 87-97.
[238] T. V. W. Janssens, H. Falsig, L. F. Lundegaard, P. N. R. Vennestrøm, S. B. Rasmussen, P. G. Moses, F. Giordanino, E. Borfecchia, K. A. Lomachenko, C. Lamberti, S. Bordiga, A. Godiksen, S. Mossin, P. Beato, A consistent reaction scheme for the selective catalytic reduction of nitrogen oxides with ammonia, ACS Catal. 5 (2015) 2832-2845.
[239] J-C. Chen, G-C. Fang, S-S. Shi, Activities of different metal oxide catalysts on NO reduction and CO oxidation, Int. J. Environment and Pollution, 37 (2009) 86-96.
[240] K. Frey, D.J. Schmidt, W.F. Schneider, Implications of coverage-dependent O adsorption for catalytic NO oxidation on the late transition metals, Catal. Sci. Technol. 4 (2014) 4356-4365.
[241] I. Atribak, I. Such-Basáñez, A. Bueno-López, A. García- García, Comparison of the catalytic activity of MO_2 (M = Ti, Zr, Ce) for soot oxidation under NOx/O_2, J. Catal. 250 (2007) 75–84.
[242] Z. Wu, M. Li M, S.H. Overbury, On the structure dependence of CO oxidation over CeO_2 nanocrystals with well-defined surface planes. J Catal 285, (2012), 61–73.
[243] I. Atribak, B. Azambre, A. Bueno López, A. García-García, Effect of NOx adsorption/desorption over ceria-zirconia catalysts on the catalytic combustion of model soot, Applied Catal. B. 92 (2009) 126-137.
[244] I. Atribak, A. Bueno López, A. García-García, Combined removal of diesel soot particulates and NOx over CeO_2–ZrO_2 mixed oxides, J. Catal. 259 (2008) 123–132.
[245] M. Adamowska, S. Muller, P. Da Costa, A. Krzton, P. Burg, Correlation between the surface properties and deNOx activity of ceria-zirconia catalysts, Appl. Catal., B: Environmental 74 (2007) 278–289.
[246] M. Yu. Sinev, G. W. Graham, L. P. Haack and M. Shelef, Kinetic and structural studies of oxygen availability of the mixed oxides $Pr_{1-x}M_xO_y$ (M=Ce or Zr), J. Mater. Res. 11 (1996) 1960-1971.
[247], J. Gimenez-Manogil, N. Guillen-Hurtado, N, S. Fernandez-Garcia, X.W. Chen, J.J. Calvino-Gamez, A. Garcia-Garcia, Ceria-Praseodymia Mixed Oxides: Relationships Between Redox Properties and Catalytic Activities Towards NO Oxidation to NO_2 and CO-PROX Reactions, Topics in Catalysis 59 (2016) 1065-1070.
[248] J. Giménez-Mañogil, A. Bueno-López, A. García-García, Preparation, characterisation and testing of $CuO/Ce_{0.8}Zr_{0.2}O_2$ catalysts for NO oxidation to NO_2 and mild temperature diesel soot combustion, Appl. Catal. B. 152-153 (2014) 99-107.
[249] Z. Wang, X. Sun, J.Liu, X. Li, The NO oxidation performance over $Cu/Ce_{0.8}Zr_{0.2}O_2$ catalyst, Surfaces and Interfaces 6 (2017) 103-109.
[250] F. Lin, X. Wu, D. Weng, Effect of barium loading on CuO_x–CeO_2 catalysts: NOx storage capacity, NO oxidation ability and soot oxidation activity, Catal. Today 175 (2011) 124-132.
[251] H-Y. Chen, Z. Wei, M. Kollar, F. Gao, Y. Wang, J. Szanyi, C.H.F. Peden, NO oxidation on zeolite supported Cu catalysts: Formation and reactivity of surface nitrates, Catal. Today 267 (2016) 17-27.
[252] F. Gao, E. D. Walter, M. Kollar, Y. Wang, J. Szanyi, C.H.F. Peden, Understanding ammonia selective catalytic reduction kinetics over Cu/SSZ-13 from motion of the Cu ions, J. Catal. 319 (2014) 1–14
[253] A.A.Verma, S.A. Bates, T. Anggara, C. Paolucci, A.A. Parekh, K. Kamasamudram, A. Yezerets, J.T. Miller, W.N. Delgass, W.F. Schneider, F.H. Ribeiro, NO oxidation: A probe reaction on Cu-SSZ-13, J. Catal. 312 (2014) 179-190.
[254] C. Zhou, X. Liu, C. Wu, Y. Wen, Y. Xue, R. Chen, Z. Zhang, B. Shan, H. Yin, W.G. Wang, NO oxidation catalysis on copper doped hexagonal phase $LaCoO_3$: a combined experimental and theoretical study, Phys.Chem.Chem.Phys., 16 (2014) 5106-5112.

[255] K. Shiba, H. Hinode, M. Wakihara, Catalytic oxidation of NO to NO_2 over Cr/TiO_2 and Cu/TiO_2 under oxidizing atmosphere, React. Kinet. Catal. Lett. 58 (1996) 133-137.
[256] M.F. Irfan, J.H. Goo, S.D. Kim, Co_3O_4 based catalysts for NO oxidation and NO_x reduction in fast SCR process, Appl. Catal. B: Environmental 78 (2008) 267–274.
[257] Y. Huang, D. Gao, Z. Tong, J. Zhang, H. Luo, Oxidation of NO over cobalt oxide supported on mesoporous silica J. Nat. Gas Chem. 18 (2009) 421–428.
[258] D.S. Kim, Y.H. Kim, J.E. Yie, E.D. Park, NO oxidation over supported cobalt oxide catalysts, Korean J. Chem. Eng. 27 (2010) 49–54.
[259] S.K. Megarajan, S. Rayalu, Y. Teraoka, N. Labhsetwar, High NO oxidation catalytic activity on non-noble metal based cobalt-ceria catalyst for diesel soot oxidation, J. Mol. Cat. A. 385 (2014) 112-118.
[260] E. Park, S. Chin, J. Jeong, J. Jurng, Low-temperature NO oxidation over Mn/TiO2 nanocomposite synthesized by chemical vapor condensation: effects of Mn precursor on the surface Mn species, Microporous and Mesoporous Materials 163 (2012) 96–101.
[261] Z.B. Wu, N.A. Tang, L. Xiao, Y. Liu, H.C. Wang, MnOx/TiO2 composite nanoxides synthesized by deposition–precipitation method as a superior catalyst for NO oxidation, J. Colloid Interface Sci. 352 (2010) 143–148
[262] Z.H. Chen, F.R. Wang, H. Li, Q. Yang, L.F. Wang, X.H. Li, Low-temperature selective catalytic reduction of NOx with NH_3 over Fe-Mn mixed-oxide catalysts containing $Fe_3Mn_3O_8$ phase, Ind. Eng. Chem. Res. 51 (2012) 202–212.
[263] W.W. Zhao, C.T. Li, P. Lu, Q.B. Wen, Y.P. Zhao, X. Zhang, C.Z. Fan, S.S. Tao, Iron, lanthanum and manganese oxides loaded on γ-Al2O3 for selective catalytic reduction of NO with NH_3 at low temperature, Environ. Technol. 34 (2013) 81–90.
[264] M. Zhang, C. Li, L. Qu, M. Fu, G. Zeng, C. Fan, J. Ma, F. Zhan, Catalytic oxidation of NO with O2 over FeMnOx/TiO2: Effect of iron and manganese oxides loading sequences and the catalytic mechanism study, Appl. Surf. Sci. 300 (2014) 58-65.
[265] Y. Wen, C. Zhang, H. He, Y. Yu, Y. Teraoka, Catalytic oxidation of nitrogen monoxide over $La_{1-x}Ce_xCoO_3$ perovskites, Catal. Today 126 (2007) 400–405.
[266] C.H. Kim, G. Qi, K. Dahlberg, W. Li, Strontium-doped perovskites rival platinum catalysts for treating NOx in simulated diesel exhaust, Science 237 (2010) 1624–1627.
[267] N. Akter, L. Han, D. Huaman, Y. Kang, T. Kim, NO and NH_3 Oxidation over zeolite materials, Materials Today: Proceedings, 3 (2016) 550-555.
[268] J.A. Loiland, R. F. Lobo, Low temperature catalytic NO oxidation over microporous materials, J Catal. 311 (2014) 412-423.
[269] N. Artioli, R.F. Lobo, E. Iglesia, Catalysis by confinement: Enthalpic stabilization of NO oxidation transition states by micropororous and mesoporous siliceous materials, J. Phys. Chem C., 117(40) (2013) 20666-20674.
[270] I. Halasz, A. Brenner, Active sites of H-ZSM5 catalysts for the oxidation of nitric oxide by oxygen, Catal. Letters, 34 (1995) 151-161.
[271] P.S. Metkar, V. Balakotaiah, M.P. Harold, Experimental and kinetic modeling study of NO oxidation: Comparison of Fe and Cu-zeolite catalysts, Catalysis Today, 184 (2012) 115-128.
[272] N.I. Il'chenko, Catalytic Oxidation of Ammonia, Russ. Chem. Rev. 45 (12) (1976) 1119-1134.
[273] N.N. Sazonova, A.V. Simakov, H. Veringa, Selective catalytic oxidation of ammonia to nitrogen, React. Kinet. Catal. Lett. 57(1) (1996) 71-79.
[274] R.Q. Long and R.T. Yang, Selective catalytic oxidation of ammonia to nitrogen over Fe2O3–TiO2 prepared with a sol–gel method, J. Catal. 207 (2002) 158-165.
[275] L. Gang, B.G. Anderson, J.V. Grondelle, R.A. van Santen, NH_3 oxidation to nitrogen and water at low temperatures using supported transition metal catalysts, Catal. Today 61 (2000) 179-185.
[276] Y. Li, J.N. Armor, Selective NH_3 oxidation to N_2 in a wet stream, Appl. Catal. B: Environmental 13 (1997) 131-139.
[277] M. Koebel, M. Elsener, M. Kleemann, Urea-SCR: a promising technique to reduce NOx emissions from automotive diesel engines, Catal. Today 59 (2000) 335-235.
[278] M. Koebel, E.O. Strutz, Thermal and hydrolytic decomposition of urea for automotive selective catalytic reduction systems: Thermochemical and practical aspects, Ind. Eng. Chem. Res. 42 (2003) 2093-2100.
[279] A.M. Berhard, D. Peitz, M. Elsener, T. Schildhauer, O. Kröcher, Catalytic urea hydrolysis in the selective catalytic reduction of NOx: catalyst screening and kinetics on anatase TiO_2 and ZrO_2, Catal. Sc. Technol. 3 (2013) 942-951.

[280] P.M. Schaber, J. Colson, S. Higgins, D. Thielen, B. Anspach, J. Brauer, Thermal decomposition (pyrolysis) of urea in an open reaction vessel, Thermochim. Acta. 424 (2004) 131-142.
[281] M. Seneque, F. Can, D. Duprez, X. Courtois, Use of a μ-scale synthetic gas bench for direct comparison of Urea-SCR and NH_3-SCR reactions over an oxide based powdered catalyst, Catalysts 5 (2015) 1535-1553.
[282] M. Seneque, F. Can, D. Duprez, X. Courtois, NOx Selective catalytic reduction (NO_x-SCR) by urea: Evidence of the reactivity of HNCO, including a specific reaction pathway for NOx reduction involving NO + NO_2, ACS Catal., 6 (7) (2016) 4064–4067.
[283] D. Fino, N. Russo, G. Saracco, V. Specchia, Removal of NOx and diesel soot over catalytic traps based on spinel-type oxides, Powder Technology, 180 (2008) 74-78.
[284] Z. Say, M. Tohumeken, E. Ozensoy, NO_x storage and reduction pathways on zirconia and titania functionalized binary and ternary oxides as NO_x storage and reduction (NSR) systems, Catal. Today, 231, 2014, 135-144.
[285] R. You, Y. Zhang, D. Liu, M. Meng, L. Zheng, J. Zhang, T. Hu, YCeZrO ternary oxide solid solution supported nonplatinic lean-burn NOx trap catalysts using $LaCoO_3$ perovskite as active phase, J. Phys. Chem. C., 118 (44) (2014) 25403-25420.
[286] F. Garin, Mechanism of NOx decomposition, Appl. Catal. A: General. 222 (2001) 183-219.
[287] A. Ogata, A. Obuchi, K. Mizuno, A. Ohi, H. Ohuchi, Active sites and redox properties of supported palladium catalysts for nitric oxide direct decomposition, J. Catal. 144 (1993) 452-459.
[288] M. Haneda, Y. Kintaichi, I. Nakamura, T. Fujitan, H. Hamada, Effect of surface structure of supported palladium catalysts on the activity for direct decomposition of nitrogen monoxide, J. Catal. 218 (2003) 405-410.
[289] A. Pulido, P. Nachtigall, Correlation between catalytic activity and metal cation coordination: NO decomposition over Cu/Zeolites, ChemCatChem, 1 (2009) 449–453.
[290] M. Iwamoto, H. Hamda, Removal of nitrogen monoxide from exhaust gases through novel catalytic processes, Catal. Today, 10 (1991), 57–71.
[291] E.R.S. Winter, The catalytic decomposition of nitric oxide by metallic oxides, J. Catal., 22 (1971), 158–170.
[292] G.K. Boreskov, Forms of oxygen bonds on the surface of oxidation catalysts, Discuss. Faraday Soc., 41 (1966), 263–276.
[293] S. Shin, Y. Hatakeyama, K. Ogawa, K. Shimomura, Catalytic decomposition of NO over brownmillerite-like compounds, $Ca_2Fe_2O_5$ and $Sr_2Fe_2O_5$, Mater. Res. Bull., 14 (1979) 133–136.
[294] H. Shimada, S. Miyama, H. Kuroda, Decomposition of nitric oxide over Y–Ba–Cu–O mixed oxide catalysts, Chem. Lett., 17 (1988) 1797–1800.
[295] H. Yasuda, N. Mizuno, M. Misono, Role of valency of copper in the direct decomposition of nitrogen monoxide over well characterized $La_{2x}A'_xCu_{1-y}B'_yO_4$, J. Chem. Soc., Chem. Commun., 16 (1990) 1094–1096.
[296] N. Imanaka, T. Masui, H. Masaki, Direct decomposition of nitric oxide over C-Type Cubic $(Gd_{1-x-y}Y_xBa_y)_2O_{3-y}$ solid solutions, Adv. Mater., 19 (2007) 3660–3663.
[297] H. Masaki, T. Masui, N. Imanaka, Direct decomposition of nitric oxide into nitrogen and oxygen over C-type cubic Y_2O_3–ZrO_2 solid solutions, J. Alloys Compd., 451 (2008) 406–409.
[298] N. Imanaka, T. Masui, Advances in direct NOx decomposition catalysts, Appl. Catal. A: General, 431–432 (2012) 1–8.
[299] M.A. Vannice, A.B. Walters, X. Zhang, The kinetics of NOx decomposition and NO reduction by CH_4 over La_2O_3 and Sr/La_2O_3, J. Catal., 159 (1996) 119–126.
[300] S. Xie, G. Mestl, M.P. Rosynek, J.H. Lunsford, Decomposition of nitric oxide over barium oxide supported on magnesium oxide. 1. Catalytic results and in situ Raman spectroscopic evidence for a barium–nitro intermediate, J. Am. Chem. Soc., 119 (1997) 10186–10191.
[301] S. Xie, M.P. Rosynek, J.H. Lunsford, Catalytic Reactions of NO over 0–7 mol% Ba/MgO Catalysts: I. The direct decomposition of NO, J. Catal., 188 (1999) 24–31.
[302] H. Iwakuni, Y. Shinmyo, H. Yano, H. Matsumoto, T. Ishihara, Direct decomposition of NO into N_2 and O_2 on $BaMnO_3$-based perovskite oxides, Appl. Catal. B: Environmental, 74 (2007) 299–306.
[303] K. Goto, H. Matsumoto, T. Ishihara, Direct Decomposition of NO on Ba/Ba–Y–O Catalyst, Top. Catal., 52 (2009) 1776–1780.
[304] T. Ishihara, K. Goto, Direct decomposition of NO over BaO/Y_2O_3 catalyst, Catal. Today, 164 (2011) 484–488.
[305] K. Goto, T. Ishihara, Direct decomposition of NO into N_2 and O_2 over $Ba_3Y_{3.4}Sc_{0.6}O_9$, Appl. Catal. A: Gen., 409–410 (2011) 66–73.
[306] S. Iwamoto, R. Takahashi, M. Inoue, Direct decomposition of nitric oxide over Ba catalysts supported on CeO2-based mixed oxides, Appl. Catal. B: Environmental, 70 (2007) 146–150.

[307] W.J. Hong, S. Iwamoto, S. Hosokawa, K. Wada, H. Kanai, M. Inoue, Effect of Mn content on physical properties of CeO_x–MnO_y support and BaO–CeO_x–MnO_y catalysts for direct NO decomposition, J. Catal. 277 (2011) 208–216.
[308] W.J. Hong, M. Ueda, S. Iwamoto, S. Hosokawa, K. Wada, H. Kanai, H. Deguchi, M. Inoue, Effect of Fe content on physical properties of BaO–CeOx–FeOy catalysts for direct NO decomposition, Appl. Catal. B: Environmental, 106 (2011) 142–148.
[309] Y. Doi, M. Haneda, M. Ozawa, Direct decomposition of NO an Ba catalysts supported on rare earth oxides, J. Mol. Cat. A. 383-384 (2014) 70-76.
[310] F. Arena, R. Di Chio, B. Gumina, L. Spadaro, G. Trunfio, Recent advances on wet air oxidation catalysts for treatment of industrial wastewaters, Inorg. Chim. Acta 431 (2015) 101-109.
[311] G. Jing, M. Luan, T. Chen, Progress of catalytic wet air oxidation technology, Arabian J. Chem. 9 (2016) S1208–S1213.
[312] J. Fu, G. Z. Kyzas, Wet air oxidation for the decolorization of dye wastewater: An overview of the last two decades, Chin. J. Catal. 35 (2014) 1-7.
[313] F. Xie, L. Wang, K. Wang, D. Hua, W. Li, Preparation of CuO/SiO_2 hollow spheres for catalytic oxidation of phenol, Catal. Surv. Asia 20 (2016) 74-81.
[314] X. Zhong, J. Barbier Jr., D. Duprez, H. Zhang, S. Royer, Modulating the copper oxide morphology and accessibility by using micro-/mesoporous SBA-15 structures as host support: Effect on the activity for the CWPO of phenol reaction, Appl. Catal. B: Environmental 121-122 (2012) 123-134.
[315] O. P. Taran, A. B. Ayusheev, O. L. Ogorodnikova, I. P. Prosvirin, L. A. Isupova, V. N. Parmon, Perovskite-like catalysts LaBO3(B = Cu, Fe, Mn, Co, Ni) for wet peroxide oxidation of phenol, Appl. Catal. B: Environmental 180 (2016) 86-93.
[316] H. Min, X. Ran, J. Fan, Y. Sun, J. Yang, W. Teng, W.-X. Zhang, G. Li, D. Zhao, Preparation of a mesoporous Cu-Mn/TiO_2 composite for the degradation of Acid Red 1, J. Mater. Chem. A 3 (2015) 7399-7405.
[317] M. Das, K. G. Bhattacharyya, Oxidation of Rhodamine B in aqueous medium in ambient conditions with raw and acid-activated MnO2, NiO, ZnO as catalysts, J. Mol. Catal. A: Chemical 391 (2014) 121-129.
[318] Anushree, S. Kumar, C. Sharma, Synthesis, characterization and catalytic wet air oxidation property of mesoporous $Ce_{1-x}Fe_xO_2$ mixed oxides, Mater. Chem. Phys. 155 (2015) 223-231.
[319] Anushree, S. Kumar, C. Sharma, $Ce_{1-x}Co_xO_y$ nanocatalysts: synthesis, characterization and environmental application, Catal. Sci. Technol. 6 (2016) 2101-2111.
[320] M. Zhu, G. Diao, Synthesis of porous Fe_3O_4 nanospheres and its application for the catalytic degradation of xylenol orange, J. Phys. Chem. C, 115 (2011) 18923-18934.
[321] Z. Wan, J. Wang, Ce-Fe-reduced graphene oxide nanocomposite as an efficient catalyst for sulfamethazine degradation in aqueous solution, Environ. Sci. Pollut. Res. 23 (2016) 18542-18551.
[322] J. Han, H.-Y. Zeng, S. Xu, C.-R. Chen, X.-J. Liu, Catalytic properties of CuMgAlO catalyst and degradation mechanism in CWPO of methyl orange, Appl. Catal. A: General 527 (2016) 72-80.
[323] H. Li, Y. Li, L. Xiang, Q. Huang, J. Qiu, H. Zhang, M. V. Sivaiah, F. Baron, J. Barrault, S. Petit, S. Valange, Heterogeneous photo-Fenton decolorization of Orange II over Al-pillared Fe-smectite: Response surface approach, degradation pathway, and toxicity evaluation, J. Hazard. Mater. 287 (2015) 32-41.
[324] F. Schmit, L. Bois, F. Chassagneux, C. Descorme, Catalytic wet air oxidation of methylamine over supported manganese dioxide catalysts, Catal. Today 258 (2015) 570-575.